UNIVERSIDADE FEDERAL DE SANTA CATARINA
PROGRAMA DE PÓS-GRADUAÇÃO EM ENGENHARIA CIVIL

LUCAS RAFAEL DO NASCIMENTO

PERFORMANCE ASSESSMENT OF SOLAR PHOTOVOLTAIC TECHNOLOGIES UNDER DIFFERENT CLIMATIC CONDITIONS IN BRAZIL

Florianópolis
2019

LUCAS RAFAEL DO NASCIMENTO

PERFORMANCE ASSESSMENT OF SOLAR PHOTOVOLTAIC TECHNOLOGIES UNDER DIFFERENT CLIMATIC CONDITIONS IN BRAZIL

Tese submetida ao Programa de Engenharia Civil da Universidade Federal de Santa Catarina para a obtenção do Grau de Doutor em Engenharia Civil
Orientador: Prof. Ricardo Rüther, Ph.D.

Florianópolis
2019

Ficha de identificação da obra elaborada pelo autor através do Programa de Geração Automática da Biblioteca Universitária da UFSC.

Nascimento, Lucas Rafael
Performance assessment of solar photovoltaic technologies under different climatic conditions in Brazil/ Lucas Rafael do Nascimento; orientador, Ricardo Rüther, 2019.
104 p.

Tese (doutorado) - Universidade Federal de Santa Catarina, Centro Tecnológico, Programa de Pós-Graduação em Engenharia Civil, Florianópolis, 2019.

Inclui referências.
1. Engenharia Civil. 2. Photovoltaics. 3.
1. Photovoltaics. 2. Performance ratio. 3. Overirradiance. I. Rüther, Ricardo. II. Universidade Federal de Santa Catarina. Programa de Pós-Graduação em Engenharia Civil. III. Título.

LUCAS RAFAEL DO NASCIMENTO

PERFORMANCE ASSESSMENT OF SOLAR PHOTOVOLTAIC TECHNOLOGIES UNDER DIFFERENT CLIMATIC CONDITIONS IN BRAZIL

O presente trabalho em nível de doutorado foi avaliado e aprovado por banca examinadora composta pelos seguintes membros:

Prof. Dr. Roberto Zilles
Universidade de São Paulo

Prof. Dr. Arno Krenzinger
Universidade Federal do Rio Grande do Sul

Prof. Fernando Oscar Ruttkay Pereira, PhD
Universidade Federal de Santa Catarina

Prof. Roberto Lamberts, PhD
Universidade Federal de Santa Catarina

Certificamos que esta é a **versão original e final** do trabalho de conclusão que foi julgado adequado para obtenção do título de doutor em Engenharia Civil.

Assinado de forma digital por Roberto Lamberts:29400384068
Dados: 2019.08.14 17:24:27 -03'00'

Prof. Roberto Lamberts, PhD
Coordenador do Programa

Assinado de forma digital por Ricardo Ruther:38822385004
Dados: 2019.08.14 14:03:48 -03'00'

Prof. Ricardo Rüther, PhD
Orientador

Florianópolis, 29 de Março de 2019.

ACKNOWLEDGEMENTS

I would like to start by thanking Prof. Ricardo Rüther for all the knowledge shared over these fourteen years since I started as an undergraduate student at UFSC. Thank you for your guidance throughout my doctorate period and your dedication to the growth of the Solar Research Group (Fotovoltaica-UFSC) into a reference on the photovoltaic scene in Brazil.

To the Brazilian Electricity Regulatory Agency (ANEEL), as well as ENGIE Brasil Energia and the 11 cooperating electric utility companies for sponsoring project PE-0403-0027/2011. Statkraft must also be acknowledged with thanks for sponsoring the project where the Solar Monitoring Station of Brotas de Macaúbas – BA is situated. I would also like to thank the Brazilian Post-Graduate Council – CAPES for a doctoral scholarship.

Thanks are also due to the Australian Government and the Australian Academy of Science for sponsoring my Ph.D. Exchange with the University of New South Wales (UNSW) and Dr. Anna Bruce and Prof. Muriel Watt for supporting me during my doctorate's sandwich period.

I would also like to extend my thanks to my colleagues and friends from Fotovoltaica-UFSC Pedro Veríssimo, Álvaro do Nascimento, Eduardo Deschamps, Julio Dal Bem, Bernardo Hickel, Alexandre Montenegro, André Nobre, Clarissa Zomer, Andrigo Filippo, Juliane Almeida, Kathlen Schneider, Isadora Custódio, Lucas Sergio, Junior Cruz and Delma Camargos for their contribution and help in the development of this work.

To those directly involved in the endless analyses, treatment, and interpretation of the data presented in this thesis, my special thanks to colleagues Anelise Medeiros, André Cechinel, Ruany Dolla, Gustavo Xavier, Eduardo Watzko, Julio Boing and Danilo Neto.

Special thanks also to colleagues Aline Kirsten and Caroline Bedin for performing the night electroluminescence measurements used in this work, and to Ernesto Moscardini for the cleaning of PV systems and performing of I-V curve measurements to quantify the soiling shown in this thesis.

I would like to extend my sincere gratitude to colleagues Marília Braga and Trajano Viana for the many discussions on the extensive amount of results stemming from this project, co-authoring of scientific articles, and revision of this thesis.

I also would like to express my gratitude to Rafael Campos for prolonged nights of data processing, interpretation of results and co-authorship of articles.

To Dr. Gilberto Figueiredo for the insights of low-cost electroluminescence that were used in this study.

To the members of the evaluation committee, I express my gratefulness in taking your time to read this thesis, and for your invaluable suggestions for the overall enrichment of my thesis.

I would like to acknowledge Prof. Hans Helmut Zürn and Prof. Helena Flavia Naspolini, for having given me guidance and support during all these years since my early beginning at UFSC.

A special thanks to my friend Juan Debali for the professional ABNT formatting, and to all my friends who helped and contributed to making this happen.

To my four mothers (Maristela, Marise, Marlene and Marli*) for all the support, dedication, affection, and for teaching me the important values in life.

To my friend, and beloved wife Kamila for all the partnership, understanding and joy of the past days and of many others that will still come.

“O otimista é um tolo. O pessimista, um chato. Bom mesmo é ser um realista esperançoso”

Ariano Suassuna.

RESUMO

A geração fotovoltaica (FV) centralizada tem apresentado um importante crescimento no Brasil nos últimos anos, consequência de intensa redução de seus custos de produção. As elevadas temperaturas de operação, os altos níveis de umidade e irradiância e uma distribuição de irradiância em um espectro desviado para o azul em comparação com o espectro padrão ASTM G-173, levam a resultados operacionais contrastantes das várias tecnologias FV comercialmente disponíveis, que são evidenciados nesta tese. Este trabalho avalia oito Módulos de Avaliação (MAs) idênticos instalados em oito regiões climáticas do Brasil, cada um possuindo uma potência instalada de 54 kWp e utilizando as seguintes tecnologias fotovoltaicas: Silício amorfo (a-Si), Silício microcristalino (µc-Si), Telureto de Cádmio (CdTe), Disseleneto de Cobre-Índio-Gálio (CIGS), Silício mono e multi-cristalino (c-Si e m-Si). Todas os sistemas operam com inclinação idêntica à latitude local correspondente. Parâmetros elétricos e ambientais em todos os locais são medidos continuamente em intervalos de um segundo. Os resultados mostram uma análise detalhada das perdas de energia para todas as tecnologias. Os módulos fotovoltaicos de filmes finos com baixo coeficiente de temperatura apresentaram elevada taxa de desempenho. Módulos de silício cristalino revelaram intensa degradação em áreas com alta umidade relativa e temperatura. Apesar das diferentes tecnologias FV avaliadas, os resultados encontrados estão diretamente associados aos fabricantes dos módulos utilizados e não necessariamente refletem o comportamento destas tecnologias como um todo. Os efeitos de sobreirradiância causados por eventos de borda de nuvem resultaram em picos de irradiância de até 1845 W/m², com eventos que duraram vários minutos acima de 1600 W/m², resultando em frequentes queimas de fusíveis, mesmo quando foram observadas as recomendações dos fabricantes dos módulos fotovoltaicos. A soma de todos os efeitos observados e descritos nesta tese demonstra que o dimensionamento e operação de usinas solares fotovoltaicas de grande porte nas distintas regiões do Brasil apresentam peculiaridades que até o presente pouco foram descritas na literatura científica especializada.

Palavras-chave: Energia solar fotovoltaica. Desempenho de sistemas fotovoltaicos. Coeficiente de desempenho. PID. Sobreirradiância.

RESUMO EXPANDIDO

Introdução

Nos últimos anos a aplicação da geração solar FV vem apresentando desenvolvimento notável, tanto em escala de produção e aplicação, como em redução de custos, atingindo resultados cuja consequência são o reconhecimento de que esta tecnologia deverá integrar a matriz energética brasileira de forma competitiva, inclusive no curto prazo. Com isto o conhecimento técnico do desempenho das tecnologias FV comercialmente disponíveis é de grande importância, não somente no âmbito científico e tecnológico, mas também econômico. Esta tese mostra os resultados da avaliação de seis tecnologias FV fixas instaladas em oito diferentes regiões climáticas do Brasil. Os resultados também apresentam algumas das peculiaridades observadas durante o monitoramento em alta resolução temporal dos geradores FV. Eventos de sobreirradiância resultaram em problemas operacionais que não foram descritos anteriormente na literatura. Estas informações são de grande importância científica e econômica à medida que a penetração da energia solar aumenta e faz parte do planejamento estratégico do sistema elétrico no Brasil.

Objetivos

Avaliar como os fatores ambientais podem afetar a expectativa de geração elétrica de diferentes tecnologias solares FV em diferentes condições climáticas na matriz elétrica brasileira.

Metodologia

Em agosto de 2011 com os principais objetivos de facilitar a inserção da geração FV na matriz energética brasileira, viabilizar economicamente a produção, instalação e monitoramento e incentivar o desenvolvimento e nacionalização no país de toda a cadeia produtiva FV, foi lançada a chamada de projeto de P&D Estratégico 013 da ANEEL intitulada: Arranjos Técnicos e Comerciais para Inserção da Geração Solar Fotovoltaica na Matriz Energética Brasileira. Nesta chamada de projetos de P&D as empresas Tractebel Energia (atualmente Engie) e outras 11 empresas cooperadas, com a coordenação da Universidade Federal de Santa Catarina, iniciaram um projeto de P&D com o objetivo de avaliar técnica e economicamente a geração FV em diferentes condições climáticas na matriz elétrica brasileira.

O projeto teve como premissa a instalação de oito sistemas FV, denominados Módulos de Avaliação (MA). Os sistemas foram instalados em diferentes regiões climáticas do Brasil, cada um possuindo uma potência instalada de 54 kWp e utilizando as seguintes tecnologias FV: Silício amorfo (a-Si), Silício microcristalino (a-Si/μc-Si), Telureto de Cádmio (CdTe), Disseleneto de Cobre-Índio-Gálio (CIGS), Silício mono e multi-cristalino (c-Si e m-Si). Todas os sistemas operam com inclinação idêntica à latitude local correspondente. Os Parâmetros elétricos e ambientais em todos os locais são medidos continuamente em intervalos de um segundo. A única diferença entre os oito MA é o ângulo de inclinação dos módulos FV que é idêntica à latitude local em cada caso. Os MA são constantemente monitorados, variáveis ambientais como irradiância, temperatura (ambiente e módulo FV) e parâmetros elétricos são medidos e registrados em intervalos de um segundo.

Resultados e Discussões

Em ambientes quentes e ensolarados a temperatura é o principal fator de perdas em sistemas FV. A avaliação de desempenho das tecnologias FV nas diferentes regiões climáticas do Brasil, relevou que a tecnologia de filme fino de silício amorfo (a-Si), que apresenta baixo coeficiente de temperatura para potência, apresentou desempenho elétrico superior quando comparada as demais tecnologias avaliadas. Sistemas FV de silício monocristalino (c-Si) e multi-cristalino (m-Si) apresentaram elevado desempenho em vários dos MA. Contudo, revelaram intensa

degradação em áreas costeiras com alta temperatura e alta umidade relativa, alcançando reduções de potência de até 60% e 40% para módulos individuais, respectivamente. As avaliações realizadas apontam padrões de degradação compatível com degradação induzida por potencial (PID) para módulos FV da tecnologia de m-Si e degradação induzida por penetração de umidade nas células para a tecnologia de c-Si. Os resultados também mostram baixa potência de pico medida para os módulos de silício microcristalino (a-Si/μc-Si) que operaram por dois anos consecutivos, indicando uma redução de 7% na potência nominal, o que pode estar associado a uma degradação inicial maior do que a esperada pelo fabricante. Para a tecnologia de Disseleneto de Cobre-Índio-Gálio (CIGS) medições da curva I-V realizadas em módulos novos indicam uma redução de potência média de 6,2% em relação a dados de placa. Mesmo que uma pequena amostra tenha sido analisada, isso poderia indicar uma discrepância entre a potência declarada pelo fabricante e a potência real dos módulos FV.

Para a tecnologia de Telureto de Cádmio (CdTe), importantes avanços foram realizados pelo fabricante First Solar desde a instalação dos MA e as características de desempenho da Série 2 dos módulos instalados nessa avaliação foram consideravelmente melhoradas no atual produto da Série 4. Avaliações de desempenho com Performance Ratio (PR) 2-3% superiores à tecnologia de m-Si foram relatados na literatura para o Nordeste do Brasil em avaliações similares utilizando módulos de Série 3. Embora seis tecnologias FV distintas tenham sido avaliadas, os resultados apresentados nesta tese estão diretamente relacionados aos fabricantes específicos dos módulos empregados no projeto e não refletem necessariamente o comportamento das tecnologias FV como um todo.

Os efeitos dos eventos de sobreirradiância solar, além de serem de interesse científico e tecnológico, apresentaram impactos importantes no desempenho operacional de usinas FV de grande porte. Sete dos dez maiores eventos de sobreirradiância medidos mundialmente e registrados na literatura ocorreram no Brasil e foram medidos no âmbito desta tese. Todos esses eventos ocorreram em locais onde usinas FV de grande porte estão sendo implantadas no Brasil, e todos esses locais estão localizados em altitudes relativamente baixas, onde não há benefício de uma absorção atmosférica reduzida, tornando essas observações ainda mais notáveis. O maior evento de sobreirradiância registrado em Caucaia-CE, a uma altitude de cerca de 32 m acima do nível do mar, foi de 1845 W/m². O valor medido é semelhante ao relatado para Colorado-EUA, onde 1891 W/m² foi registrado a 1829 m acima do nível do mar, e para Andes-Equador, onde 1832 W/m² foi medido a 3400 m acima do nível do mar. Os resultados mostraram que quando longos eventos de sobreirradiância (maior que cinco minutos), estão associados às temperaturas elevadas de operação dos fusíveis de proteção dos sistemas, consequências deletérias podem ser observadas. Estes impactos podem incluir o rompimento de fusíveis, se forem dimensionados de acordo com as especificações do fabricante do módulo fotovoltaico. Portanto, recomenda-se que os fabricantes de módulos FV reavaliem suas classificações de máximo fusível permitido e que projetos de usinas FV de grande porte dimensionem as caixas de proteção de maneira a evitar que os fusíveis atinjam elevadas temperaturas. Nas condições mostradas nesta tese, o projeto de usinas FV de grande porte precisa ser realizado com cuidado devido à grande fração da energia solar disponível em elevados valores de irradiância, acima da irradiância padrão de 1000 W/m2, normalmente causada por eventos de sobreirradiância. Para tais casos, os intervalos de aquisição de dados com resolução de um minuto apresentaram resultados satisfatórios para modelagem e dimensionamento dos sistemas.

Considerações Finais

Nesta tese a avaliação de desempenho de seis tecnologias FV distintas, instaladas em oito locais no Brasil foi descrita e avaliada em um experimento científico de médio prazo. Os resultados apresentados fornecem uma visão geral dos principais aspectos (dimensionamento, degradação,

perdas por sujeira, incertezas de geração) que deverão ser considerados com mais detalhes conforme as usinas fotovoltaicas de grande porte começam a ser instaladas no Brasil.
Medições de alta resolução temporal da irradiância solar medidos em outros lugares do mundo podem revelar que eventos de sobreirradiância, como os apresentados nesta tese, podem ser ainda mais comuns do que os relatados neste trabalho. Especialmente em locais onde usinas FV de grande porte serão implantadas no futuro.

Palavras-chave: Energia solar fotovoltaica. Desempenho de sistemas fotovoltaicos. Coeficiente de desempenho. PID. Sobreirradiância.

ABSTRACT

Utility-scale photovoltaic (PV) generation is being ramped-up in Brazil in recent years, as a result of intense price reductions. Extreme operating temperatures, high humidity, and irradiance levels, and a blue-biased distribution of irradiance in comparison with the standard ASTM G-173 spectrum lead to contrasting operational outputs of the various commercially-available PV technologies. The performance assessment of six different PV technologies installed at eight different climatic regions in Brazil is presented. This thesis evaluates eight identical, 54 kWp Evaluation Sites (ESs), all with the following PV technologies: amorphous-silicon (a-Si), microcrystalline-silicon (a-Si/µc-Si), cadmium-telluride (CdTe), copper-indium-gallium-diselenide (CIGS), mono- and multi-crystalline silicon (c-Si and m-Si). All installations operate at a fixed-tilt equal to the corresponding local latitude. Electrical and environmental parameters at all sites are measured continuously at one-second intervals. A detailed energy loss analysis for all technologies is presented. Thin-film PV modules with a low temperature-coefficient of power presented superior performance. Crystalline silicon modules revealed severe degradation in areas with high relative humidity and temperature. Even though several PV technologies were assessed, the results presented are directly related to the specific manufacturers of the modules employed in the project, and not necessarily reflect the PV technologies' behavior as a whole. Cloud-edge and cloud-enhancement effects of solar irradiance resulted in irradiance peaks of up to 1845 W/m², with long overirradiance events which lasted many minutes over 1600 W/m², resulting in the frequent blowing of string fuses when manufacturers' maximum fuse ratings were employed. The combined effect of all the phenomena observed and described in this thesis demonstrates that the sizing and operating of utility-scale PV in the different climatic regions in Brazil presents peculiarities which have not been extensively described in the scientific literature so far.

Keywords: Photovoltaics. PV performance. Performance ratio. PID. Overirradiance

LIST OF FIGURES

Figure 1 - Development of the production of PV modules by technology (Fraunhofer, 2018). 24
Figure 2 - Comparison of the efficiencies of the best PV cells produced in laboratory *vs.* best PV module efficiencies for the year 2011 (Fraunhofer, 2012). 25
Figure 3 - Comparison of the efficiencies of the best PV cells produced in laboratory *vs.* best PV module efficiencies for the year 2017 (Fraunhofer, 2018). 25
Figure 4 - Temperature variation of the PV generator for different types of PV integration (Nobre *et al.*, 2012). 27
Figure 5 -Spectral Response of different PV technologies (Minnaert and Veelaert, 2014). 28
Figure 6 - Response of PV technologies to different irradiance levels (N. Reich *et al.*, 2005). 31
Figure 7 - c-Si power degradation (Jordan and Kurtz, 2013). 32
Figure 8 - Degradation of a-Si power (Jordan and Kurtz, 2013) 32
Figure 9 - Evolution of the normalized DC output power of a 2kWp thin-film a-Si PV generator, and average back-of-module temperature over a 15-year period in Brazil (Nascimento, 2013). 33
Figure 10 - Solar irradiance levels throughout the day, G_{CC} being the irradiance profile measured by a clean reference solar cell (W/m²) and G_{DC} being the irradiance profile measured by a soiled reference solar cell (W/m²) (Zorrilla-Casanova *et al.*, 2013). 33
Figure 11 - Relationship between losses caused by soiling and rainfall in a PV cell (Zorrilla-Casanova *et al.*, 2013). 34
Figure 12 - Losses caused by soiling for arid and desert regions of the United States without land movement (Caron and Littmann, 2013). 35
Figure 13 -Losses caused by soiling for arid and desert regions of the United States with presence of agriculture and land movement (Caron and Littmann, 2013). 35
Figure 14 - Soiling losses on CdTe PV plants with performance reduction rates of 0.015%/day (left) and 0.15%/day (right) (Gostein *et al.*, 2014). 36
Figure 15 - Non-uniform soiling distribution profile in PV modules caused by high wind incidence (Hickel *et al.*, 2016). 36
Figure 16 - Non-uniformity of soiling in a PV system (Lorenzo *et al.*, 2013). 37

Figure 17 - Impact of non-uniform soiling on the I-V curve of a clean PV module (blue curve) and a soiled PV module (orange curve), both connected in the same string. (Lorenzo *et al.*, 2013). 37
Figure 18 - Impact of soiling density on different PV technologies (Qasem *et al.*, 2012). 38
Figure 19 - Inverter Loading Ratios (ILR) for each of the 143 power plants with successful bids in the five PV-dedicated auctions in Brazil, identified in chronological order from 2014 to 2018 by red, blue, magenta, orange and green colors. When possible, the projects are separated into fixed tilt (circles), one axis tracking (X) and both (diamonds). Adapted from (Deschamps and Rüther, 2019). 40
Figure 20 - PR values for PV systems installed between 1994 and 2010 in Germany, during the 1000 Roofs Programme (Reich *et al.*, 2012). 44
Figure 21 - PV system annual PR (%) and total annual energy yield (kWh/kWp/year) for a 2kWp, thin-film a-Si PV generator over a 15-year period, together with the total annual solar irradiation at the site (kWh/m²/year) (Nascimento, 2013)..... 45
Figure 22 - PR *vs.* PR corrected by temperature for 275 days of analysis (Dierauf *et al.*, 2013). 46
Figure 23 - General location in the 8.5 million km² Brazilian territory of the eight identical R&D ESs, located between 3°S and 28°S, each with approximately 54 kW_p of fixed, latitude-tilt PV. 51
Figure 24 - Aerial view of one (ES # Capivari de Baixo-SC, 28ºS, 48ºW) of the eight identical R&D ESs, with approximately 54 kWp of fixed, latitude-tilt PV..... 52
Figure 25 - Solar monitoring station installed at the Capivari de Baixo-SC ES, with identical sensors installed in all eight ESs and detailed in Table 5. 55
Figure 26 - General view (a) of the seven SMS installed in the Brazilian territory, and an enlarged view (b) of North and Northeast regions in which most of the utility-scale PV power plants are being installed since 2014 in the country. 59
Figure 27 - AC Performance Ratios (PR) of the PV technologies installed at the eight ESs in different climates in Brazil. 63
Figure 28 - Potential Induced Degradation (PID) effect on two p-type multi-crystalline strings from the Capivari de Baixo-SC ES (28°S, 49°W), located on the coast of Southern Brazil. (a) maps the two strings connected to independent MPPT inverter inputs: string "a" (outlined in blue, with 13 modules) and string "b" (outlined in orange, with 16 modules), with positive modules in green and negative modules in red. (b) shows the EL images made for all the m-Si modules within the two strings. (c) shows the measured

power, obtained using an I-V curve tracer, relative to the best-performing module in the string. The modules shaded in red and black on the left-hand side of all pictures are modules that were damaged and were thus disregarded in the study. 64
Figure 29 - Individually measured I-V curves for each of the PV modules belonging to the two strings shown in Figure 28. (a) displays the I-V curves measured for the modules in string "a", while (b) displays the same for string "b". 66
Figure 30 - Electroluminescence (EL) images and I-V curve results of two strings of c-Si PV modules from the Capivari de Baixo-SC ES, showing traces of humidity within the PV module encapsulation. (a) shows the EL images of the two strings (string "a" outlined in blue and string "b" in orange). (b) shows, respectively, the series resistance obtained for each PV module during the I-V curve measurements. (c) shows the measured power, obtained using an I-V curve tracer, relative to the best-performing module in the string. The modules outlined and shaded in red in the images are modules that were damaged and were thus disregarded in the study. 67
Figure 31 - I-V curve measurement of a 260 Wp c-Si PV module from the Capivari de Baixo - SC ES, showing high series resistance (5.6Ω), low shunt resistance (44.5Ω) and low fill factor (43.1%), which could be related to the humidity ingress in the PV module's encapsulation 68
Figure 32 - I-V curve measurement results of three brand-new 142 Wp a-Si/µc-Si PV modules (green squares), and three 142 Wp a-Si/µc-Si PV modules that had been operating in the ES for two years (blue triangles). The flash test results provided by the manufacturer for these specific six modules are also shown as red Xs. The tolerance indicated by the manufacturer on the PV module's datasheet is shown as yellow dashed lines. 70
Figure 33 - Weak-light response of brand-new PV modules of five technologies identical to the ones employed at the ESs. Measurements were made in a PASAN SunSim 3C LAPSS AAA solar simulator, at LABSOL-UFRGS, and corrected to STC. Results are shown in relation to each technology's STC measurement. 71
Figure 34 - Measured losses (left-hand bars in orange) and simulated losses (right-hand stacked bars) for the # Itiquira-MT ES (17°S, 54°W). 72
Figure 35 - Measured losses (left-hand bars in orange) and simulated losses (right-hand stacked bars) for the # Aratiba-RS ES (27°S, 52°W). 73

Figure 36 - Images of the CIGS (a), CdTe (b) and m-Si (c) Itiquira MT ES PV systems before and after being manually cleaned (left- and right-hand side images, respectively). The soiling shown was accumulated between December 2013 and September 2014. 75
Figure 37 - Highest overirradiance event measured in Brazil so far (1845 W/m^2), using a Delta SPN1 thermopile pyranometer installed at the # Caucaia-CE SMS. 76
Figure 38 - Picture of a broken cloud sky with overirradiance event at the # Itiquira-MT SMS. 77
Figure 39 – Extreme overirradiance events recorded at each of the seven SMSs installed at different sites in Brazil, measured with pyranometers (thermopile sensors) from different models and manufacturers. 78
Figure 40 – Extreme global horizontal overirradiance (GHI) events, recorded at the # Brotas de Macaúbas-BA and # Itiquira-MT SMS, with SMP11 and SPN1 pyranometers (both are thermopile sensors). 79
Figure 41 - Operating temperature (66.3 ºC) and maximum temperature (74.3 ºC) measured in a fuse holder, inside a combiner box. The meter's thermocouple is inserted in the fuse holder. 82
Figure 42 - Global tilted overirradiance event measured with a Kipp & Zonen CMP11 thermopile pyranometer at the # Cabo Frio-RJ SMS, around 12:30, with irradiances higher than 1500 W/m^2 and lasting longer than five minutes. The fuse of string 2 has blown with a normalized current value of 1.43. 84
Figure 43 – Inverter overload losses for a crystalline-Si PV system at the # Itiquira-MT ES, with an average PR of 75%, and ILRs varying from 100% to 140% using different data averaging intervals. 88
Figure 44 - Frequency distribution of irradiance ramps, for 50 W/m^2/s slope intervals, at the # Itiquira-MT SMS. 89

All the figures used in this thesis are original and was carried by myself except where specific contributions of other persons are acknowledged. Reference to the work published by other individuals has extensively been made throughout this thesis, and was always cited in the usual manner.

LIST OF TABLES

Table 1 - Characteristic atmospheric parameters for some Brazilian locations and ASTM G-173.The standard deviation for the concentration values of ozone, water vapor, and AOD are shown in parentheses (Haag, 2013). 29

Table 2 - Main electrical characteristics of the six commercially-available PV module technologies employed at the eight identical ESs, sorted from most to least efficient (all 2011-2013 vintage PV modules). 51

Table 3 - Main characteristics of the six PV generators installed at each of the eight identical ESs spread over the 8.5 million km^2 Brazilian territory. 53

Table 4 - Coordinates, commissioning date and climate classification according to Köppen-Geiger of the eight identical evaluation sites (ESs) spread over the 8.5 million km^2 Brazilian Territory (Cfa: Humid subtropical climate; Aw: Tropical wet-dry climate; Am: Tropical monsoon climate; As: Tropical dry summer)..... 54

Table 5 - List of sensors and variables measured at the eight identical solar monitoring stations (SMS). 56

Table 6 - Site location, altitude, geographic coordinates, climate classification and the measurement period of the seven Solar Monitoring Stations (SMS)..... 60

Table 7 - Temperature coefficient of maximum power for the PV module technologies used in this study, sorted from lowest to highest, as per each manufacturer's PV module spec sheet. 61

Table 8 - Measured peak power and power reduction relative to nameplate peak power for three brand-new 120 Wp CIGS PV modules identical to the ones used in the ESs. Results are from I-V curve measurements carried out at real sunlight, after the proper light exposure of the samples. The uncertainty of the I-V curve tracer used, PVE PVPM 1040X, is ±5%. 69

Table 9 - Summary of results for measured losses and total simulated losses for the # Itiquira-MT ES (17°S, 54°W). 73

Table 10 - Summary of results for measured losses and total simulated losses for the # Aratiba-RS ES (27°S, 52°W). 73

Table 11 - Measured soiling losses at the # Itiquira-MT ES (17°S, 54°W)..... 74

Table 12 - Maximum values of global horizontal overirradiance (GHI) events recorded around the world. Adapted from Almeida *et al.* (2014) and Gueymard (2017a) and

updated, including location, elevation, clearness index (Kt), measurement time resolution, the instrument used in the measurement and instrument response time. 80

Table 13 - Number of high global tilted irradiance (GTI) events (irradiance higher than G_0, 1367 W/m^2) measured at all seven SMS. Averaged irradiance is calculated using all instantaneous overirradiance values measured in the corresponding time span. 85

Table 14 - Annual GTI solar energy distribution (in % of annual irradiation) measured at Itiquira-MT SMS, for different ranges of irradiance (G) and different averaging periods. 87

All the tables used in this thesis are original and was carried by myself except where specific contributions of other persons are acknowledged. Reference to the work published by other individuals has extensively been made throughout this thesis, and was always cited in the usual manner.

LIST OF ABBREVIATIONS

APE	Average Photon Energy
a-Si	Amorphous Silicon
a-Si/µc-Si	Microcrystalline Silicon
BAPV	Building Applied Photovoltaics
BIPV	Building Integrated Photovoltaics
CdTe	Cadmium-Telluride
CIGS	Copper-Indium-Gallium-Diselenide
c-Si	Mono-crystalline Silicon
EL	Electroluminescence
ES	Evaluation Site
EVA	Ethylene Vinyl Acetate
GHI	Global Horizontal Irradiation
GTI	Global Tilted Irradiance
IAM	Incidence Angle Modifier
ILR	Inverter Loading Ratio
LCOE	Levelized Cost of Energy
m-Si	Multi-crystalline Silicon
O&M	Operation and Maintenance
Pmpp	Maximum Power Point Power
PR	Performance Ratio
PV	Photovoltaics
SF	Spectral Factor
SMS	Solar Monitoring Stations
STC	Standard Test Conditions
SWE	Staebler-Wronski Effect
UV	Ultraviolet
VIS-NIR	Visible and Near Infrared Regions

SUMMARY

1 INTRODUCTION 20
1.1 MOTIVATION **20**
1.2 OBJECTIVES **22**
1.2.1 Main objective 22
1.2.2 Specific objectives 22

2 LITERATURE REVIEW 23
2.1 PHOTOVOLTAIC SOLAR ENERGY 23
2.2 PHOTOVOLTAIC TECHNOLOGIES 23
2.3 PERFORMANCE OF PHOTOVOLTAIC SYSTEMS **25**
2.3.1 Temperature 26
2.3.2 Humidity 27
2.3.3 Solar spectrum 28
2.3.4 Solar irradiation 30
2.3.5 PV module degradation 31
2.3.6 Soiling 33
2.3.7 Inverter Loading Ratio (ILR) 38
2.3.8 Losses due to shading 40
2.3.9 Incidence Angle Modifier (IAM) 41
2.3.11 Potential-Induced Degradation (PID) 42
2.3.12 PV module mismatch losses **42**
2.3.13 Electrical losses in DC and AC wiring **42**
2.4 PERFORMANCE MEASUREMENT **43**
2.4.1 Performance Ratio (PR) 43
2.4.2 Corrected Performance Ratio 44
2.5 OVERIRRADIANCE IMPACTS ON PV POWER PLANTS **48**

3 MATERIALS AND METHODS 50
3.1 EXPERIMENTAL SETUP 50
3.2 PERFORMANCE EVALUATION 56
3.3 FIELD MEASURING INSTRUMENTS 57
3.4 DATA ASSESSMENT OF OVERIRRADIANCE EVENTS 58

4 RESULTS AND DISCUSSION 61
4.1 PV PERFORMANCE ASSESSMENT 61
4.2 ENERGY LOSS ANALYSIS 72
4.3. OVERIRRADIANCE IMPACTS ON PV SYSTEMS 76
4.3.1 Global Horizontal Irradiance - overirradiance events (GHI) 76
4.3.2 Impacts on PV power performance 80
4.3.2.1 Fuse rating 80
4.3.2.2 Fuse behavior with temperature 81
4.3.2.3 Blown fuses during overirradiance events 83
4.3.2.4 Inverter overload losses 86
4.3.2.5 Irradiance variability and impacts on MPPT efficiency 88

5 CONCLUSIONS 90

REFERENCES 92

1 INTRODUCTION

In recent years, due to the declining costs of photovoltaics (PV), and the excellent solar energy resource availability in the country, the Brazilian government and the electricity sector have started to evaluate and consider PV as a serious potential contributor to the national energy mix. Utility-scale PV is gaining momentum in Brazil, and after the successful introduction of large-scale wind generation in the late 1990s, solar generation is now enjoying exponential growth in the country.

This thesis presents the main results of the assessment of six, fixed-tilt, flat-plate, commercially-available solar PV technologies installed at eight different sites with distinct climatic conditions in Brazil. The PV performance at each site is evaluated through the calculation of the Performance Ratios (PRs) from measured data for each PV technology, and comprehensive analysis of these results is presented.

A detailed energy loss analysis, carried out with the use of computational simulation, is also presented for two of the evaluation sites (ESs). These results are compared with those obtained from measured data of a full year of operation of the corresponding PV systems. The differences observed between simulated and measured losses along with simulation uncertainties are discussed. The results also reveal some of the peculiarities observed during the continuous and high-temporal-resolution (one-second) monitoring of PV generators at all these warm and sunny sites.

Cloud-edge and cloud-enhancement effects on solar irradiance are also presented and discussed, together with the consequent operational issues experienced. To our knowledge, such issues have not been previously described in the literature. This study is of considerable scientific and economic interest as PV generation increases its penetration and is part of the strategic planning of the National Electricity Sector in Brazil.

1.1 MOTIVATION

Unforeseen and impressive PV module price reductions over the last 10 years (Kavlak *et al.*, 2018) have led to massive falling prices - and rising capacity factors - of utility-scale PV power plants, especially in warm and sunny climates all over the world (Bolinger *et al.*, 2015),(Reich *et al.*, 2012). Cheaper PV modules gave rise to a noticeable increase in inverter loading ratios in ground-mounted PV plants in recent years, adding more DC power to the same AC power converter (Deschamps and Rüther, 2019). Most of these large-scale PV projects aim at selling PV electricity under long-term contracts and at prices close to the $ 25/MWh mark or less. While the traditional silicon technologies (both mono- and multi-crystalline) dominate the

scene, with some 95% of the world market in 2017 (Fraunhofer, 2018), high-efficiency (18% in current production and prospects of 22% demonstrated efficiencies) (Bosio *et al.*, 2018; NREL, 2018) new generation thin-film cadmium-telluride (CdTe) PV modules have recently been introduced in the market. These improved CdTe modules present some interesting features for utility-scale PV power plants in the same warm and sunny climates where record-low prices for solar electricity are being promised. While for c-Si PV spectral effects (due to spectral shifts of the incident spectrum when compared with the standard spectral distribution of sunlight) do not play a significant role, the narrower spectral response of CdTe and a-Si results in different behaviors depending on the spectral content of sunlight at a particular site (Tsuji *et al.*, 2018). The lower temperature coefficient of power, and the blue-shifted spectral response when compared to c-Si, render thin-film CdTe - and the no longer commercially-available amorphous silicon PV technologies - good performers in the warm, sunny, humid and bluer skies predominant in sunbelt regions of the world (Rüther and Livingstone, 1995; Rüther *et al.*, 2002).

Grid-connected photovoltaic systems exhibit a close to linear response to solar irradiance (G), which plays the most important role in the power output of solar PV devices. PV modules electrical data are rated at Standard Test Conditions (STC) values (25°C cell temperature, 1000 W/m^2 solar irradiance, and AM=1.5 incident spectral distribution of sunlight). For laboratory rating purposes, an irradiance value of 1000 W/m^2 (normally emitted by a flash solar simulator) is applied perpendicularly to a PV module surface to determine its nominal maximum power value (STC-rated peak power, Wp) and other electrical data. Ground-based solar monitoring stations normally measure values lower than the extraterrestrial irradiance (G_0) because of atmospheric attenuation. In this way, irradiance values above 1000 W/m^2 are not considered as frequent or lasting long enough in the field, to play a significant role in the PV module and PV system performance. However, solar overirradiance events measured in Brazil at values considerably higher than the extraterrestrial irradiance are relatively frequent, sometimes lasting up to several minutes, a situation which might cause important impacts and harmful consequences in solar PV grid-connected systems, especially in utility-scale PV power plants as this thesis shows. Results and analyses of global horizontal and global tilted overirradiance events presented in this thesis are from irradiance data measured at seven similar ground-based Solar Monitoring Stations (SMS) installed in different Brazilian climatic regions. An extensive scientific literature search has been carried out, and no studies have been found in the literature so far, measuring and evaluating the occurrence and levels of overirradiance in a vast tropical area as presented in this thesis.

1.2 OBJECTIVES

1.2.1 Main objective

Evaluate the effects of environmental factors on the performance and reliability of different solar PV technologies in distinct climatic conditions in Brazil.

1.2.2 Specific objectives

a) Evaluate the Performance Ratio of different PV technologies in order to identify and quantify the main system losses at various climatic regions;

b) Assess the PV power degradation mechanisms of different PV technologies in various climatic regions;

c) Compare simulated and measured losses for various PV technologies in different climatic regions of Brazil;

d) Evaluate the impact of overirradiance events on the operation of PV systems and;

e) Assess the impacts of measurements' time resolution on simulation and sizing of PV systems;

2 LITERATURE REVIEW

2.1 PHOTOVOLTAIC SOLAR ENERGY

The PV effect describes the direct conversion of sunlight into electrical energy. This energy conversion phenomenon presents great advantages, such as extreme simplicity, the absence of moving parts, its modular characteristic (from mW to MW), short installation time, high reliability and low maintenance. In addition, PV conversion is silent, non-polluting and uses a renewable and inexhaustible source of energy.

PV conversion occurs using semiconductor materials, with silicon being the most used. In addition to silicon, thin-film Cadmium-Telluride (CdTe), Copper-Indium-Gallium-Diselenide (CIGS), as well as other composite semiconductors are also used (Rüther, 2004; Parida *et al.*, 2011).

2.2 PHOTOVOLTAIC TECHNOLOGIES

PV technologies can be divided into three categories or generations of PV modules. The first generation uses crystalline silicon cells, mono or multi-crystalline, with cell thickness in the 150-200 μm range, with cost reduction limited by material costs (Saga, 2010). The second generation, called thin-film technology, has an emphasis on cost reduction using very thin layers (~ 1μm) of semiconductor materials. It also uses silicon but in amorphous form (a-Si), as well as other materials such as CdTe and CIGS among others. The third generation was initially defined as technologies that should have been abundant, non-toxic, thin-layer, with extremely low production costs, and of intrinsically higher efficiency materials than single-junction devices, such as those presented in the first generation. This definition has been expanded to include other advanced PV technologies such as organic PV cells (dye-sensitized solar cells) and organic-inorganic perovskite cells. Although the third-generation of PV modules has a longer perspective of cost reduction, these are only expected to be met in the long run and limitations related to the low life expectancy and low efficiency when deposited in large areas are still to be overcome (Green, 2004; 2009; Heeger, 2010; El Chaar *et al.*, 2011; Parida *et al.*, 2011; Green, 2016). Figure 1 illustrates the production development of PV modules by technology. It can be observed that the technology of the first generation of modules presents itself as the most traditional of PV technologies and has the largest scale of commercial production, with around 95% of the market for the year 2017 (~ 62% multi-crystalline and ~ 33% mono-crystalline).

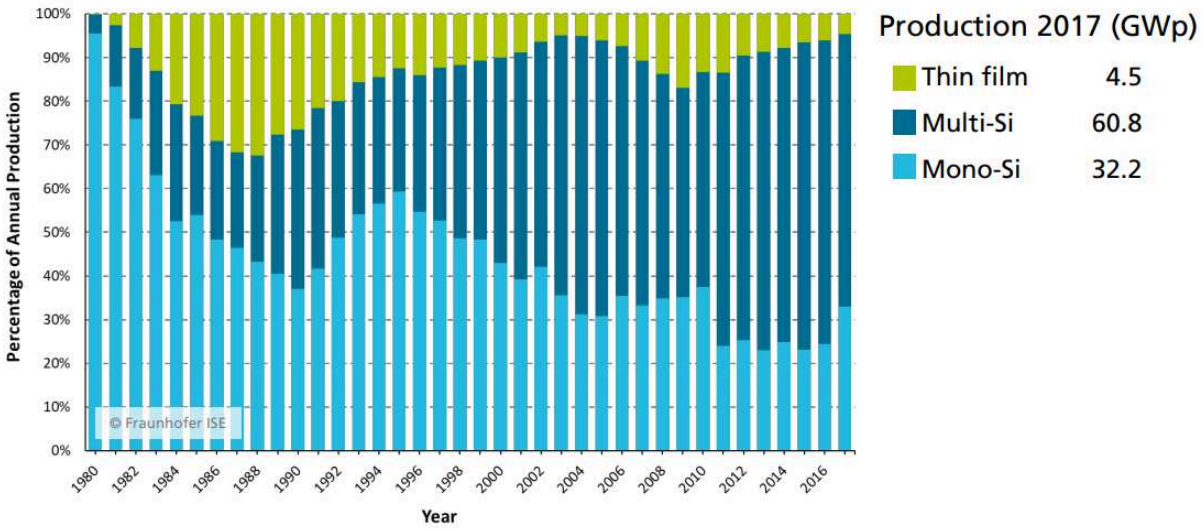

Figure 1 - Development of the production of PV modules by technology (Fraunhofer, 2018).

PV conversion efficiency is given by the ratio of the maximum power produced by the cell or PV module, under Standard Test Conditions (STC), to the product of the cell/module area and irradiance, also under STC (ABNT, 2006).

Figure 2 presents an efficiency comparison of the best PV cells produced in the laboratory and the best efficiencies of PV modules for the year 2011, while Figure 3 presents the same data for the year 2017. It is important to note that the presented efficiencies are much higher than those commercially available since laboratory studies generally use small devices, higher purity materials in well-controlled production processes with low production yields.

While the most widely used multi-crystalline silicon technology on the market had a 1.7% (absolute) efficiency increase between 2011-2017 for the best modules, the best CdTe modules for the same period increased by 5.8% (absolute).

During the last 10 years, while the efficiency of commercially-available multi-crystalline silicon modules increased from 12% to 17%, CdTe modules increased from 9% to 16% (Fraunhofer, 2018).

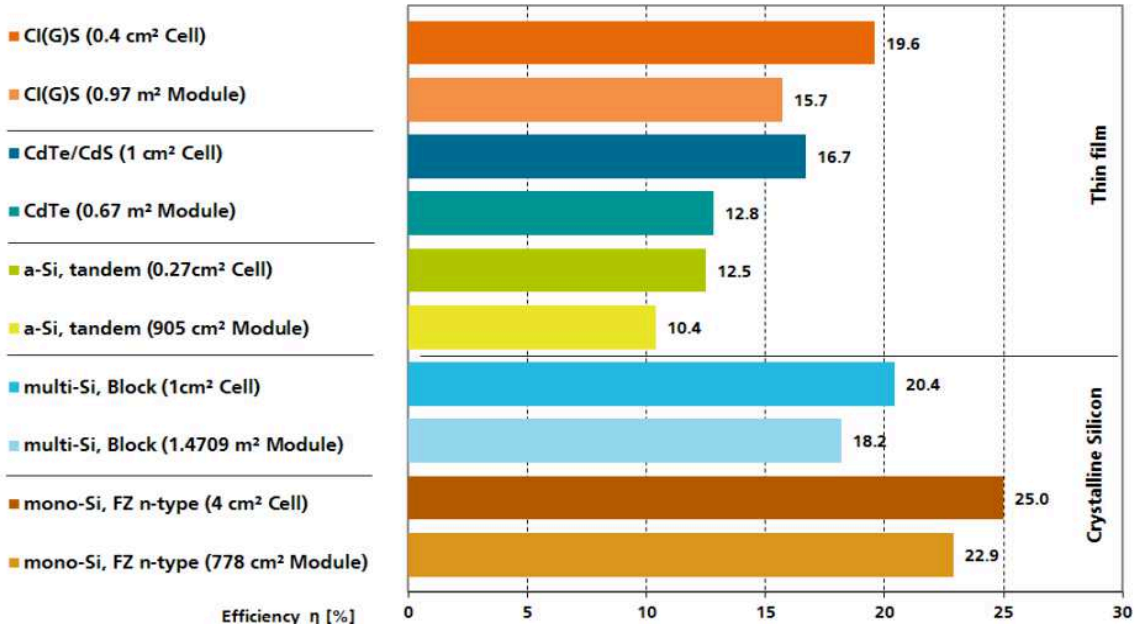

Figure 2 - Comparison of the efficiencies of the best PV cells produced in laboratory *vs.* best PV module efficiencies for the year 2011 (Fraunhofer, 2012).

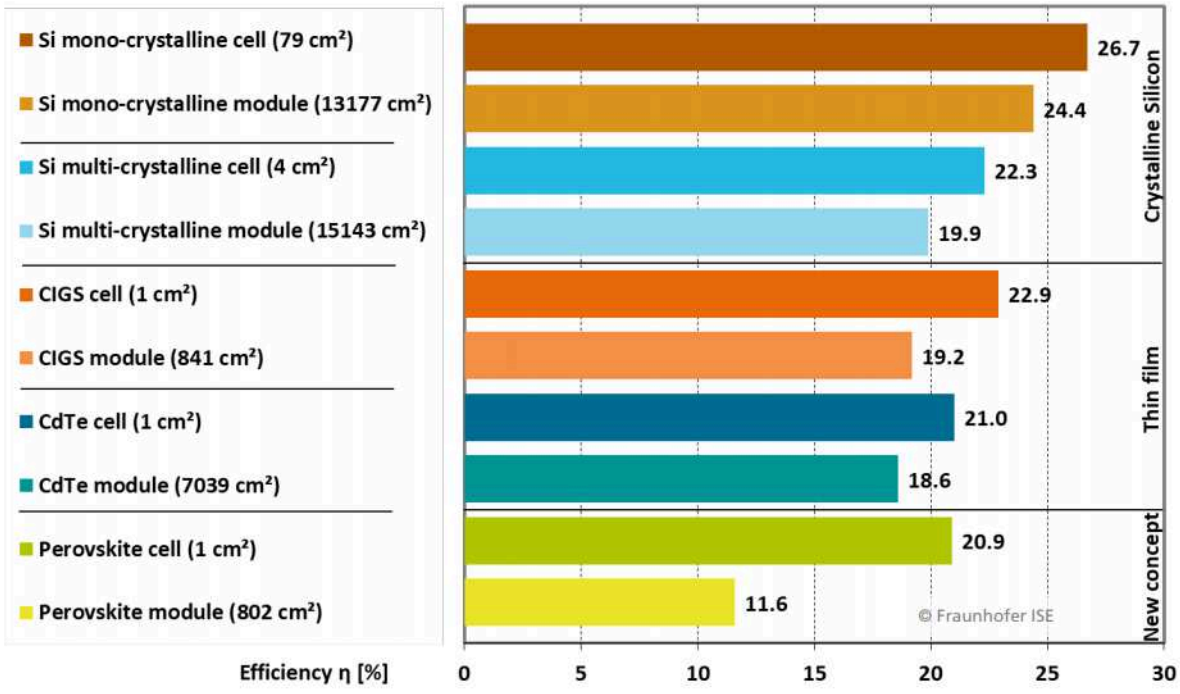

Figure 3 - Comparison of the efficiencies of the best PV cells produced in laboratory *vs.* best PV module efficiencies for the year 2017 (Fraunhofer, 2018).

2.3 Performance of photovoltaic systems

There are several environmental factors that can affect the overall performance of PV systems. These factors may depend exclusively on the environmental characteristics of where

the system is installed, as in the case of solar irradiance profile, temperature, the spectral content of sunlight, among others. Other characteristics - such as soiling - are both related to the environmental characteristics of the site and to the frequency of Operation and Maintenance (O&M) practices on the PV system.

2.3.1 Temperature

PV devices have a negative coefficient of temperature over power as a function of the increase in temperature at the P-N junction of the PV cell, a result from the voltage reduction due to the decreasing of the corresponding semiconductor energy gap (Skoplaki and Palyvos, 2009). In the literature, several PV module temperature models are proposed and evaluated as functions of irradiance, ambient temperature and wind speed (Mora Segado *et al.*, 2015).

In Building Applied and Building Integrated Photovoltaic (BAPV and BIPV, respectively) the type of PV module integration can also cause strong influences on system performance. Figure 4 shows how different architectural integrations can lead to different PV module temperatures. In hot climates, the temperature of non-ventilated PV modules integrated into the roofs can reach values above 80°C (Rüther *et al.*, 2010b), strongly affecting their electrical characteristics as the voltage of the modules decreases proportionally with the increase in temperature. In these situations, the choice of PV technology should be a point to be observed. Thin-film modules such as amorphous silicon (a-Si), microcrystalline silicon (a-Si/μc-Si) and CdTe become a suitable option for this type of architectural integration since they have a low coefficient of temperature on power (Rüther *et al.*, 2008; Rüther *et al.*, 2010a). Especially for a-Si, the temperature coefficients reported in catalogs often do not match the actual electrical characteristics of a stabilized PV module, and the coefficient may be even lower than that reported, which applies specifically to new modules and which has not yet suffered from the Staebler-Wronski Effect (SWE) (Rüther *et al.*, 2008).

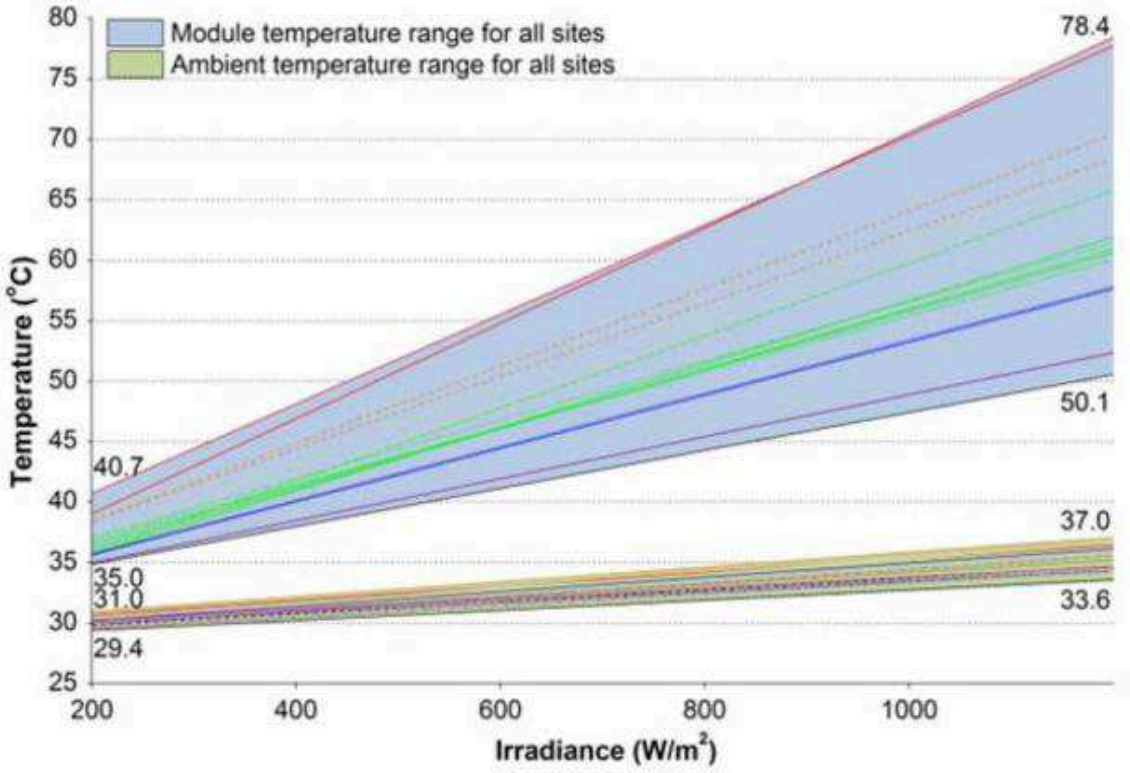

Figure 4 - Temperature variation of the PV generator for different types of PV integration (Nobre *et al.*, 2012).

High ambient temperatures, besides impacting the electrical performance of the system, can also have an impact on PV module degradation. This degradation caused by temperature can occur in different ways. Encapsulating material (e.g., Ethylene Vinyl Acetate -EVA) that protects the PV cell, may lose transparency and elasticity under high temperature conditions (Sefid *et al.*, 2012). Increased serial resistance of PV cells could be another undesirable effect of extended exposure to high temperatures when associated with poor welding on PV module fabrication (King *et al.*, 2000).

2.3.2 Humidity

Humidity can influence in three different ways the performance of a PV system. The first scenario is the effect of the water vapor of the atmosphere in the scattering, reflection, and absorption that solar irradiance is subjected to when crossing the atmosphere. The second scenario is the effects of the ingress of moisture inside the encapsulation of the PV module, which may cause embrittlement of the encapsulating material and increase the resistance of the PV cells, decreasing the performance of the device (Mekhilef *et al.*, 2012; Sefid *et al.*, 2012).

Lastly, high humidity can also lead to dew formation on the PV module. In places subject to this condition, dust clots can be formed, decreasing the performance of the system due to accumulated soiling (Mani and Pillai, 2010).

2.3.3 Solar spectrum

Due to intrinsic material properties, distinct PV technologies respond differently to the spectral distribution of sunlight. The response of the PV device to different wavelengths of solar radiation is known as the device's spectral response, and depends on both the semiconductor material and the PV device design. Figure 5 shows the typical spectral response of different PV technologies.

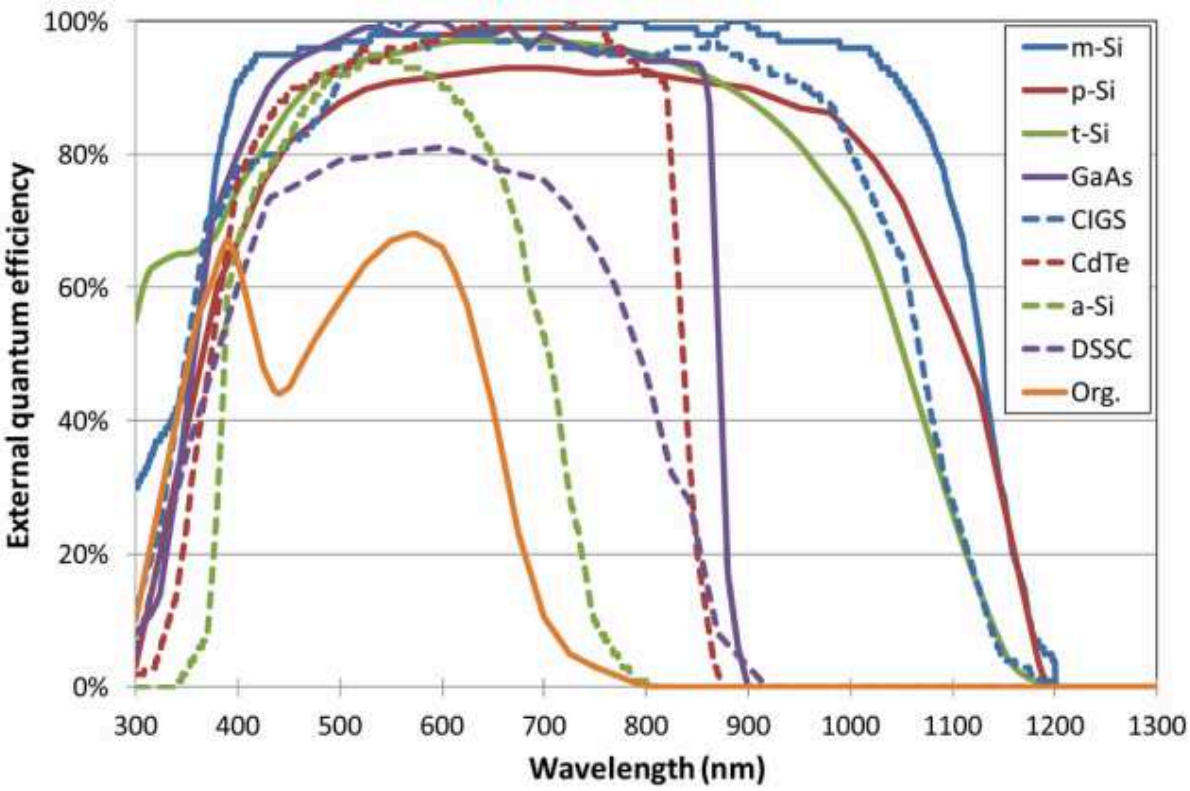

Figure 5 -Spectral Response of different PV technologies (Minnaert and Veelaert, 2014).

It can be observed that a-Si and CdTe technologies present a spectral response mainly at shorter wavelengths (blue-biased devices). In this way, these technologies will have a spectral advantage in regions with the predominance of cloudy skies and low irradiance (Rüther *et al.*, 2002; Gottschalg *et al.*, 2005).

Due to the high cost and complexity of maintenance and data acquisition, there are not many spectroradiometers globally available. In Brazil, there is currently no equipment performing continuous and long-term measurements for spectral characterization across the

country's territory. Simulation models for PV systems also do not faithfully represent spectral losses/gains, often neglecting this loss due to the complexity of modeling atmospheric dynamics and its impact on the solar spectrum (Duck and Fell, 2015). For these scenarios, an alternative used is to obtain a spectral representation of a site using radiation transfer models (Myers and Gueymard, 2004), from atmospheric data originated from measurements in the field (Núñez *et al.*, 2016) or satellite data (Amillo *et al.*, 2015).

The standard spectrum used for testing the PV modules under STC (ASTM-G173.03, 2012), was obtained through the spectral modeling aforementioned, which used as inputs Aerosol Optical Depth (AOD), amount of precipitable water, ozone column, carbon dioxide, and average air mass from representative regions of the US in order to define the standard spectrum. The atmospheric values presented in Table 1 were used to characterize the typical standard spectrum used worldwide in the characterization of PV modules; the average values for a few Brazilian locations are also presented, showing the atmospheric differences for various regions of Brazil. Using this methodology, characteristic spectra were defined for Brazil (Haag, 2013; Haag and Krenzinger, 2016).

Table 1 - Characteristic atmospheric parameters for some Brazilian locations and ASTM G-173.The standard deviation for the concentration values of ozone, water vapor, and AOD are shown in parentheses (Haag, 2013).

Location	Ozone (DU)	Water Vaper (cm)	AOD	CO_2 (ppmv)
ASTM G-173	343.8	1.42	0.084	370
Porto Alegre, RS	275.4 (9.26)	2.30 (0.24)	0.061 (0.028)	384
Petrolina, PE	286.5 (8.83)	3.24 (0.21)	0.040 (0.018)	381
Alta Floresta, MT	270.2 (9.48)	4.53 (0.24)	0.246 (0.11)	382
Manaus, AM	260.5 (9.75)	5.25 (0.15)	0.195 (0.068)	382

There are several indexes for quantifying the effects of different spectral distributions of light on PV technologies. Some of these indexes characterize the spectral distribution of light, such as the blue fraction and APE (average photon energy), while others relate a given spectral distribution with the standard spectrum and a specific spectral response (spectral factor, useful fraction, etc.) or even correlate the relative spectral impacts between two PV devices (spectral mismatch factor) (Rodrigo et al., 2017).

In order to quantify the spectral mismatch between the reference ASTM G173-03 spectrum and the local spectrum, for a particular PV spectral response, the spectral factor (SF),

a dimensionless coefficient is typically used (Rodrigo et al., 2017). This index is chosen because it quantifies the actual spectral gains of a PV technology regardless of the reference irradiance sensor used. It must be noted that when correcting IV curve measurements or other irradiance-dependent parameters, the mismatch factor (MM) is a more suitable index, considering that it correlates the spectral response of the reference sensor and the device under test as well as the reference and the measured spectra (Rodrigo et al., 2017). The formula for the spectral factor (SF) calculation is shown in Equation 1.

$$SF = \frac{\int E_G(\lambda) SR(\lambda) d\lambda}{\int E_G^*(\lambda) SR(\lambda) d\lambda} \cdot \frac{\int E_G^*(\lambda) d\lambda}{\int E_G(\lambda) d\lambda} \quad (1)$$

Were:
SF = spectral factor
$E_G(\lambda)$ = local spectrum
$E_G^*(\lambda)$ = reference ASTM G173-03 spectrum
$SR(\lambda)$ = spectral response of the PV device

This spectral correction is discrete, and for an extended analysis over a time period, it is necessary to perform a point-by-point correction in order to quantify the impact of the SF over the analyzed period. The mean SF for the period can be calculated as an irradiance-weighted mean of point-by-point SF (Duck and Fell, 2015); thus SF values for moments with higher irradiance have a greater weight on the mean.

2.3.4 Solar irradiation

The level or intensity of solar radiation (irradiance) is also an important parameter that influences the performance of PV systems. When PV modules are tested in the laboratory, their efficiency is measured under an irradiance of 1000 W/m², which corresponds approximately to the irradiance around solar noon on a clear day. Although much of the energy of a PV system is generated at high irradiance levels (Burger and Rüther, 2006), depending on the time of year and cloud cover ratio, low irradiance can have a significant influence on the performance of a PV system (Rüther *et al.*, 2010b). The behavior of a PV device under low irradiance levels is called weak light performance or low light performance (N. Reich *et al.*, 2005).

Figure 6 shows the efficiency of different PV technologies relative to STC conditions as a function of irradiance. It can be seen that the a-Si PV technology achieves nominal efficiency at practically any level of irradiance, but the same is not true for the other PV technologies analyzed.

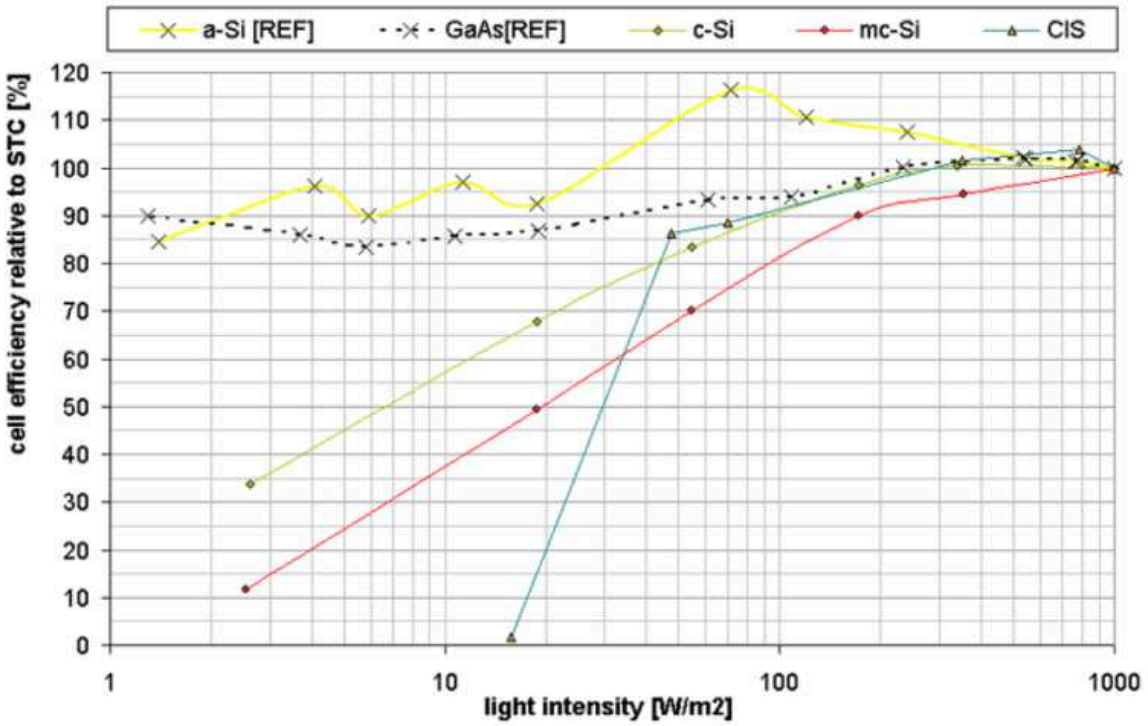

Figure 6 - Response of PV technologies to different irradiance levels (N. Reich *et al.*, 2005).

2.3.5 PV module degradation

PV modules have a warranty against manufacturing defects that are typically offered in 5- to 12-year periods. The product warranty is usually related to cracks in the front glass, detachment of the connection box, delamination of the encapsulating layers, EVA yellowing, among others. In addition to the product warranty, the manufacturers provide guarantees regarding the peak power of the PV module. Typically, it is guaranteed by the manufacturer that the nominal peak power of the module should have a maximum reduction of 10% in the first 10 years of operation and another 10% on the next 10 to 25 years. This represents a degradation of the PV module rated power of about 0.8% per year.

The degradation of PV modules is not identical for all technologies, and it is very much related to the climate where the system is installed. For crystalline silicon modules, a survey conducted in 1751 PV systems showed that the median degradation for this technology is about 0.5% per year (Figure 7). For a-Si 169 PV systems were analyzed, showing a median degradation of around 1.0% per year (Figure 8) (Jordan and Kurtz, 2013). In Brazil, limited literature is available on this topic, but long-term evaluations of a PV generator installed in 1997 showed performance reduction rates of 0.55% per year (Figure 9), values similar to the averages found in the international literature (Nascimento and Rüther, 2014).

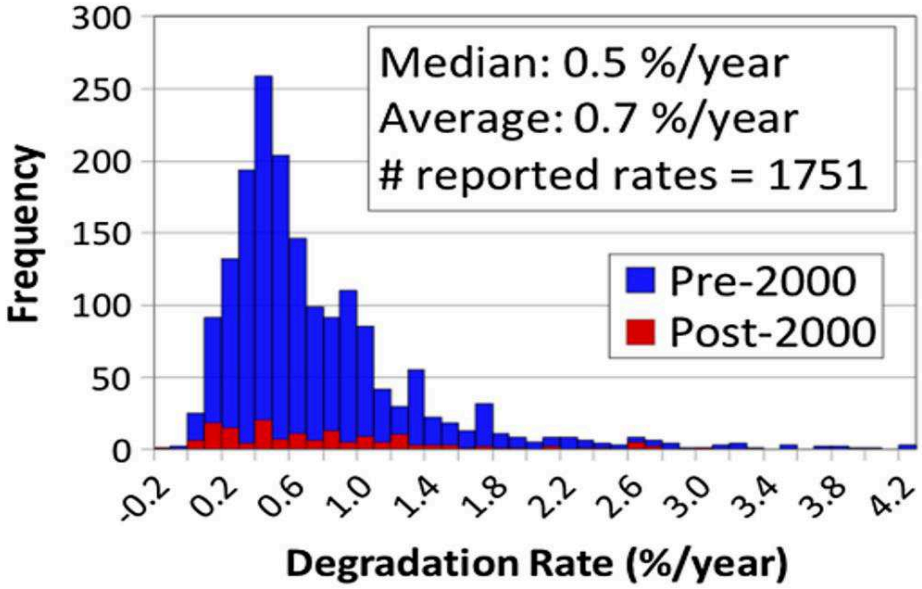

Figure 7 - c-Si power degradation (Jordan and Kurtz, 2013).

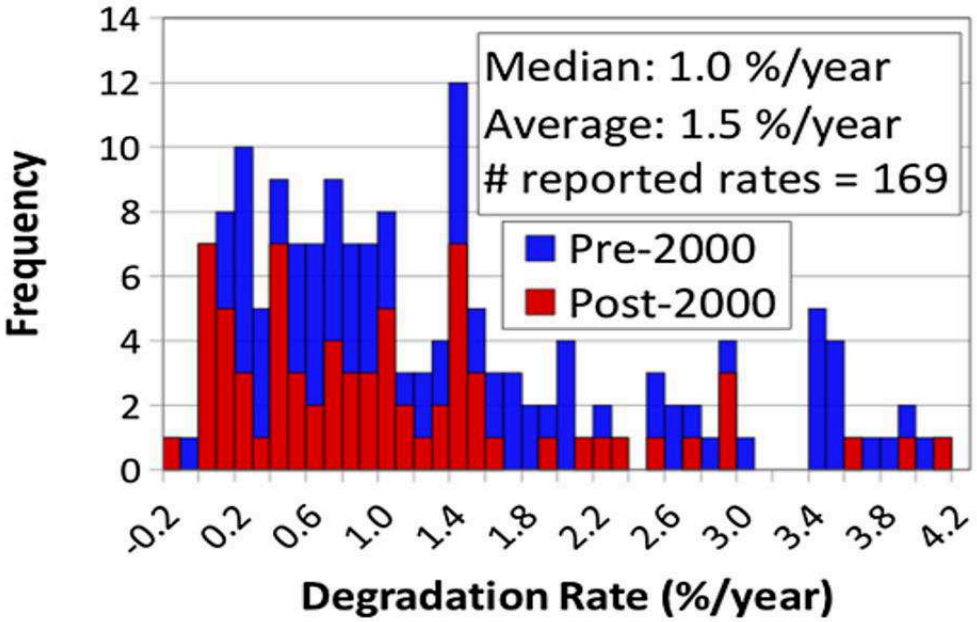

Figure 8 - Degradation of a-Si power (Jordan and Kurtz, 2013).

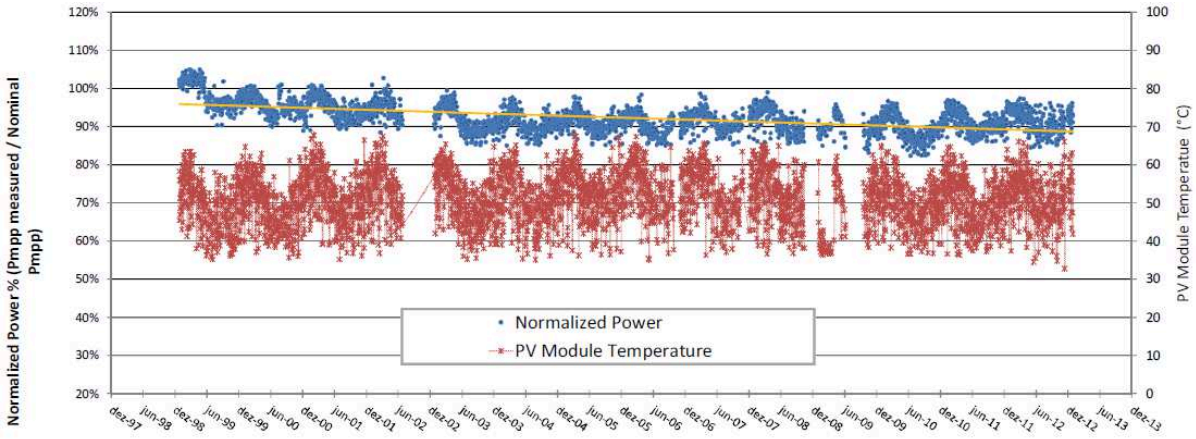

Figure 9 - Evolution of the normalized DC output power of a 2kWp thin-film a-Si PV generator, and average back-of-module temperature over a 15-year period in Brazil (Nascimento, 2013).

2.3.6 Soiling

After irradiance and temperature, soiling may be the third most important environmental factor impacting the performance of PV systems. Soiling can be defined as the reduction of effective solar irradiance reaching the PV device due to absorption and reflection by contaminants present on the surface of a PV module (Sinha *et al.*, 2014).

As seen in Figure 10, when solar irradiance reaches a PV module with a uniform soiling distribution, it is attenuated, reducing the energy received by the device.

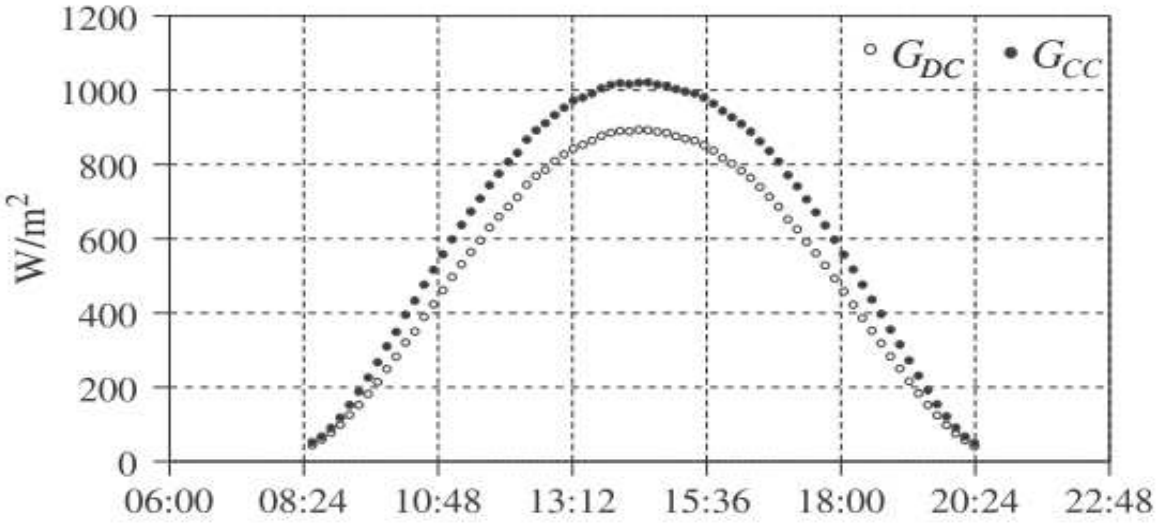

Figure 10 - Solar irradiance levels throughout the day, G_{CC} being the irradiance profile measured by a clean reference solar cell (W/m²) and G_{DC} being the irradiance profile measured by a soiled reference solar cell (W/m²) (Zorrilla-Casanova *et al.*, 2013).

Soiling losses will always be related to the context of the local climatic characteristics (e.g., frequency and intensity of rainfall, humidity, speed and predominant wind direction, bush fire events, soil type in the vicinity of the site) and type of PV module used (framed, glass/glass, coated, textured glass, etc.). However, in places with non-impregnating dirt and suitable PV tilting angle, typically the rain itself cleans the modules and no additional cleaning is required if there is enough rainfall throughout the year. Figure 11 shows the relationship between the losses caused by soiling on a PV cell and rainfall. It can be seen that when there is rain at the site, the losses caused by soiling virtually disappear. Therefore, with regard to the cleaning of PV modules, it is desired that there are no long periods without rain; otherwise, manual cleaning may be necessary.

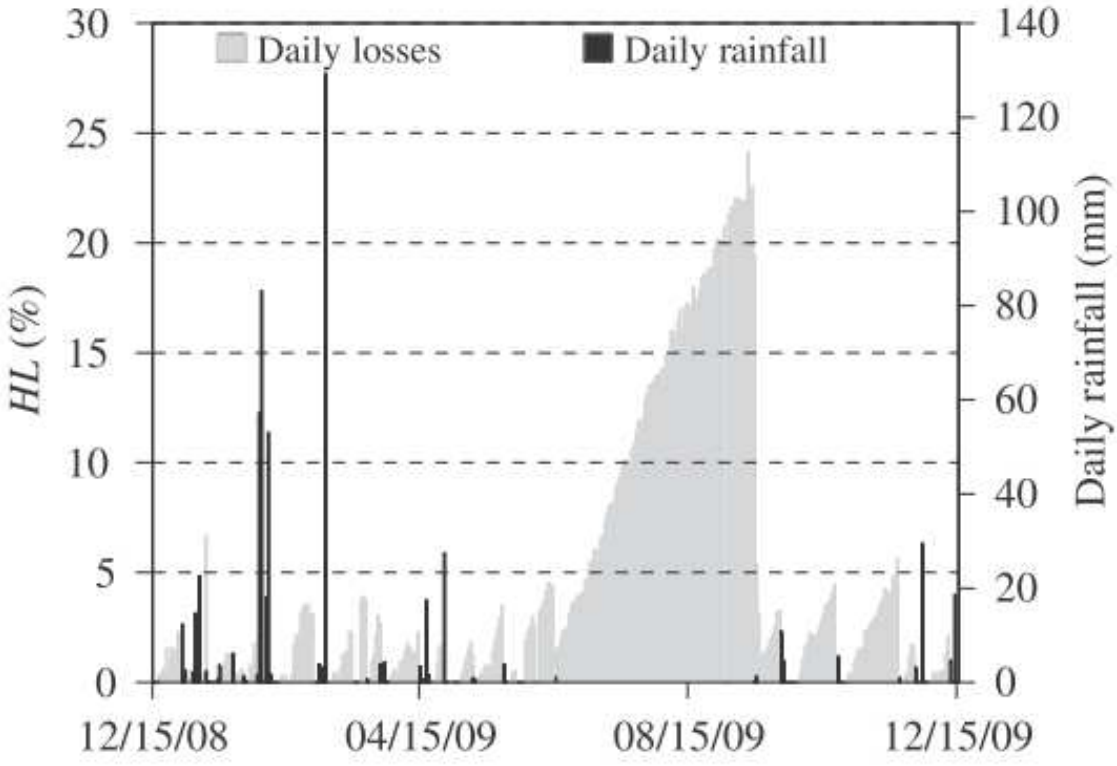

Figure 11 - Relationship between losses caused by soiling and rainfall in a PV cell (Zorrilla-Casanova *et al.*, 2013).

The studies on electrical losses caused by soiling presented in the literature vary mainly from the methodology used for the evaluation (Hickel *et al.*, 2016), the type of PV module and the system location. For large-scale plants using modules with frameless CdTe thin-film technology, soiling losses with rates of approximately 0.03%/day to 0.12%/day can be found for arid regions without soil movement (Figure 12) and arid regions with the presence of agriculture and land movement (Figure 13), respectively.

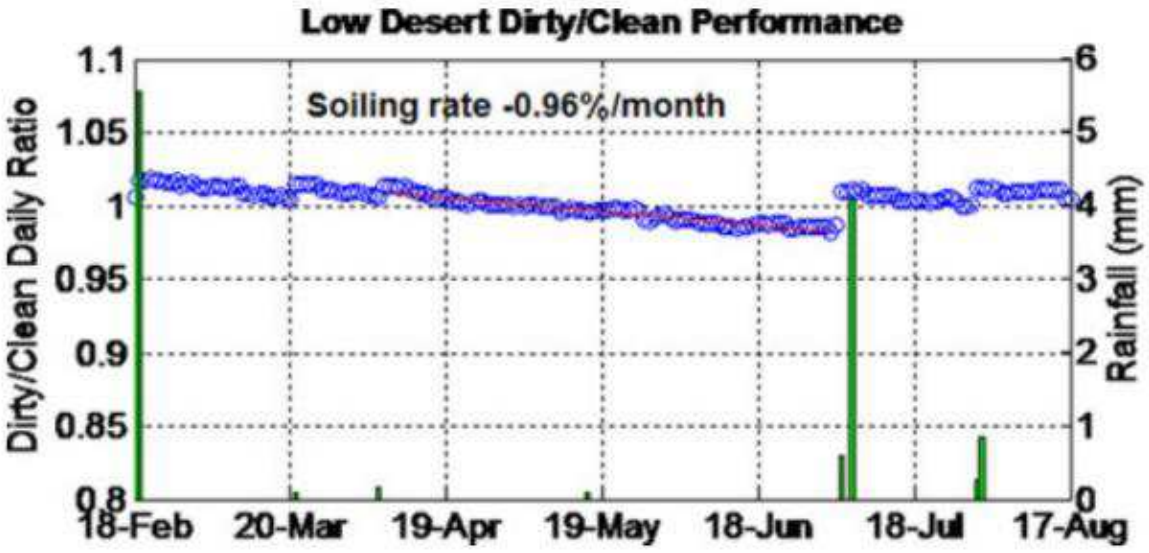

Figure 12 - Losses caused by soiling for arid and desert regions of the United States without land movement (Caron and Littmann, 2013).

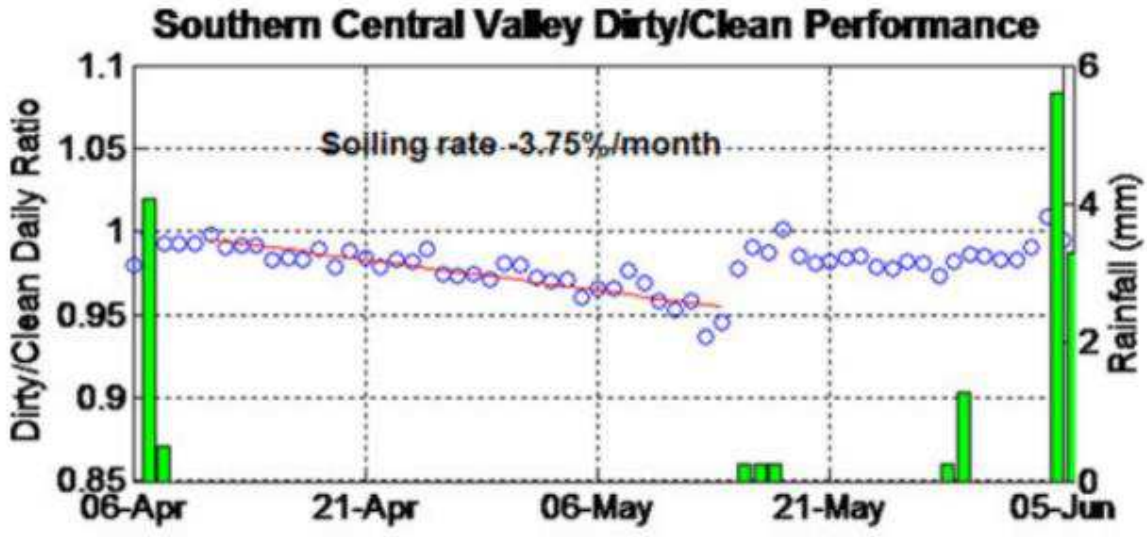

Figure 13 -Losses caused by soiling for arid and desert regions of the United States with presence of agriculture and land movement (Caron and Littmann, 2013).

In another study involving 10 to 200 MWp PV plants using frameless CdTe modules with several soiling monitoring stations, losses with rates of approximately 0.015%/day to 0.15%/day (Figure 14) can be found for PV plants in various climates and regions (Gostein *et al.*, 2014).

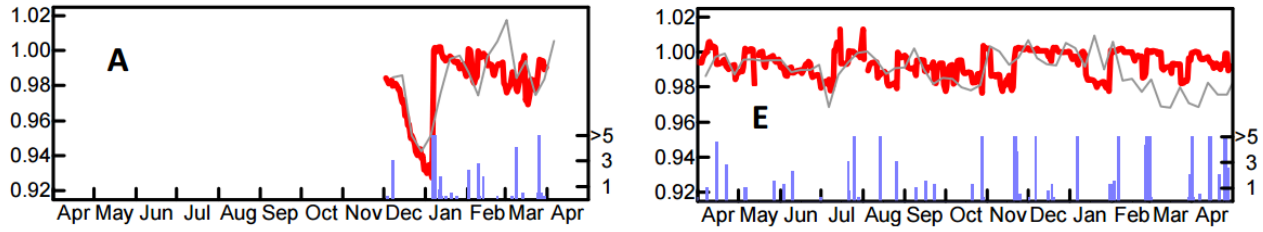

Figure 14 - Soiling losses on CdTe PV plants with performance reduction rates of 0.015%/day (left) and 0.15%/day (right) (Gostein *et al.*, 2014).

In regions with a predominance of strong winds, such as in the vicinity of wind farms where many PV solar plants will coexist in the near future, soiling may often be deposited in a non-uniform way (Hickel *et al.*, 2016; Nascimento *et al.*, 2016), as shown in Figure 15. This non-uniform soiling pattern results not only on irradiance attenuation, but also on electric mismatch, which occurs when the electrical parameters of one solar cell or module are significantly different from those of the remaining devices, considerably increasing soiling losses (Lorenzo *et al.*, 2013).

Figure 15 - Non-uniform soiling distribution profile in PV modules caused by high wind incidence (Hickel *et al.*, 2016).

Figure 16 illustrates the non-uniformity of dust distribution over a PV system and in Figure 17 the electrical impact on the I-V curve of a clean and a soiled module, both connected in series on the same string[1].

[1] String: association of PV modules in series.

Figure 16 - Non-uniformity of soiling in a PV system (Lorenzo *et al.*, 2013).

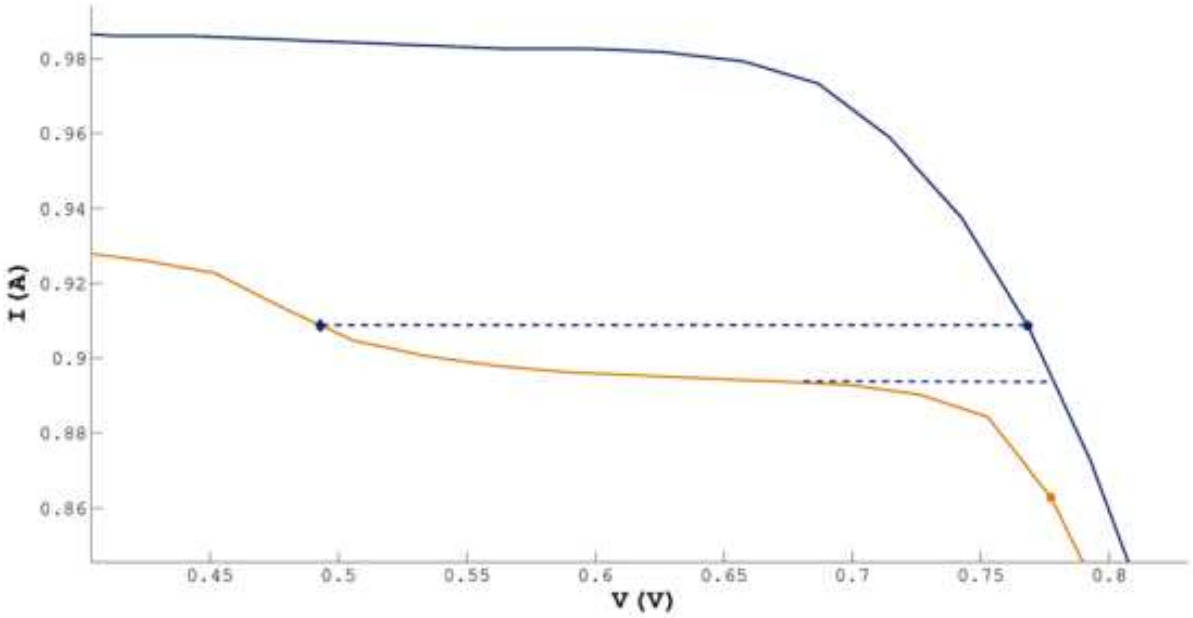

Figure 17 - Impact of non-uniform soiling on the I-V curve of a clean PV module (blue curve) and a soiled PV module (orange curve), both connected in the same string. (Lorenzo *et al.*, 2013).

Soiling also has different impacts depending on the PV technology. Figure 18 shows how electrical losses increase as the dust density is increased on PV cells of different technologies. It can be observed that soiling has a slightly higher impact on a-Si and CdTe. This happens due to these technologies having a higher bandgap, resulting in an effective spectral

response between 300 and 800 nm, in which the spectral transmittance of the front of the modules decreases as a result of dust accumulation, i.e. soiling acts as a blue-filter, impacting more blue-biased PV technologies (Qasem *et al.*, 2012)**.**

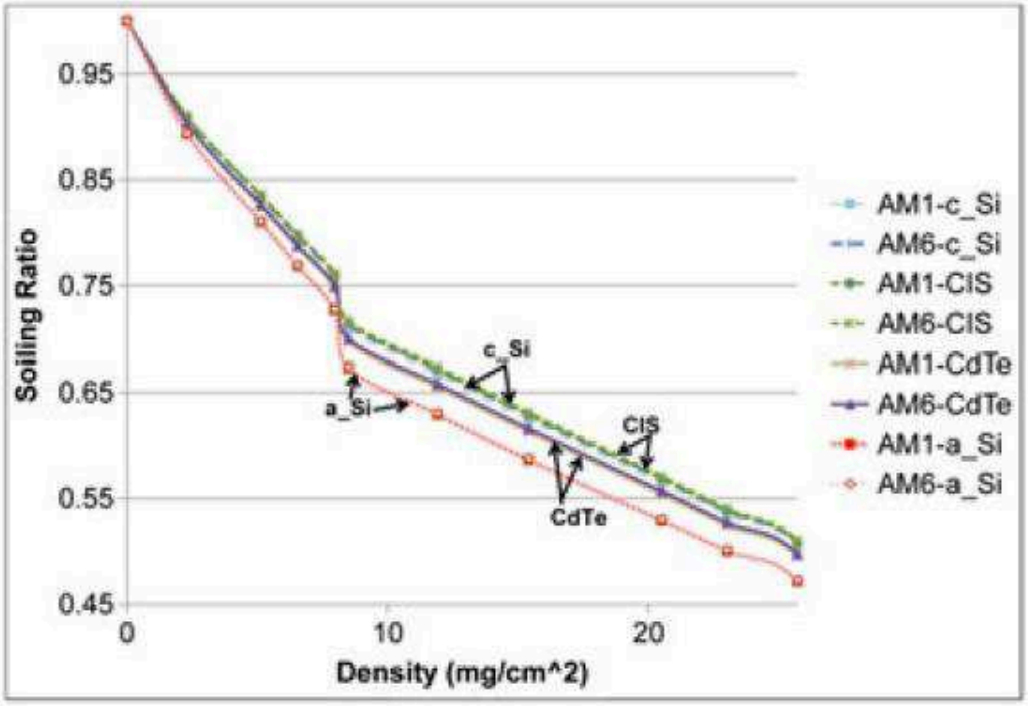

Figure 18 - Impact of soiling density on different PV technologies (Qasem *et al.*, 2012).

2.3.7 Inverter Loading Ratio (ILR)

Due to the negative temperature coefficient of power and the distribution of irradiance over a day, PV systems hardly ever reach their nominal peak power; this effect being even more intense for c-Si when compared to thin-film modules (Virtuani *et al.*, 2010). This physical characteristic of PV devices, associated with the economic optimization of PV systems (i.e., a trend to add more PV modules to the same PV inverter, increasing the PV system ILR), leads to the recommendation to undersize PV inverters. Typical ILR has changed over the years, especially because PV modules are showing pronounced price reductions in recent years. Inverters have also undergone price reductions, but not at the same impressive level as PV modules (Feldman *et al.*, 2015). This has led to a trend in optimizing the ILR - which is defined as the ratio between the DC STC installed power and the AC inverter nominal power, as shown in Equation 2 - in order to obtain a more competitive Levelized Cost of Energy (LCOE) (Kratzenberg *et al.*, 2014).

$$ILR = \frac{P_{DC_{STC}}}{P_{AC}} \qquad (2)$$

Where:

ILR = Inverter Loading Ratio (dimensionless)

$P_{DC_{STC}}$ = Peak STC power of the PV system [kWp]

P_{AC} = Inverter nominal power [kW]

Figure 19 shows the trends in ILR of the 143 utility-scale PV power plants that were won the last PV energy auctions carried out in Brazil (Deschamps and Rüther, 2019). It can be noted that the ILR ranges from 104% up to 162%, averaging 124%.

When sizing a PV plant most PV Softwares use synthetized average hourly irradiance data for simulation, and this typical one-hour resolution often underestimates high irradiance levels (Ransome and Funtan, 2005). In practice, underestimating high irradiance will directly affect systems with relatively high ILRs, since inverter saturation will be reached at a lower irradiance limit.

ILR optimization requires numerical simulation that must be performed by an experienced project designer. For m-Si/c-Si and a-Si technologies, the following ILR are commonly found in the literature.

m-Si/c-Si: 0.9 < ILR <1.66 (Burger and Rüther, 2006; Dias, 2006; Macêdo and Zilles, 2007).
a-Si: 0.9 < ILR < 1.2 (Jiang *et al.*, 2008; Notton *et al.*, 2010; Hussin *et al.*, 2012).

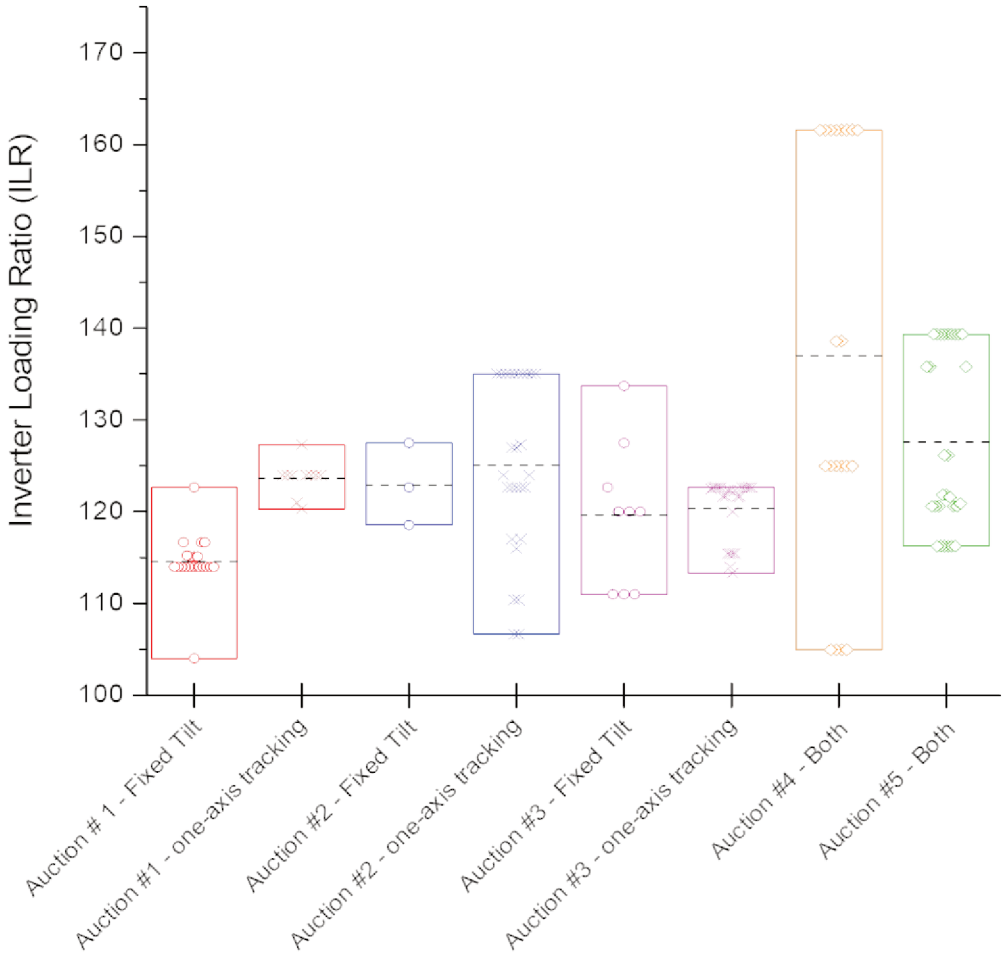

Figure 19 - Inverter Loading Ratios (ILR) for each of the 143 power plants with successful bids in the five PV-dedicated auctions in Brazil, identified in chronological order from 2014 to 2018 by red, blue, magenta, orange and green colors. When possible, the projects are separated into fixed tilt (circles), one axis tracking (X) and both (diamonds). Adapted from (Deschamps and Rüther, 2019).

2.3.8 Losses due to shading

Losses caused by shading can be defined by three components: horizon shading, shading between rows and shading caused by objects.

The horizon shading is caused by mountains, valleys and large, distant objects that are in the solar trajectory, usually diminishing the solar availability at sunrise and sunset.

The shading losses between rows indicate the losses caused by the shading of one row of PV modules on the next one. These electrical losses, caused by the blocking of direct and diffuse irradiation (Duffie and Beckman, 2013) are more pronounced for PV systems that do not have adequate spacing between rows of PV modules, with the most intense losses occurring in winter months when the sun is lower in the sky.

Shading loss of objects is caused by objects near the photovoltaic system, such as trees and buildings, usually affecting only a few areas of the system.

2.3.9 Incidence Angle Modifier (IAM)

The effect of the angle of incidence, also called IAM (incidence angle modifier) corresponds to the reduction of the irradiance that effectively reaches the surface of the PV cell, in relation to irradiance incident normal to the plane, due to the reflections that occur in the glass of the PV module.

There are several analytical models that allow describing the IAM factor. The PVsyst software (PVsyst, 2016) uses the model presented by the ASHRAE 93-77 standard (ASHRAE, 1978). This model, presented in Equation 3, depends on a single parameter to represent the losses by reflection on the glass of a PV module.

$$\boldsymbol{FIAM = 1 - b_0 \cdot \left(\frac{1}{\cos i} - 1\right)} \qquad \textbf{(3)}$$

Where:
i = angle of incidence on the plane;
b_0 = coefficient of modification of the angle of incidence (PVsyst standard $b_0 = 0.05$)

The advantage of the ASHRAE model is the simplicity of a single parameter to determine reflection losses. The PVsyst software uses a standard value for the b_0 coefficient. However, this simplification is often inaccurate to represent PV modules with antireflective coating, textured glass or other strategies designed to allow more light to be captured at sharper angles of incidence. (Dynge, 2013).

2.3.10 Light-Induced Degradation (LID)

Light-induced degradation (LID) is a phenomenon where crystalline silicon cells present an initial degradation of power when exposed to light (Weizer *et al.*, 1979). This effect is typically attributed to a defect in the silicon wafer due to the presence of oxygen ions in the boron dopant (Sopori *et al.*, 2012). This defect affects more intensely mono-crystalline silicon (c-Si) modules when compared to multi-crystalline silicon (m-Si) modules. In an evaluation using c-Si PV modules from 24 manufacturers, a mean power reduction of 1.31% was observed, while the evaluation of m-Si modules from 22 manufacturers showed a mean power reduction of 0.16% (Munoz *et al.*, 2011). PV cell level degradation has been reported in the literature with

similar results: with degradation of approximately 0.5% and 0.1% for c-Si and m-Si, respectively (Sopori *et al.*, 2012).

2.3.11 Potential-Induced Degradation (PID)

Potential Induced Degradation (PID) is a phenomenon that mainly affects crystalline silicon PV modules, leading to a gradual reduction of power of the PV module. This characteristic is associated to the presence of sodium ions on the PV module front glass and the migration of these ions due to the electric field imposed by the inverter of the PV system in high voltage PV series (Schmidt, 2007; Pingel *et al.*, 2010). In humid regions with high PV module operating temperatures, this characteristic can be accentuated by the ingress of moisture on the PV module, increasing leakage currents (Hoffmann and Koehl, 2014). In order to test the stability of the PV modules under these conditions, manufacturers typically submit their PV modules to electrical tests to ensure the device's resistance to the PID effect. PV modules with a power reduction of less than 5% are considered to be resistant to PID (IEC-62804.1, 2015).

2.3.12 PV module mismatch losses

The electrical mismatch between identical PV modules is one of the main forms of energy loss in the series/parallel connection of PV systems. These losses occur due to the association in series/parallel of solar cells or modules with different electrical parameters. Cells or modules do not operate at their individual maximum power point when they are associated in series or parallel, operating therefore at a combined maximum power point of the cell or module of lower performance, which results in a decrease in overall system performance. In this case, the performance of the system occurs according to the association of cells or modules of lower power or current (Forniés *et al.*, 2013).

2.3.13 Electrical losses in DC and AC wiring

The electrical losses in the electric wiring are caused by the intrinsic resistance of the material, length, and cross-section of the wiring. These losses, usually associated with the voltage drop and Joule effect, are calculated so that the wiring has sufficient ampacity to carry the circuit currents and admitting an acceptable voltage drop (typically in the order of 1.5% or less).

2.4 PERFORMANCE MEASUREMENT

2.4.1 Performance Ratio (PR)

The performance of a PV system is typically measured by the Performance Ratio (PR), which is defined as the ratio of the actual system performance to the maximum possible theoretical performance. This relationship is a parameter to evaluate the electric power generation of a given PV system, considering the nominal power of the system under operating conditions and all losses involved, such as losses due to temperature, soiling, mismatching, inverter losses, among others. Equation 4 presents the equation used to calculate PR.

$$\boldsymbol{PR_t = \frac{E_t}{P_o}\frac{G}{H_t}} \qquad \textbf{(4)}$$

Where:

t = period considered;

PR_t= performance ratio [%] for period "t";

E_t = AC energy generated [kWh] by PV system for period "t";

P_o = total nominal power of the photovoltaic system [kWp];

G = reference irradiance [1 kW/m²];

H_t = irradiation on the plane-of-array (POA) for the period "t" [kWh/m²], calculated from the irradiance values [W/m²].

Due to improvements in the quality and performance of PV modules and inverters in the last decade, PR values have been increasing systematically, reaching values up to 90% (Figure 20) for regions with mild climate (e.g. Germany), while in Brazil and in tropical climates PR values of up to 85% are expected (Nobre, 2015; Nascimento *et al.*, 2016), mostly due to the higher operating temperatures prevailing at warm and sunny sites.

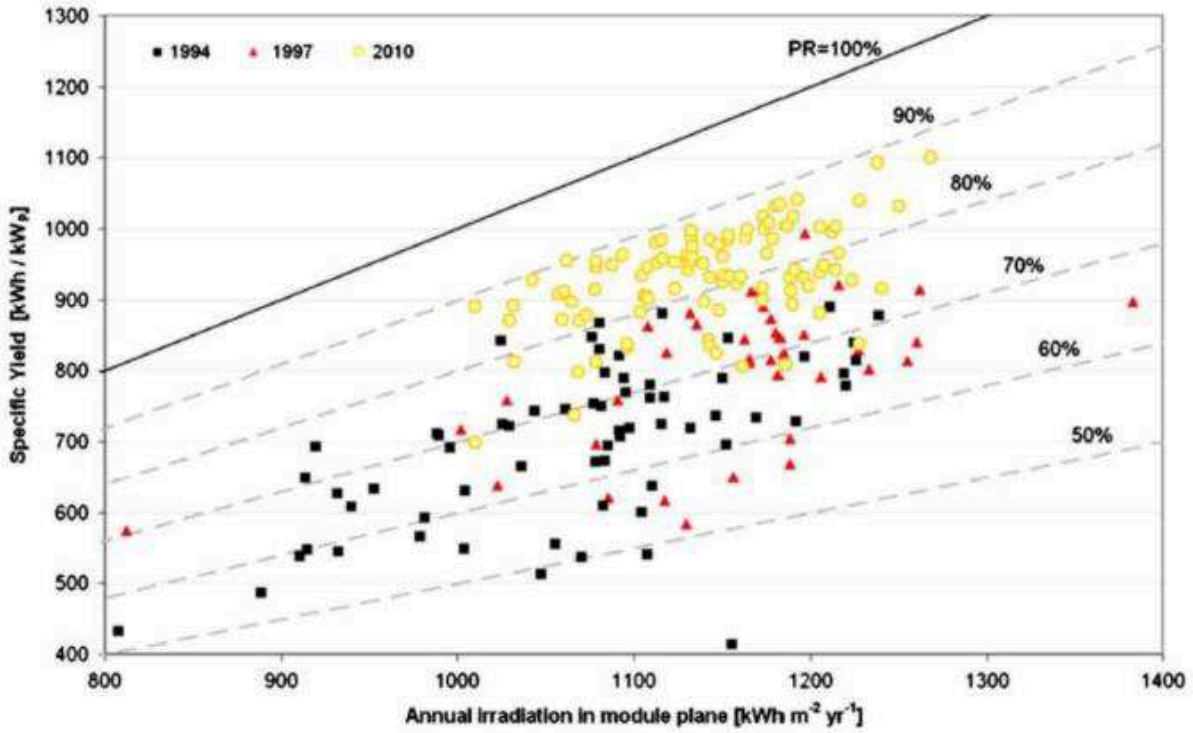

Figure 20 - PR values for PV systems installed between 1994 and 2010 in Germany, during the 1000 Roofs Programme (Reich *et al.*, 2012).

2.4.2 Corrected Performance Ratio

Despite being the most widely used metric to evaluate the performance of a PV system, PR values require caution on their interpretation, since this metric is strongly influenced by environmental characteristics (e.g., temperature, solar spectrum, irradiance distribution, soiling) of the place where the system is installed, with temperature being the primary influence component (Sinha *et al.*, 2014). Figure 21 presents the annual PR of a 2 kWp power system installed in Florianópolis-SC for the period between 1998 and 2012. Excluding the first year of operation - in which the PV modules were still experiencing the initial degradation process (Rüther *et al.*, 2008) - and years 2000 and 2008 that presented system failure - already considered in the displayed data - the PV system presented PR values ranging approximately from 72 to 80%, with an average PR of 76%. As already discussed, this fluctuation of PR values is a consequence of environmental variations during the operation of the PV system.

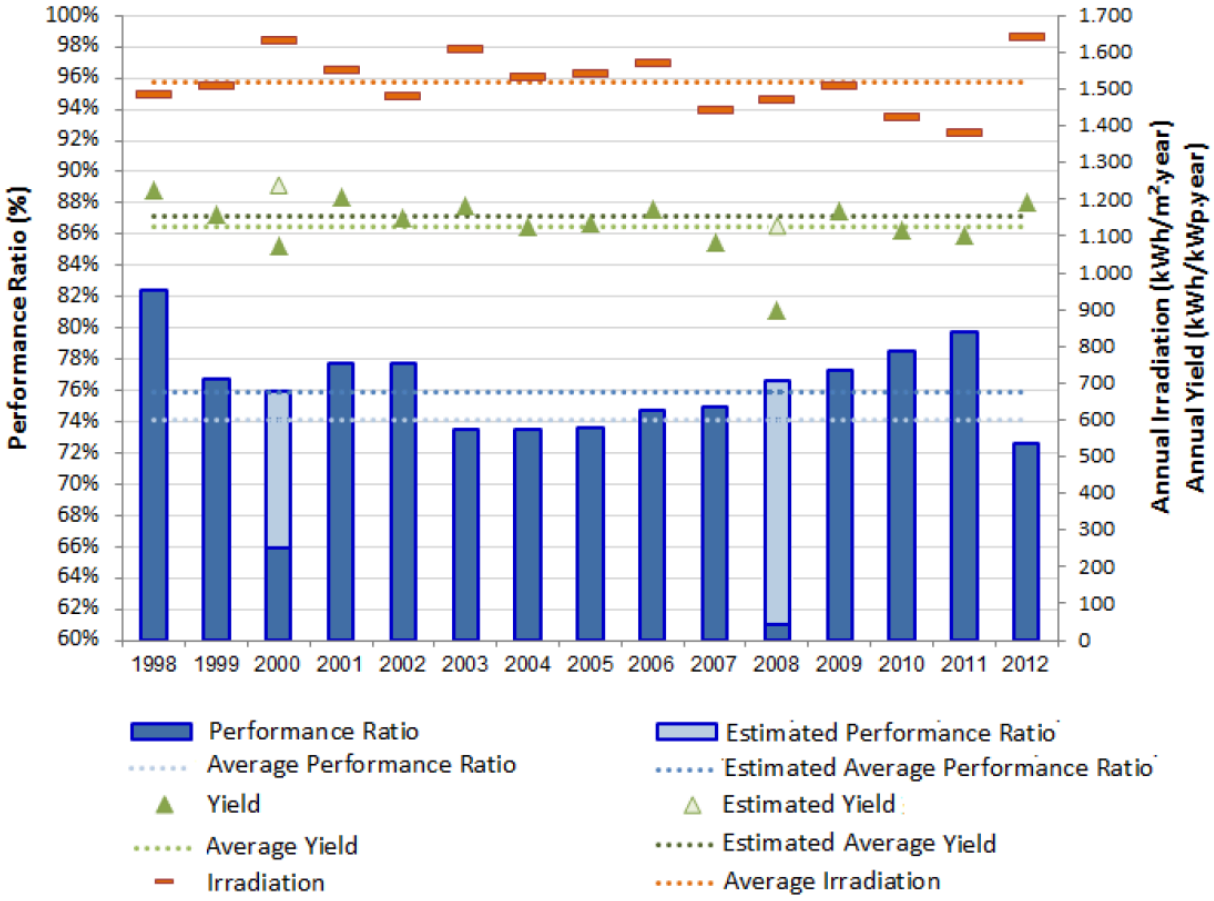

Figure 21 - PV system annual PR (%) and total annual energy yield (kWh/kWp/year) for a 2kWp, thin-film a-Si PV generator over a 15-year period, together with the total annual solar irradiation at the site (kWh/m²/year) (Nascimento, 2013).

Because temperature has such a strong influence on the performance of a PV system, other evaluation metrics are used to compensate this climatic characteristic. One of these metrics is called Temperature Corrected PR or Weather Corrected PR (Dierauf *et al.*, 2013). Equation 5 shows the formula used to correct PR in order to limit environmental influences in system performance analysis.

$$PR_{corr_t} = \frac{E_t}{P_o}\frac{G}{H_t}\frac{1}{1+\gamma\left(Tcell_{typ_{avg}} - Tcell_t\right)} \qquad (5)$$

Where:

t = time period considered;

$PRcorr_t$ = corrected performance ratio [%] for period "t";

E_t = AC energy generated [kWh] in the time period "t";

γ = temperature coefficient for Pmpp (maximum power point);

P_o = total nominal power of the photovoltaic system [kWp];

G = reference irradiance [1 kW/m^2];

H_t= irradiation on the plane of the modules for the period "t" [kWh/m²], calculated from the irradiance values [W/m²];

$Tcell_t$ = temperature of the PV cell for time period "t";

$Tcelltyp_{avg}$ = temperature of the PV cell weighted by irradiance considering the typical climate file of the region used during simulation.

Figure 22 presents an analysis of a PV system evaluated using the conventional PR metric and a comparison with the temperature corrected PR. It is possible to identify a more linear and predictable profile for temperature-corrected PR analysis when compared to conventional PR.

Despite providing more controlled values of PR due to the temperature compensation, this metric was designed to compare the actual performance of a system to that predicted in its simulation, requiring for that purpose the climatic file that gave origin to the simulation of the system.

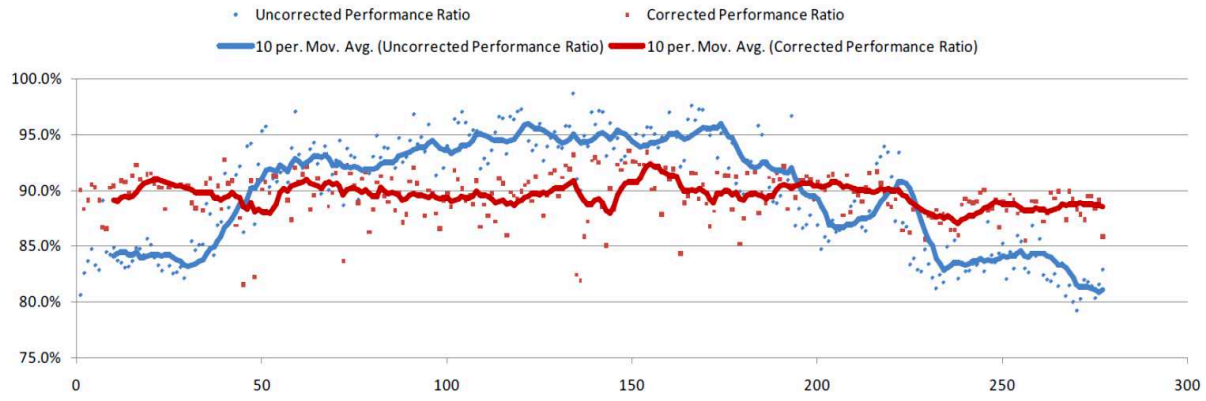

Figure 22 - PR *vs.* PR corrected by temperature for 275 days of analysis (Dierauf *et al.*, 2013).

Another metric commonly used for performance analysis of PV systems that normalizes not only the irradiance for STC conditions, but also the low light performance response is PR_{STC}, shown in Equation 6, adapted from Martínez-Moreno *et al.* (2014).

$$PR_{STC} = \frac{E_t\, G}{P_o H_t [(1+\gamma(Tcell_t - Tstc)]\left[1+cLn\frac{G_t}{G}\right]} \qquad (6)$$

Where:

t = period considered;

PR_{STC} = corrected performance ratio [%] for period "t";

E_t = AC energy generated [kWh] by the PV system for the period "t";

γ = temperature coefficient for Pmpp;

P_o = total nominal power of the photovoltaic system [kWp];

G = reference irradiance [1 kW/m^2];

G_t = average irradiance for the period "t" [W/m^2];

H_t = POA irradiation for the period "t" [kWh/m²], calculated from the values of irradiance [W/m²];

c = the c value is derived from the ratio between the module efficiencies at 200 W/m² and at 1000 W/m², which must also be given by the manufacturer. For crystalline silicon modules, this efficiency ratio is often $\frac{\eta_{200W/m^2}}{\eta_{1000W/m^2}} = 0.95$, which corresponds to c = 0.031.

Other authors, such as Ishii *et al.* (2011) take into account not only temperature, but also spectral mismatch when correcting PR. Equation 7 presents the proposed normalization, where TF is the thermal factor, for temperature correction (Equation 8) and SF is the spectral factor, as previously defined in Equation 1.

$$\boldsymbol{PRcorr_t = \frac{E_t}{P_o}\frac{G}{H_t} \times TF \times \frac{1}{SF}} \qquad \textbf{(7)}$$

$$\boldsymbol{TF = \frac{1}{1 + \gamma(Tcell_t - Tstc)}} \qquad \textbf{(8)}$$

2.5 OVERIRRADIANCE IMPACTS ON PV POWER PLANTS

Overirradiance events have been observed and reported since the 1990s, mainly directed to the ultraviolet (UV) region of the solar radiation spectrum because of its effects on human health and for its scientific relevance (Mims III and Frederick, 1994; Estupinan *et al.*, 1996; Parisi *et al.*, 2003; Parisi and Downs, 2004; Gallagher and Lee, 2006). For PV applications, the occurrence of overirradiance events in global horizontal (GHI) and global tilted irradiance (GTI) in the visible and near-infrared regions (VIS-NIR, 400-2500 nm) has only been studied more recently (Gu *et al.*, 2001; Walker, 2001; Pfister *et al.*, 2003; Tomson and Tamm, 2006; Emck and Richter, 2008; Clifford W. Hansen, 2010; Piacentini *et al.*, 2011; Luoma *et al.*, 2012; Yordanov *et al.*, 2013; Almeida *et al.*, 2014; Piedehierro *et al.*, 2014; Tapakis and Charalambides, 2014; Yordanov *et al.*, 2014; Yordanov *et al.*, 2015; Andrade and Tiba, 2016; Inman *et al.*, 2016; Gueymard, 2017b; a; Jazayeri *et al.*, 2017; McCormick and Suehrcke, 2018; Avila *et al.*, 2019).

Overirradiance is a phenomenon characterized by the short-term enhancement of solar irradiance measured on the Earth's surface that happens under broken cloud fields, when irradiance is significantly increased (Pfister *et al.*, 2003). During overirradiance events, a visible cloud brightening effect (commonly called cloud-enhancement or cloud-edge-effect) takes place. These overirradiance events are observed for all wavelengths in global horizontal and global tilted irradiance.

The extraterrestrial solar irradiance is the radiation incident at the top of the atmosphere, on a surface plane placed perpendicular to the solar rays. At the average Sun-Earth distance, the extraterrestrial irradiance is called solar constant (G_0). Although not strictly constant, in this work the value of 1367 W/m^2 was adopted for G_0, which is the annual average amount of solar power flux (irradiance, in W/m^2) that passes through the mean Sun-Earth orbit (Piacentini *et al.*, 2003; Piacentini *et al.*, 2011; Yordanov *et al.*, 2014).

During the path to the Earth's surface, solar irradiance is attenuated by the atmosphere's components. However, due to physical interactions between solar radiation and particles present in the atmosphere under certain conditions, scattering and other effects take place and irradiance values higher than the global horizontal extraterrestrial values can be measured even near sea level (Suehrcke and McCormick, 1988; Yordanov *et al.*, 2015; Andrade and Tiba, 2016; Gueymard, 2017a).

Absorption and scattering are processes in which electromagnetic radiation interacts with the atmosphere. In the absorption process, energy is removed from incident radiation and converted into some other form of energy, such as heat. Absorption can be due to molecules or

aerosols in the atmosphere. Scattering is a physical process by which a particle in the path of an electromagnetic wave, at any wavelength and covering the entire electromagnetic spectrum, continuously extracts energy from the incident wave and re-radiates that energy in all directions. Scattering processes do not remove energy from incident radiation but change its original direction of propagation (Iqbal, 1983). The particle could be considered as a point source of the scattered energy, called diffuse radiation. A solution of Maxwell's electromagnetic wave equation in spherical polar coordinates gives the theoretical energy scattered by spherical particles. A particular solution, derived by Lord Rayleigh (*Rayleigh's Theory*), is applied when the particle is spherical and much smaller than the wavelength of incident radiation, which is useful in studying the scattering of solar radiation by air molecules (*Rayleigh's Scattering*). Another solution, derived by Gustav Mie (*Mie Theory*), is applied when the particle size is of the same order of magnitude or higher than the wavelength of the incident radiation, which is used in scattering by water vapor molecules and dust particles (*Mie Scattering*) (Iqbal, 1983; Liou, 2002; Träger, 2012). Strong forward Mie scattering within low optical-depth clouds could be the main factor for overirradiance events, as recent studies suggest (Thuillier *et al.*, 2013; Yordanov *et al.*, 2013; Yordanov, 2015; Pecenak *et al.*, 2016).

Frequent overirradiance events, lasting as long as several minutes, could cause important impacts and deleterious consequences, especially on solar utility-scale PV power plants (Rüther *et al.*, 2017). Since electrical current in PV modules is roughly proportional to POA incident irradiance and is not capped at the STC-rated values, peak currents under natural sunlight can be much higher than those rated at STC. These factors could be an important issue affecting the performance of PV systems in the field, because of their consequences on components such as fuses and inverters (Burger and Rüther, 2006; Chen *et al.*, 2010; Luoma *et al.*, 2012; Rüther *et al.*, 2017).

The rapid passage of clouds in front of, or around the Sun results in large irradiance ramps with different slopes (Inman *et al.*, 2016). These variations, besides directly affecting the power grid stability, could have important impacts on inverter maximum power point tracking (MPPT) efficiency (Piotrowicz and Marańda, 2013). The effect of the intermittency of solar radiation could also affect the performance of off-grid PV and grid-connected systems with battery storage. Variations in solar radiation can cause significant fluctuations in system currents, directly affecting the performance of diesel generators in hybrid off-grid systems and battery currents for battery storage systems. These fluctuations can lead to instability of systems and reduction of battery lifetimes (McCormick and Suehrcke, 2018).

3 MATERIALS AND METHODS

This section aims to present the materials and methods used in order to allowing for the scientific objectives of the thesis to be achieved. Most of the experimental work described in this thesis was carried out at the Fotovoltaica/UFSC solar energy laboratory (www.fotovoltaica.ufsc.br) and at the many experimental sites distributed over the Brazilian National territory in which Fotovoltaica/UFSC coordinates R&D projects together with electricity companies under the Brazilian Regulatory Agency ANEEL's R&D program. Most of the hardware described and used throughout the development of this thesis either belongs to Fotovoltaica/UFSC or to these industrial partners and was acquired with public funds and research grants awarded by the Brazilian National Research Council CNPq, the Brazilian Ministry of Science and Technology MCT or the ANEEL R&D program.

3.1 EXPERIMENTAL SETUP

Eight identical, fully-monitored, 54 kWp PV Evaluation Sites (ESs), each using six different, commercially-available PV technologies (mono- and multi-crystalline silicon, and the thin-film PV technologies CdTe, CIGS, a-Si, and a-Si/µc-Si), were installed in eight different regions in Brazil between 2013 and 2015. The objective of this setup was to evaluate the performance of different PV technologies in various climatic regions in the country. Figure 23 shows the map of Brazil and the location of the eight ESs, while Figure 24 shows an aerial view of one of the eight ES (ES # Capivari de Baixo-SC).

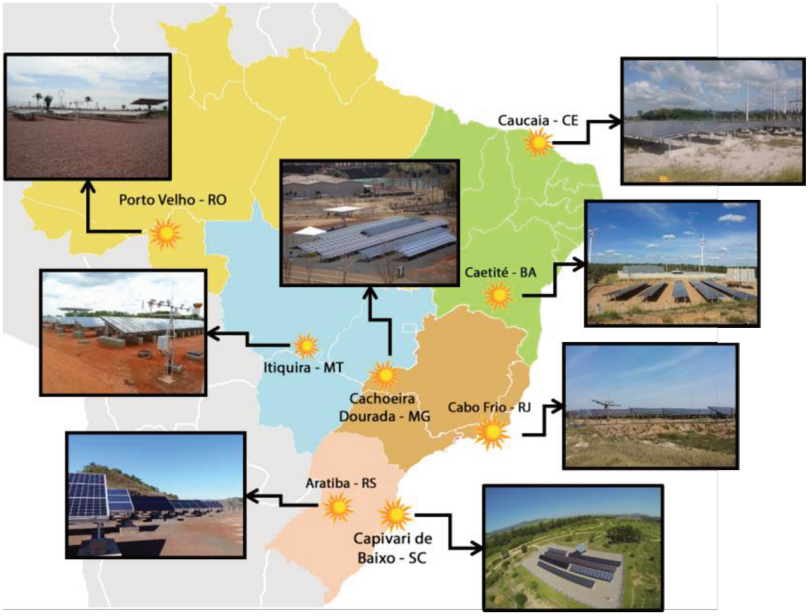

Figure 23 - General location in the 8.5 million km² Brazilian territory of the eight identical R&D ESs, located between 3°S and 28°S, each with approximately 54 kW_p of fixed, latitude-tilt PV.

The main electrical characteristics of the PV modules employed at the ESs are shown in Table 2, while Table 3 describes the six fixed-tilt systems at each ES. The six latitude-tilted systems were sized to have similar total power, inverter loading ratio (ILR), and operational voltage in order to reduce influences other than the module performance. Isolated inverters were used for technologies requiring function earthing (active polarity to be earthed either directly or via a resistor).

Table 2 - Main electrical characteristics of the six commercially-available PV module technologies employed at the eight identical ESs, sorted from most to least efficient (all 2011-2013 vintage PV modules).

PV Technology	Nominal Power [W_p]	Efficiency [%]	Open-Circuit Voltage* [V]	Short-Circuit Current* [A]
c-Si (Yingli, 2012)	260	15.9	38.6	8.91
m-Si (Hanwha, 2011)	235	12.9	36.8	8.44
CIGS (Avancis, 2011)	120	11.2	58.5	3.21
CdTe (First-Solar, 2007)	280	11.1	94	1.23
a-Si/µc-Si (Dupont, 2012)	142	9.1	156	1.43
a-Si (Dupont, 2011)	100	6.4	97	1.77

* @ STC (1000W/m² irradiance, AM 1.5 spectrum, and module temperature of 25°C).

Figure 24 - Aerial view of one (ES # Capivari de Baixo-SC, 28ºS, 48ºW) of the eight identical R&D ESs, with approximately 54 kWp of fixed, latitude-tilt PV.

The eight ESs are identical, with the only difference being the module tilt angle at each site, which corresponds to the site's local latitude. A complete list of the ESs, their exact coordinates, commissioning date and climate classification according to Köppen-Geiger (Peel *et al.*, 2007; Alvares, 2013) can be found in Table 4.

The ESs are monitored continuously, with irradiance, temperature (ambient and back-of-module), and electrical parameters measured and logged at one-second intervals. High-quality, research-grade and state-of-the-art irradiance, electrical parameters, temperature measurement devices, and data loggers were used.

Table 3 - Main characteristics of the six PV generators installed at each of the eight identical ESs spread over the 8.5 million km^2 Brazilian territory.

PV Technology	Number of PV Modules	PV Modules in Series	Number of Strings	Total Power [kW_p]	Inverter Power	DC to AC Inverter Load Ratio [%]	DC Voltage at 50°C [V]
c-Si	34	17	2	8.84	10.0 TL	88	480
m-Si	38	19	2	8.93	10.0 TL	89	509
CIGS	75	9 and 7 (2 MPPTs)	6 and 3 (2 MPPTs)	8.97	10.0 (I)	88	332 and 291 (2 MPPTs)
CdTe	112	8	14	8.96	10.0 TL	90	558
a-Si/μc-Si	63	3	21	8.95	10.0 (I)	89	324
a-Si	90	5	18	9.00	10.0 (I)	90	333

Table 4 - Coordinates, commissioning date and climate classification according to Köppen-Geiger of the eight identical evaluation sites (ESs) spread over the 8.5 million km² Brazilian Territory (Cfa: Humid subtropical climate; Aw: Tropical wet-dry climate; Am: Tropical monsoon climate; As: Tropical dry summer).

City – State	Coordinates	Commissioning Date [dd/mm/yyyy]	Köppen-Geiger Climate Classification
Capivari de Baixo – SC	28°27‘ S 48°57‘ W	17/08/2013	Cfa
Aratiba – RS	27°17‘ S 52°23‘ W	04/10/2013	Cfa
Itiquira – MT	17°36‘ S 54°55‘ W	22/11/2013	Aw
Porto Velho – RO	09°17‘ S 64°33‘ W	18/11/2013	Am
Caetité – BA	14°11‘ S 42°30‘ W	28/08/2015	Aw
Caucaia – CE	03°41‘ S 38°52‘ W	23/01/2015	Aw
Cachoeira Dourada – MG	18°30‘ S 49°29‘ W	16/08/2014	Aw
Cabo Frio – RJ	22°49‘ S 41°59‘ W	17/10/2015	Aw

Figure 25 shows the solar monitoring station installed at the Capivari de Baixo-SC ES. This same identical setup is repeated for each of the eight ESs. The sensors installed at each solar monitoring station are listed in Table 5, along with their measurements and the reference number from Figure 25.

Measuring environmental and PV operational electrical parameters at the individual PV string level, and at one-second time resolution at all the eight sites, leads to very large amounts of data, which have to be verified and qualified every day. This high time-resolution was chosen in order to enable the detection and evaluation of fast-changing environmental conditions (particularly irradiance, which was measured with SMP11 and/or CMP11 Kipp and Zonen pyranometers and IMT reference cells), and their influence on the response and performance of PV devices operating in a utility-scale PV power plant environment. The decision of measuring all parameters at the one-second time resolution was made in the context of previous experience with solar irradiance variations in a sunbelt region, in contrast with that measured in higher latitude climates (Piacentini *et al.*, 2011; Almeida *et al.*, 2014; Yordanov *et al.*, 2014; Andrade and Tiba, 2016), and the effects of a larger fraction of solar energy availability at higher irradiances on PV generator inverter sizing (Burger and Rüther, 2006; Luoma *et al.*, 2012; Kratzenberg *et al.*, 2014).

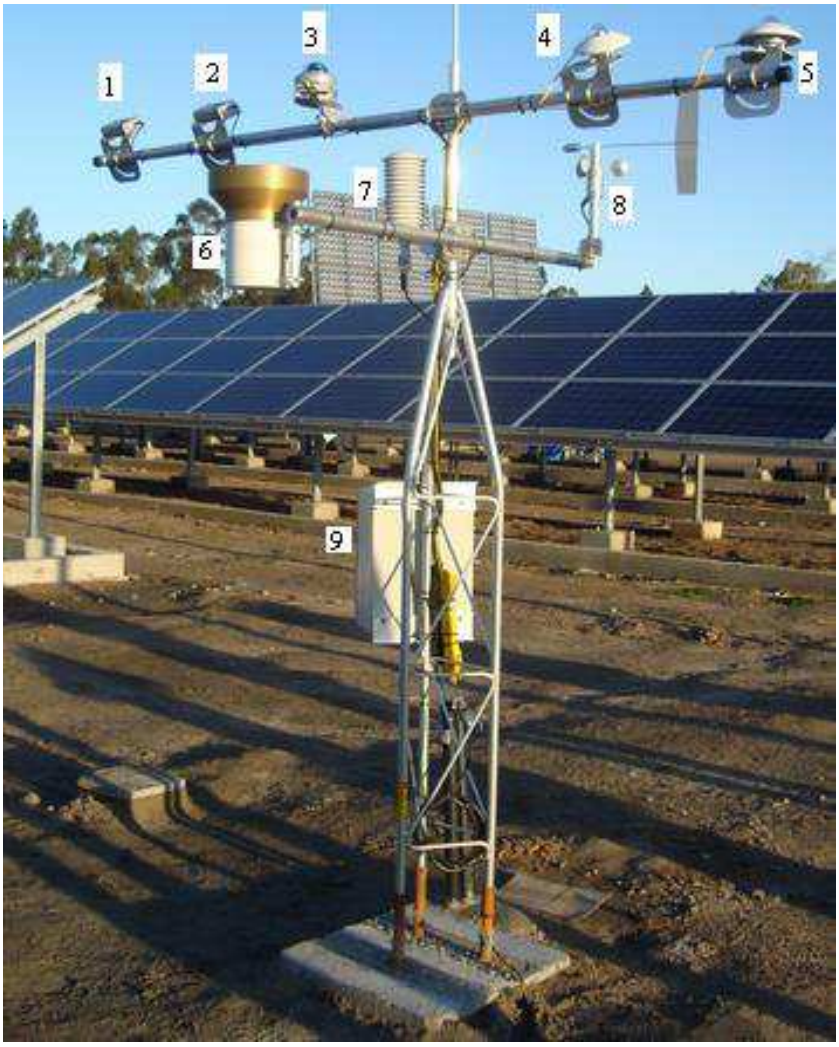

Figure 25 - Solar monitoring station installed at the Capivari de Baixo-SC ES, with identical sensors installed in all eight ESs and detailed in Table 5.

Table 5 - List of sensors and variables measured at the eight identical solar monitoring stations (SMS).

Reference in Figure 25	Sensor type	Brand	Model	Quantity
1	Reference Cell	Mencke und Tegtmeyer	Si-02-Pt100	Global Tilted Irradiance (clean)
2	Reference Cell	Mencke und Tegtmeyer	Si-02-Pt100	Global Tilted Irradiance (soiled)
3	Pyranometer	Delta	SPN1	Global, Diffuse and Direct Horizontal Irradiance
4	Pyranometer	Kipp & Zonen	SMP11 or CMP11	Global Tilted Irradiance
5	Pyranometer	Kipp & Zonen	SMP11 or CMP11	Global Horizontal Irradiance
6	Pluviometer	Texas Electronics	TE525MM-L15	Rainfall
7	Temperature and Relative Humidity	Vaisala	HMP155C-L12	Ambient Temperature and Relative Humidity
8	Anemometer	Met One	034B-L34	Wind Speed and Direction
9 (enclosed)	Barometer	Vaisala	CS106	Local Atmospheric Pressure

3.2 PERFORMANCE EVALUATION

As previously mentioned, the operational performance of a PV system is typically assessed by the performance coefficient (Performance Ratio - PR), which is defined as the relationship between the actual system performance and the maximum possible theoretical performance. PR is a widely used metric because it allows comparing PV systems installed in different locations and/or orientations, and evaluates the generation of electric power taking into account the actual power of the system under operating conditions. In this work, PR was considered the best metric to assess the losses of the evaluated PV systems in different ESs. The monthly PR was calculated according to Equation (4).

The global plane-of-array (POA) irradiation data used was obtained from SMP11 and/or CMP11 Kipp & Zonen pyranometers installed at the local solar monitoring stations with the same tilt as the PV systems at each specific location. The maximum uncertainty of these secondary standard pyranometers in the hourly radiation totals is about 3%. The solar monitoring station takes measurements at a one-second time interval, and the data used for the analysis was the one-minute average of these measurements. The irradiance data collected by the solar monitoring stations were treated, flagged and filtered according to the algorithm proposed by the Baseline Surface Radiation Network (BSRN) (Long and Dutton, 2002).

The AC power output of the PV systems is recorded every minute by the inverters and independent energy meters (Carlo Gavazzi WM5-96), and this data are collected by a data

logger installed at each ES. The precision of these power measurements is respectively 2% and 0.5%, according to the inverters' and energy meters' manufacturers.

The data from all the PV systems and the pyranometers at each ES were cross-checked, and only data points where all PV systems were operating simultaneously, and for which there is irradiance data available, were used. The data were then integrated into daily values, and only days with more than 500 data points (500 minutes) were considered valid. The daily values were then integrated into monthly values. With monthly values of energy and irradiation, the monthly PR was then calculated, and values were only considered representative of the full month when more than half of the days in the respective month were valid. The final performance result is the average of all valid month's PRs. The maximum overall uncertainty of the analysis is estimated to be around 3.6%.

3.3 FIELD MEASURING INSTRUMENTS

A Sony Cyber-shot DSC-WX9 16.2 megapixel digital camera with an sCMOS sensor was used to obtain the Electroluminescence (EL) images during field analysis. The conventional camera was adapted removing the infrared filter of the camera, allowing the visualization of the luminescence in the range of the crystalline silicon spectrum. The evaluation of EL images used in this thesis uses the general methodologies presented in IEA (2014), using a polarization current of 100% of Isc, since the technical specification IEC 60904-13 (2018) - Photovoltaic Devices Part 13: Electroluminescence of PV Modules, was only published by the end of 2018, seeking to standardize the EL tests by injecting certain current values (multiples of Isc), to evaluate different characteristics and defects of the junction.

The equipment used for the I-V curve measurements at the field was the PV Engineering - PVPM 1040X I-V curve tracer. The instrument performs I-V curve measurement using 4-wire topology, avoiding systematic errors in the measurement of voltage due to the resistance of the cables. For solar irradiance data at the time of measurements, a Mencke & Tegtmeyer polycrystalline reference cell with an accuracy of 2.5% ± 5W/m² of the measured value, was connected to the I-V curve tracer and positioned in the same plane as the PV module evaluated. For PV module temperature measurement during the measurements, a PT100 sensor, accuracy: 0.20% ± 0.3 °C was used. The measuring process for PV modules is defined for STC, which are not reproduced simultaneously in the field, requiring the normalization of the measured values (IEC-60891, 2009). The combined uncertainty of the I-V measurements, reference cell, module temperature and normalization of measurements is ± 5%.

3.4 DATA ASSESSMENT OF OVERIRRADIANCE EVENTS

For the evaluation of the overirradiance events and their impacts on PV performance, not all the sensors of all ESs could be used, due to data acquisition problems with one-second data resolution. Therefore, for these analyses, both the # Porto Velho-RO and the # Capivari de Baixo-SC ESs were withdrawn and a new site at Brotas de Macaúbas-BA Solar Monitoring Site (SMS) was inserted in their place, thus totaling seven SMS for this particular focus of the thesis.

Figure 26 shows the general view (a) of the seven SMS installed over the Brazilian territory, and an enlarged view (b) of the North and Northeast regions, in which most of the utility-scale PV power plants are being installed in Brazil since dedicated PV energy auctions started in 2014 in the country.

Table 6 shows the location, altitude, geographic coordinates, climate classification, and the measurement period of the seven SMS. Global horizontal irradiance (GHI) data were obtained using Kipp & Zonen (CMP11 or SMP11) and Delta-T (SPN1) pyranometers installed horizontally.

The tilted (plane-of-array, or G_{POA}) irradiance data were obtained from IMT reference cells installed at the same tilt angle as the PV arrays, coincident with the local latitude at each specific SMS location. The irradiance data collected were treated, flagged and filtered according to the algorithm proposed by the Baseline Surface Radiation Network (BSRN) (Long and Shi, 2008).

As previously mentioned, overirradiance is a phenomenon characterized by short-term enhancements of the solar irradiance, that is significantly increased compared to equivalent cloud-free, clear sky conditions and extraterrestrial irradiance expected values. In this work, by definition global horizontal solar overirradiance events are considered always when measured one-second values are higher than the extraterrestrial global horizontal irradiance ($Kt > 1$) (Gueymard, 2017a). For quantifying the impact of overirradiance events on PV systems, this work considers measured one-second values higher than G_0.

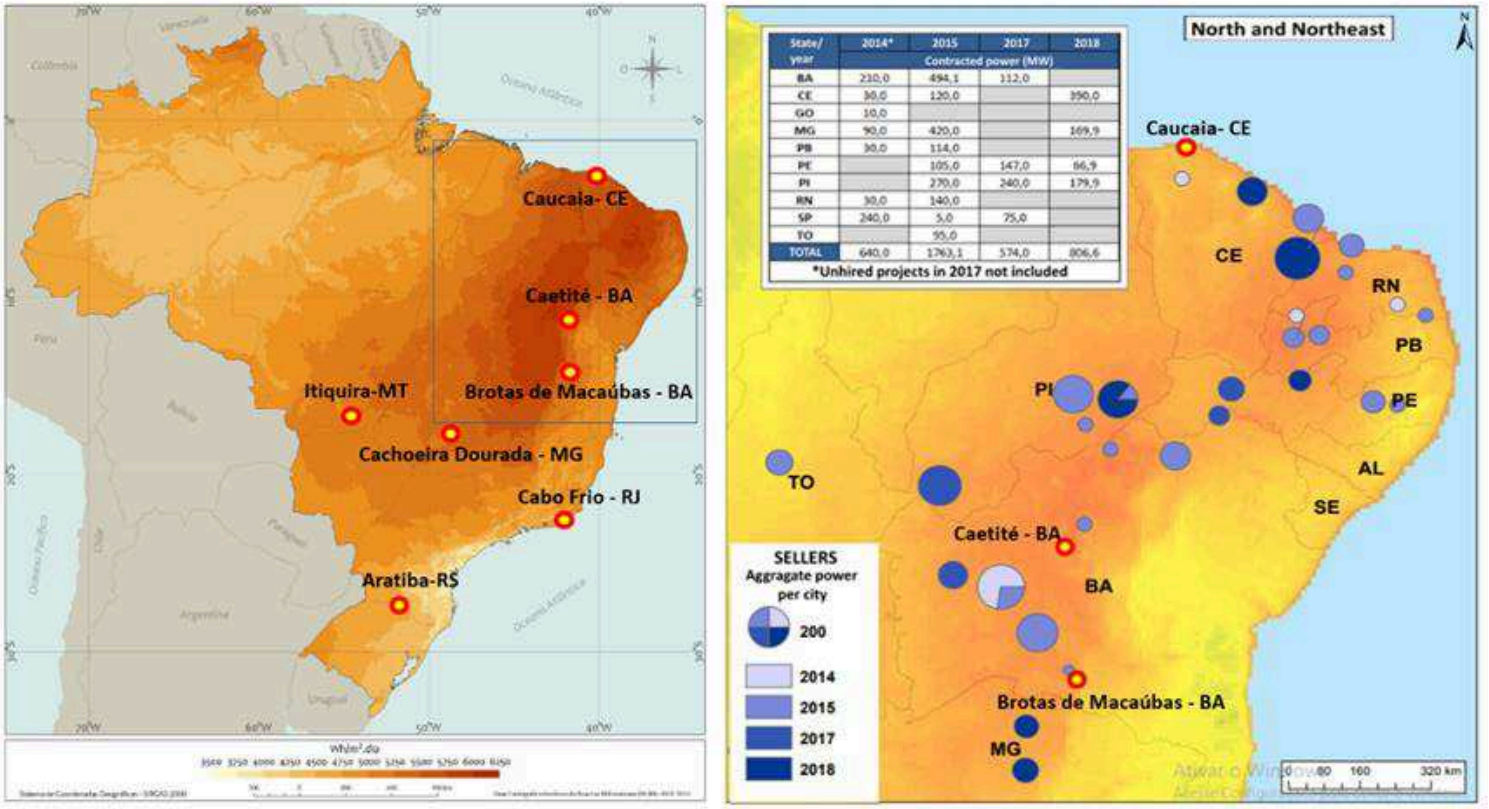

(a) (b)

Figure 26 - General view (a) of the seven SMS installed in the Brazilian territory, and an enlarged view (b) of North and Northeast regions in which most of the utility-scale PV power plants are being installed since 2014 in the country.

Table 6 - Site location, altitude, geographic coordinates, climate classification and the measurement period of the seven Solar Monitoring Stations (SMS).

Site location (City-State)	Altitude (m)	Geographic coordinates	Climate classification	Measurement period (month/year)
Aratiba-RS	404	27°17 S 52°23 W	Cfa	07/2015 – 03/2017
Cachoeira Dourada-MG	430	18°30 S 49°29 W	Aw	03/2015 – 02/2017
Itiquira-MT	392	17°36 S 54°55 W	Aw	01/2015 – 03/2017
Caucaia-CE	32	03°41 S 38°52 W	As	12/2015 – 03/2017
Caetité-BA	1193	14°11 S 42°30 W	Aw	02/2016 – 03/2017
Cabo Frio-RJ	5	22°49 S 41°59 W	Aw	09/2015 – 11/2016
Brotas de Macaúbas-BA	1068	12°18 S 42°20 W	BSh	01/2018 – 09/2018

4 RESULTS AND DISCUSSION

4.1 PV PERFORMANCE ASSESSMENT

In warm and sunny environments, the temperature is the main cause of energy losses in PV systems. Table 7 shows the temperature coefficient of maximum power for the PV module technologies used in this study. It can be observed that the crystalline-silicon-based technologies (mono- and multi-crystalline silicon) are the ones more strongly affected by high temperatures. Meanwhile, the fixed-tilt PV technologies least affected by extreme temperatures are the thin-film technologies, with a-Si and CdTe having the lowest temperature coefficients among them.

Table 7 - Temperature coefficient of maximum power for the PV module technologies used in this study, sorted from lowest to highest, as per each manufacturer's PV module spec sheet.

PV Technology	Temperature Coefficient of P_{mpp} [%/°C]
a-Si (Dupont, 2011)	-0.25
CdTe (First-Solar, 2007)	-0.25
a-Si/µc-Si (Dupont, 2012)	-0.32
CIGS (Avancis, 2011)	-0.39
c-Si (Yingli, 2012)	-0.42
m-Si (Hanwha, 2011)	-0.45

The irradiance-weighted back-of-module average temperature of the six fixed-tilt PV module technologies at the ESs varied from 44°C up to 51°C during the analyzed periods. These high temperatures have favored the thin-film PV technologies, especially a-Si and CdTe, which have the lowest temperature coefficient of power among all evaluated PV technologies.

Another advantage reported in the literature for thin-film technologies in Brazil is related to the spectral response of these PV technologies. Amorphous silicon and cadmium-telluride are known for having a blue-biased spectral response (Rüther and Livingstone, 1995; Rüther *et al.*, 2002; Reich *et al.*, 2005; Dirnberger *et al.*, 2015), which matches the bluer spectral content of light found in several regions of Brazil (Haag, 2013; Haag and Krenzinger, 2016). The AC Performance Ratio (PR) assessment of the six fixed-tilt PV technologies installed at the eight ESs is presented in Figure 27. The period analyzed for each ES includes only simultaneous valid data for all the PV technologies at the specific site. This is the reason why the analyzed period varies from one ES to another, and why some of these sites have only a few months of available data. At the Porto Velho-RO ES, problems in the communication system - especially those related to the lack of internet connection - were frequent, and long periods of data were

lost before these problems could be solved, due to the site's remote location in the Amazon region. Hence, only a couple of months of valid data were available for the performance assessment shown here for that ES. For this reason, the results for the # Porto Velho-RO ES have been disregarded in further analyses. For the # Capivari de Baixo-SC ES, problems related to the a-Si inverter led this technology also to be disregarded in the analyses shown in this thesis.

For the data shown it can be observed that the thin-film a-Si technology resulted in a superior PR than the other technologies for most of the ESs. This behavior is due to the lower temperature coefficient of this technology (as noted in Table 7), which results in an excellent performance in warm climates (Rüther *et al.*, 2003). A bluer spectral content of sunlight in the region might also have been beneficial for these blue-biased PV devices. The analyzed period comprehends data acquired after the stabilization of the Staebler-Wronski Effect (SWE), which strongly affects the output performance of thin-film a-Si PV modules during the first year of outdoor operation, and stabilizes after some 1000 kWh/m^2 of sunlight exposure (Rüther *et al.*, 2008).

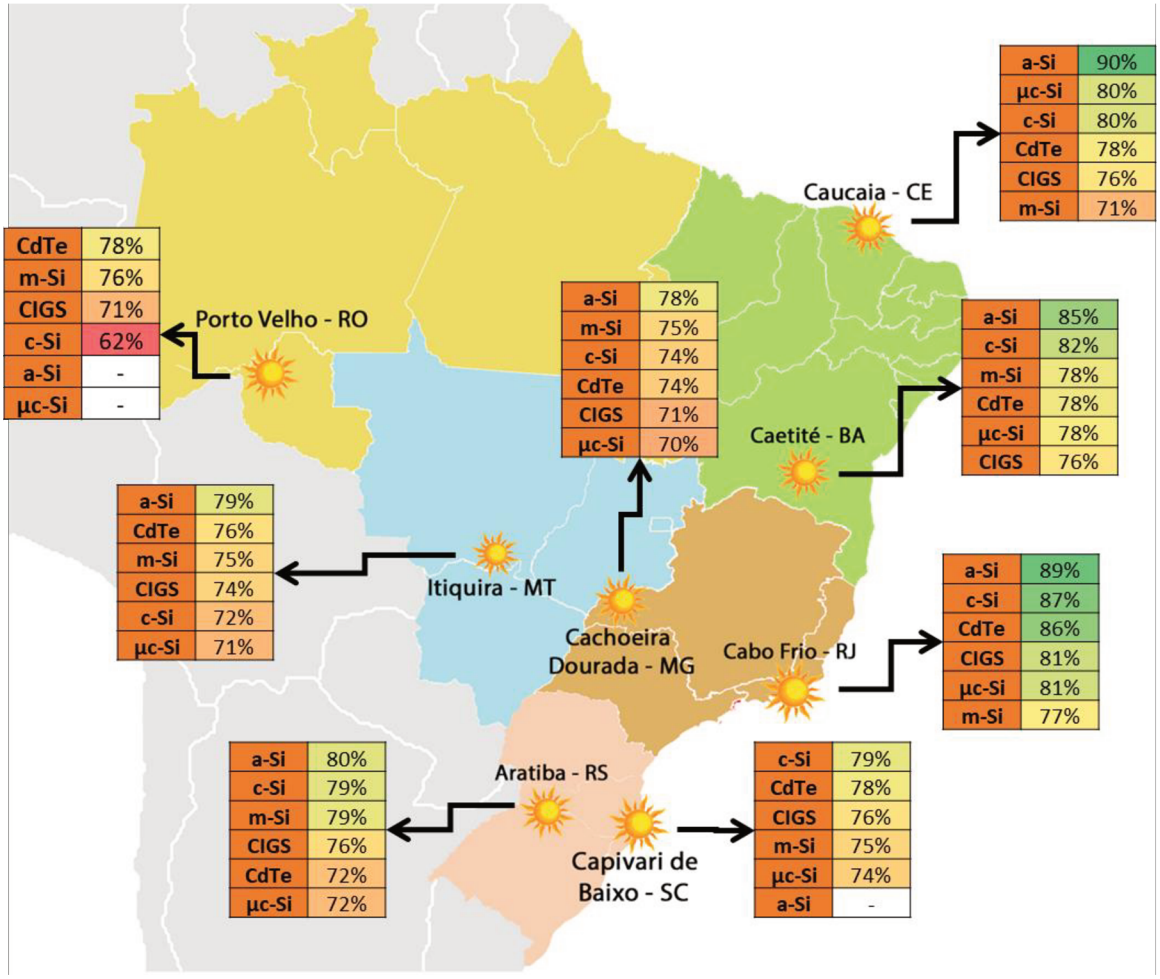

Figure 27 - AC Performance Ratios (PR) of the PV technologies installed at the eight ESs in different climates in Brazil.

For the c-Si and m-Si technologies, a good performance is observed in most of the ESs, with both technologies presenting very similar PRs. However, a few ESs have presented a marked discrepancy between the two technologies. Field evaluations revealed intense potential induced degradation (PID) in coastal areas with high relative humidity and temperature, environmental factors that favor the appearance of such degradation (Pingel *et al.*, 2010). Figure 28 shows the effect of PID in two p-type multi-crystalline silicon strings from the # Capivari de Baixo-SC ES, located on a coastal area of Southern Brazil.

Figure 28 (a) maps the individual modules of the two strings of the m-Si fixed-tilt system at the # Capivari de Baixo-SC ES: string "a" outlined in blue, and string "b" outlined in orange, with 13 and 16 modules, respectively. In the image, modules in green belong to the positive end of the string, while modules in red belong to the negative end. Figure 28 (b) shows the electroluminescence (EL) images made for the modules that belong to the same two strings shown in Figure 28 (a). Finally, Figure 28 (c) shows the measured power relative to the best-

performing module on the string, obtained from individually measured I-V curves for the m-Si modules.

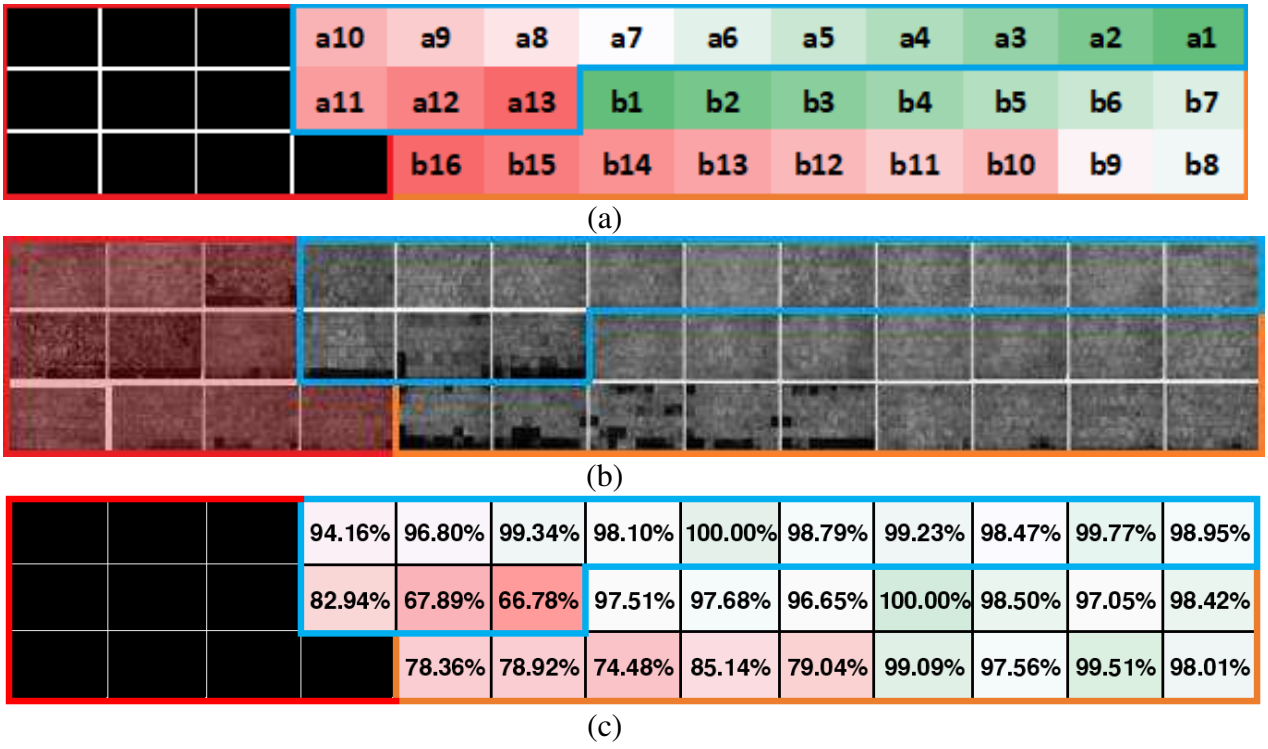

Figure 28 - Potential Induced Degradation (PID) effect on two p-type multi-crystalline strings from the Capivari de Baixo-SC ES (28°S, 49°W), located on the coast of Southern Brazil. (a) maps the two strings connected to independent MPPT inverter inputs: string "a" (outlined in blue, with 13 modules) and string "b" (outlined in orange, with 16 modules), with positive modules in green and negative modules in red. (b) shows the EL images made for all the m-Si modules within the two strings. (c) shows the measured power, obtained using an I-V curve tracer, relative to the best-performing module in the string. The modules shaded in red and black on the left-hand side of all pictures are modules that were damaged and were thus disregarded in the study.

The modules marked in black in Figure 28 (a) and (c), and shaded and outlined in red on image (b), are modules that were blown away from the metallic structure during an extreme meteorological event that hit the region on October 16th, 2016, with strong winds (up to 200 km/h gusts), prior to the EL imaging and the measuring of the modules' I-V curves. Many modules were severely damaged, and not all of them could be replaced, and therefore were put back on the structure, but not connected back to the strings they originally belonged to; they should hence be disregarded in this analysis. In Figure 28 (b), it can be easily seen that the modules located towards the negative end of the strings present more darkened cells on the EL image, and a lower peak power when measured with the I-V curve tracer, as seen in Figure 28 (c). The relation between light intensity during EL imaging and peak power measured in I-V

curve tests has also been recently reported for laboratory as well as in situ measurements (Pinto Filho, 2017; Islam *et al.*, 2018).

Figure 29 shows the individually measured I-V curves for each of the modules in the two strings shown in Figure 28; curves of modules from string “a” are shown in Figure 29 (a), and those for modules from string “b” are shown in Figure 29 (b). A reduction in shunt resistance, as well as a decrease in Voc, can be seen for the most negative modules of each string, resulting in the junction to be less capable of separating holes and electrons (Pingel *et al.*, 2010).

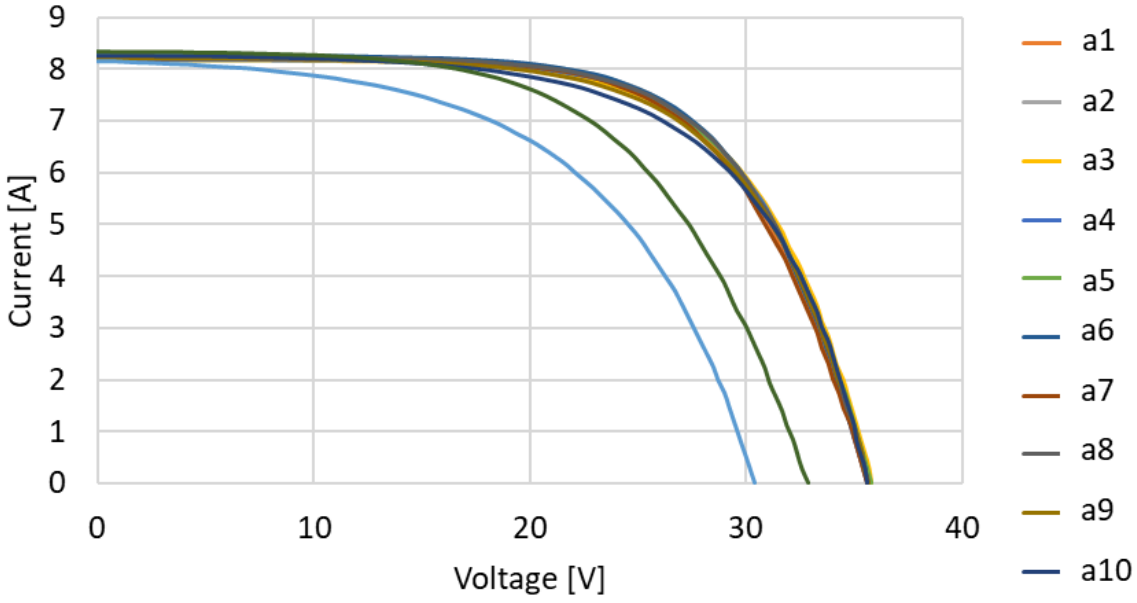

(a)

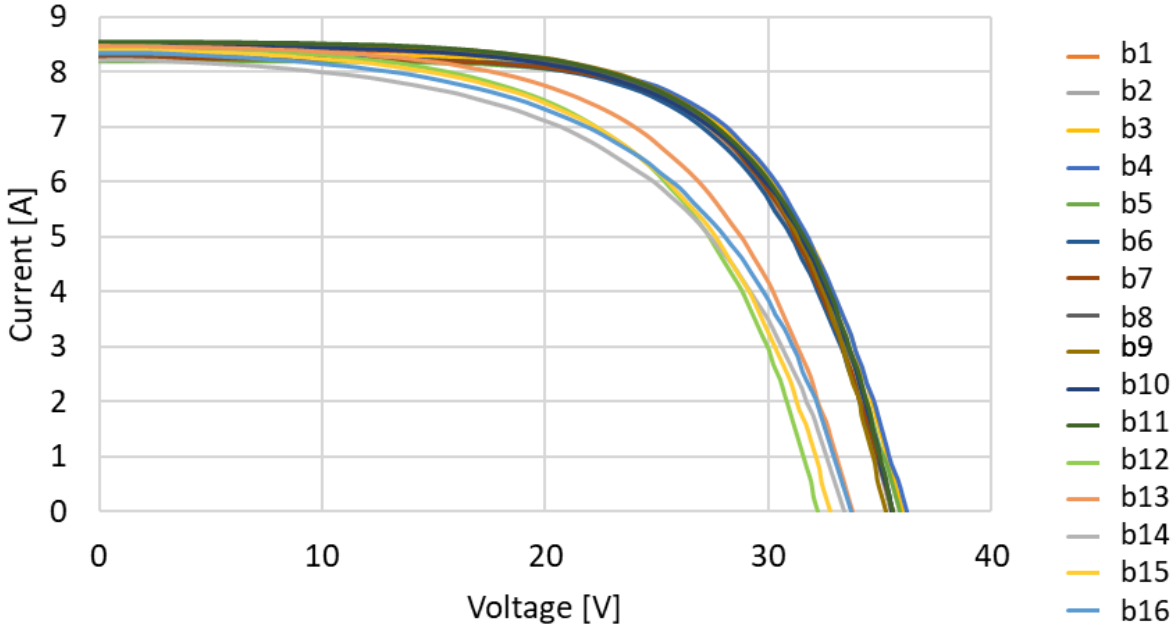

(b)

Figure 29 - Individually measured I-V curves for each of the PV modules belonging to the two strings shown in Figure 28. (a) displays the I-V curves measured for the modules in string "a", while (b) displays the same for string "b".

Electroluminescence (EL) imaging of c-Si modules from the # Capivari de Baixo-SC ES was also carried out, with results shown in Figure 30 (a). Regions with circular shapes are perceptible in some cells, and such pattern is called striation ring. They are related to the distribution of oxygen and carbon impurities in the crystal that leads to the formation of oxygen

conglomerates, associated with the losses by recombination in areas of loading (Manshanden and Bronsveld, 2016). The discoid appearance is due to the curved shape of the interface used in the growth of the silicon ingot in the Czochralski process. These patterns, however, do not represent a significant loss of efficiency (IEA, 2014).

Dark areas in the central region of PV cells are frequently observed, as well as the spreading of this dark area in the peripheral region, indicating the presence of moisture that penetrated from the ambient into the PV module.

The moisture infiltrated into the PV module becomes a basis for the hydrolysis of EVA; the most common PV module encapsulant for crystalline silicon (J. Zhu, 2017). The main byproduct of EVA hydrolysis is acetic acid, which can cause the corrosion of the silver gridline interface with the silicon on PV cells - a crucial current path for the generated electrical current - hence increasing the PV module's series resistance (Kempe *et al.*, 2006), as shown in Figure 30 (b) and Figure 31 and presenting a lower peak power when measured with the I-V curve tracer, as seen in Figure 30 (c). The extensive results of (Pinto Filho, 2017) for c-Si modules shows early degradation after relatively short exposure (<5 years) to hot and humid climates in Brazil, and corroborate these findings.

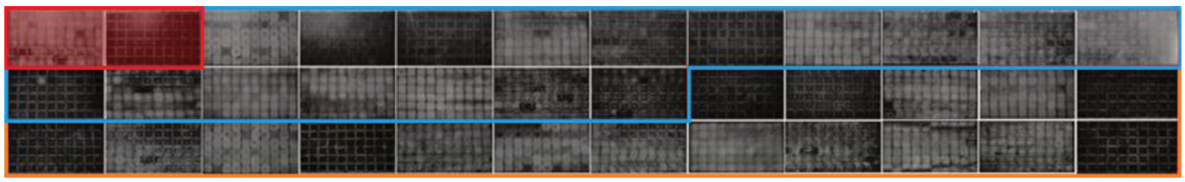

(a)

3.07	5.42	1.53	4.05	4.12	2.56	3.68	3.68	2.10	3.42	3.52	2.41
4.49	3.30	1.67	2.32	1.83	3.83	4.26	4.27	3.96	2.49	1.72	5.46
4.92	3.38	1.45	4.33	2.06	1.71	3.44	2.61	3.93	3.27	3.20	5.29

(b)

90.57%	38.69%	100.00%	62.87%	58.68%	91.34%	59.21%	59.21%	95.34%	68.59%	78.02%	91.73%
41.58%	79.05%	96.02%	89.15%	95.30%	71.90%	62.10%	54.11%	64.51%	90.64%	100.00%	37.95%
38.96%	69.73%	97.52%	51.45%	94.14%	99.77%	82.04%	88.12%	66.93%	84.70%	82.72%	41.02%

(c)

Figure 30 - Electroluminescence (EL) images and I-V curve results of two strings of c-Si PV modules from the Capivari de Baixo-SC ES, showing traces of humidity within the PV module encapsulation. (a) shows the EL images of the two strings (string "a" outlined in blue and string "b" in orange). (b) shows, respectively, the series resistance obtained for each PV module during the I-V curve measurements. (c) shows the measured power, obtained using an I-V curve tracer, relative to the best-performing module in the string. The modules outlined and shaded in red in the images are modules that were damaged and were thus disregarded in the study.

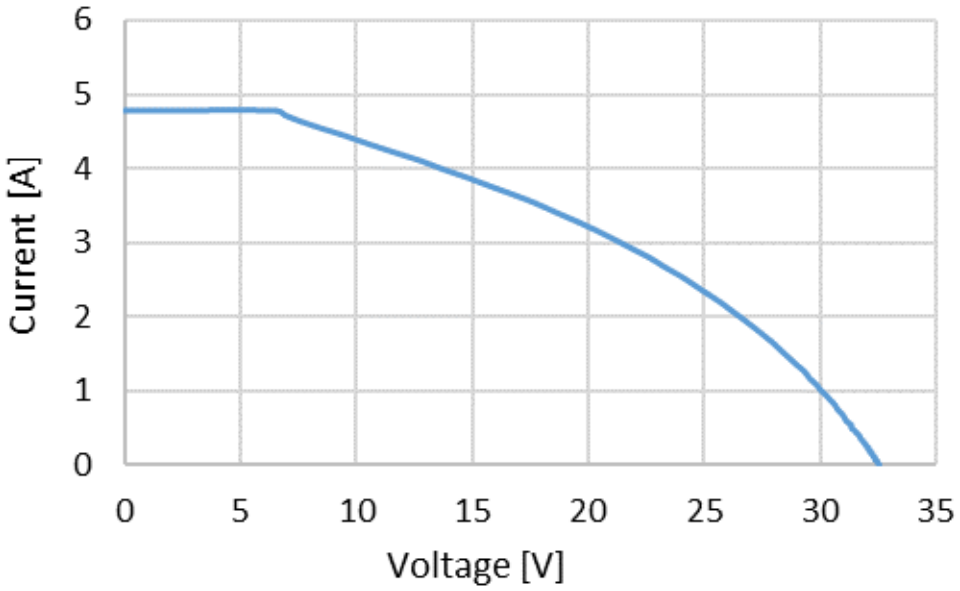

Figure 31 - I-V curve measurement of a 260 Wp c-Si PV module from the Capivari de Baixo - SC ES, showing high series resistance (5.6Ω), low shunt resistance (44.5Ω) and low fill factor (43.1%), which could be related to the humidity ingress in the PV module's encapsulation.

For CIGS and a-Si/µc-Si thin-film PV technologies, a slight negative discrepancy between the measured power and the power declared by the manufacturer was observed at the commissioning of these technologies in various ESs. For these thin-film PV technologies, flash tests are not conclusive due to the Staebler-Wronski and light soaking effects respectively, which cause a-Si/µc-Si and CIGS modules to have their peak power stabilized only after several hours of light exposure (Muñoz-García *et al.*, 2012; Mateo *et al.*, 2018).

Therefore, I-V curve measurements were carried out in brand-new 120 Wp CIGS modules identical to the ones deployed at the ESs after the proper light exposure period. The results are shown in Table 8. On average, the power reduction relative to nameplate peak power was 6.2%. It can also be observed that the measured peak power for these modules varies significantly from sample to sample. Even though a small sample was analyzed, these results could indicate a discrepancy between nameplate and actual power for modules of this technology used in the project. The uncertainty of the equipment used in these measurements was ±5%.

Table 8 - Measured peak power and power reduction relative to nameplate peak power for three brand-new 120 Wp CIGS PV modules identical to the ones used in the ESs. Results are from I-V curve measurements carried out at real sunlight, after the proper light exposure of the samples. The uncertainty of the I-V curve tracer used, PVE PVPM 1040X, is ±5%.

Sample	Measured Peak Power [W_p]	Power Reduction Relative to Nameplate Peak Power
Module #1	114.5	-4.6%
Module #2	113.8	-5.2%
Module #3	109.5	-8.8%

For the thin-film a-Si/µc-Si modules, *in situ* I-V curve measurements were carried out in three brand-new modules, as well as in three clean modules that had been operating for two years in the # Capivari de Baixo-SC ES. Figure 32 presents the results of these measurements, along with the flash test results provided by the manufacturer. On the modules' datasheet, the manufacturer states that the peak power tolerance of this product is ±5% and that in order to account for the Staebler-Wronski (Parida *et al.*) degradation, the initial peak power is approximately 10-16% higher than the stabilized power. The manufacturer also guarantees the performance of 90% of nominal power after 10 years of continuous operation. Considering a stable degradation, the a-Si/µc-Si PV modules that have been operating for two years might present a 2% power reduction due to their natural degradation after stabilization of the SWE degradation. The results show that the measured peak power for the brand-new modules corresponds to the flash test results provided by the manufacturer, and the information on the module's datasheet (10-16% higher than nominal peak power). However, the modules that had been operating presented much lower peak power, placing them on the edge of the manufacturer's negative power tolerance of 5%, plus a 2% degradation for the two-year exposure period (-7% of nominal power), which could indicate a greater than expected initial degradation.

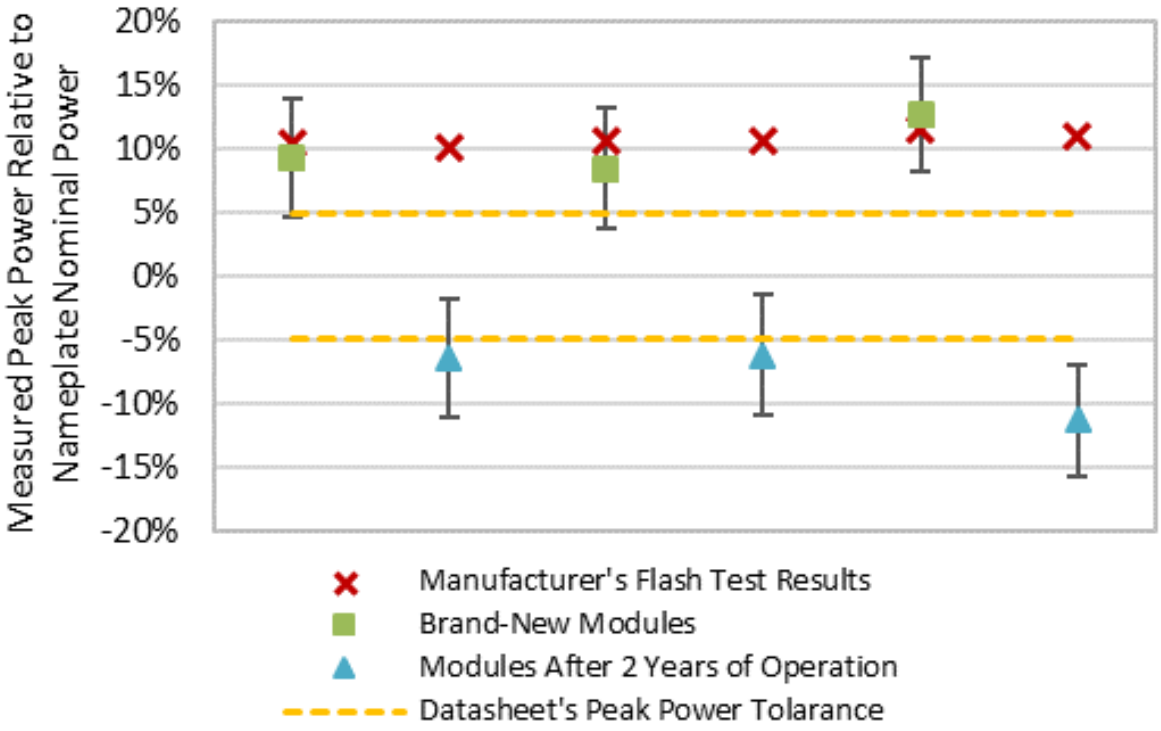

Figure 32 - I-V curve measurement results of three brand-new 142 Wp a-Si/µc-Si PV modules (green squares), and three 142 Wp a-Si/µc-Si PV modules that had been operating in the ES for two years (blue triangles). The flash test results provided by the manufacturer for these specific six modules are also shown as red Xs. The tolerance indicated by the manufacturer on the PV module's datasheet is shown as yellow dashed lines.

For the thin-film CdTe technology, important advances have been made by the manufacturer First Solar since the installation of these systems (Strevel *et al.*, 2014), and the output characteristics of the First Solar Series 2 PV modules installed at the eight ESs were considerably improved in the later Series 4 and more recently in the large-area Series 6 product. AC performance ratios 2-3% higher than multi-crystalline silicon have been reported in the literature for Northern Brazil in a similar R&D project using CdTe First Solar Series 3 modules (Braga *et al.*, 2018).

An experiment to evaluate the weak-light response of the PV modules employed at the ESs was also carried out at the Solar Energy Laboratory (LABSOL) at Universidade Federal do Rio Grande do Sul (UFRGS). LABSOL operates a PASAN SunSim 3C LAPSS (Large Area Pulsed Solar Simulator). The PASAN SunSim 3C LAPSS has a 10ms flash, an illuminated area of 2m x 2m, and the light collimation is less than 15°. This device complies with the

international standard IEC 60904-9 (2007) and is rated AAA, even exceeding the minimum requirements. The accuracy of the simulator is at least 2% (60904-9, 2007; Ruschel *et al.*, 2016).

The experiment was carried out using brand-new multi-crystalline silicon (m-Si), thin-film amorphous silicon (a-Si), microcrystalline silicon (a-Si/µc-Si), cadmium-telluride (CdTe) and copper-indium-gallium-diselenide (CIGS) PV modules, identical to the ones deployed at the ESs. The experiment was not performed on mono-crystalline modules due to the lack of availability of brand-new spare modules of this technology, but results can be expected to be similar to those presented for multi-crystalline modules. Each module had its I-V curve traced at irradiances that ranged from 100 to 1000 W/m², with 50 W/m² intervals. A set of six attenuation masks and different flash intensities were used to obtain the desired irradiances. Due to technical limitations, the lowest irradiance attained was 75 W/m². The room temperature was kept closely at 25°C, and the resulting I-V curves were corrected to STC conditions according to the international standard. The results, all relative to the STC peak power (1000 W/m²), are presented in Figure 33.

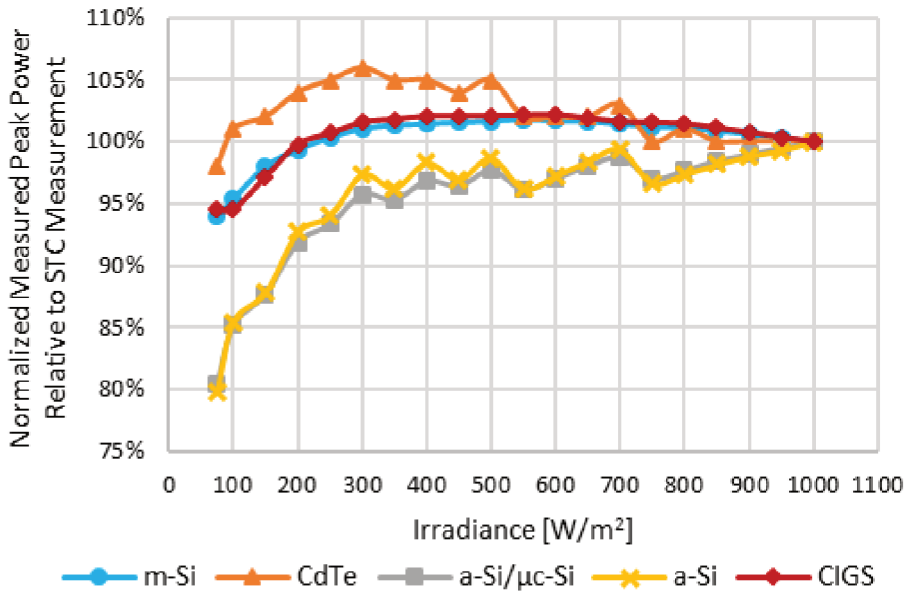

Figure 33 - Weak-light response of brand-new PV modules of five technologies identical to the ones employed at the ESs. Measurements were made in a PASAN SunSim3CLAPSS AAA solar simulator, at LABSOL-UFRGS, and corrected to STC. Results are shown in relation to each technology's STC measurement.

Results show good weak-light behavior for CdTe, m-Si and CIGS modules. CdTe presents over-performance for irradiance levels above 100 W/m^2, while for m-Si and CIGS this increase in measured power is only observed for irradiances above 200 W/m^2. For thin-film a-

Si and a-Si/µc-Si results show an underperformance for low irradiance levels, disagreeing with existent literature on the subject and resulting in poor performance during cloudy weather days.

4.2 ENERGY LOSS ANALYSIS

A detailed energy loss analysis was also carried out through simulations regarding the # Itiquira-MT ES (17°S, 54°W), and the # Aratiba-RS ES (27°S, 52°W), located in the subtropical and the tropical climatic regions of Brazil, respectively. The analyses were done through the use of PV simulation software PVsyst version 6.74 with default parameters values. The simulation was carried out using on-site measured GHI (secondary standard Kipp & Zonen SMP11 pyranometer), and ambient temperature. The total measured loss and the simulated losses are presented in Figure 34 and Figure 35 and in Table 9 and 10 a summary of the results obtained in this part of the study is shown for both sites, respectively.

Measured losses were calculated using the PRs for each technology in these specific evaluation sites using GTI data measured with secondary standard pyranometers, and energy data obtained by the PV system inverters. The evaluated period was a full year, between June 2015 and May 2016.

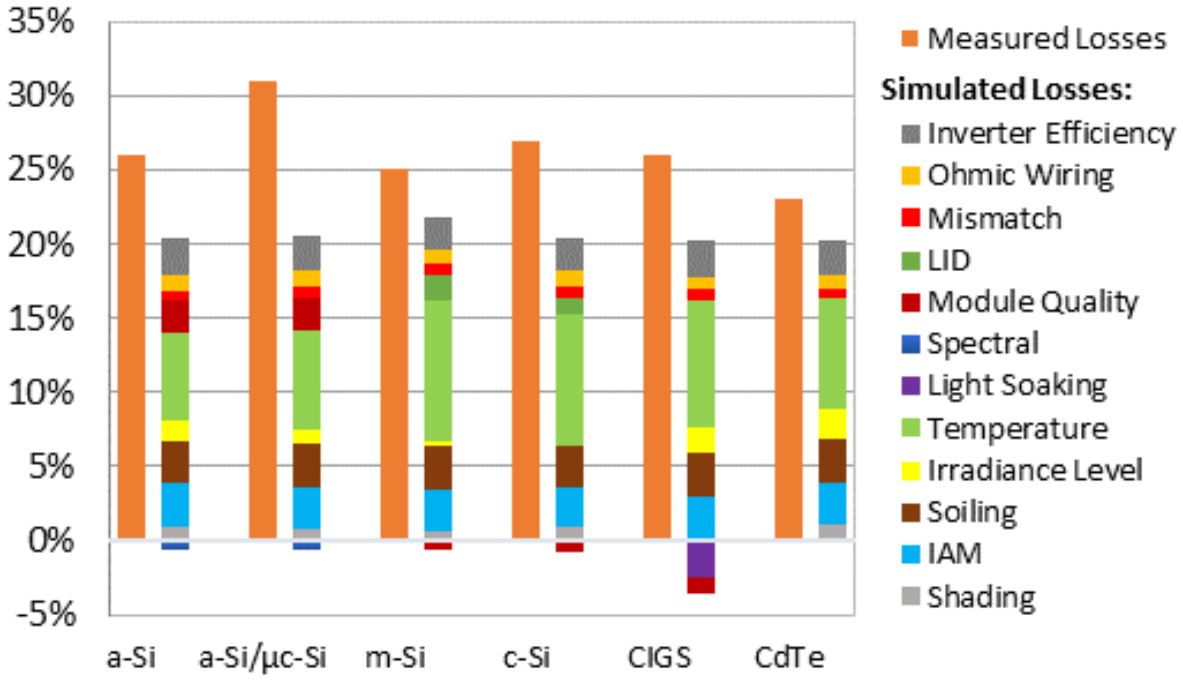

Figure 34 - Measured losses (left-hand bars in orange) and simulated losses (right-hand stacked bars) for the # Itiquira-MT ES (17°S, 54°W).

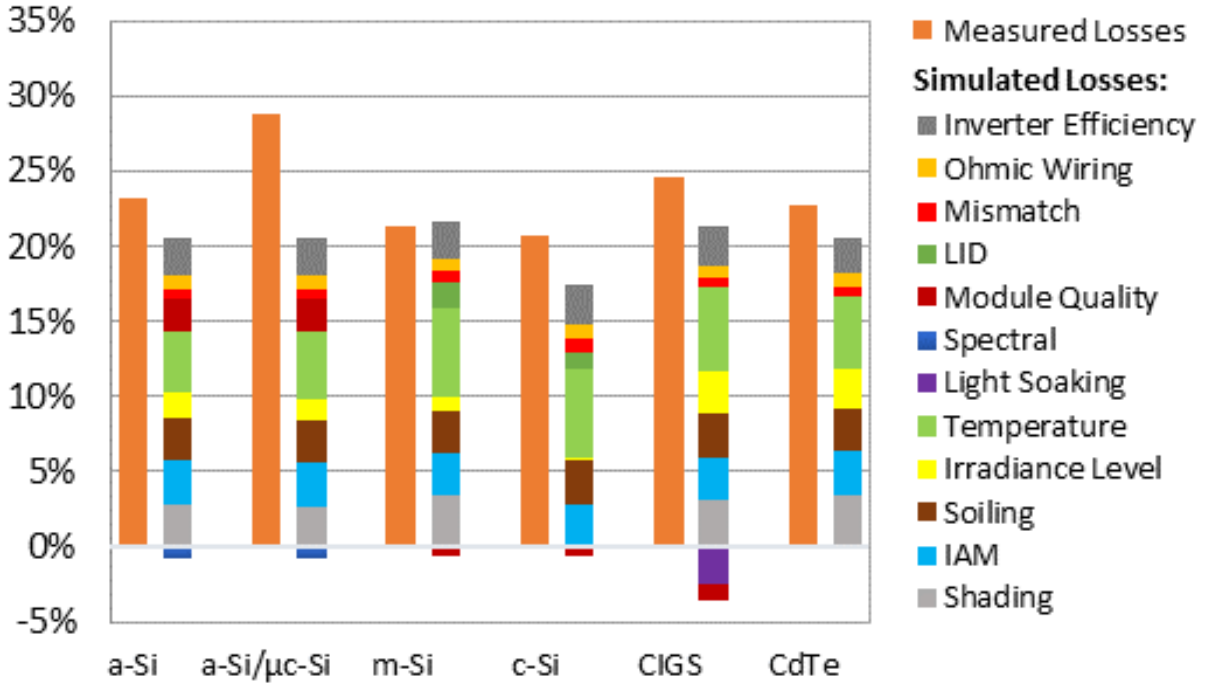

Figure 35 - Measured losses (left-hand bars in orange) and simulated losses (right-hand stacked bars) for the # Aratiba-RS ES (27°S, 52°W).

Most of the differences between simulation and measured results, as presented, are a consequence of PID effects, marked initial degradation (especially for thin-film a-Si and a-Si/µc-Si), and soiling rates different from standard simulation values, and not necessarily only due to simulation uncertainties.

Table 9 - Summary of results for measured losses and total simulated losses for the # Itiquira-MT ES (17°S, 54°W).

PV Technology	Measured Losses	Simulated Losses	Difference
a-Si/µc-Si	31%	20%	11%
CIGS	26%	17%	9%
c-Si	27%	20%	7%
a-Si	26%	20%	6%
m-Si	25%	21%	4%
CdTe	23%	22%	1%

Table 10 - Summary of results for measured losses and total simulated losses for the # Aratiba-RS ES (27°S, 52°W).

PV Technology	Measured Losses	Simulated Losses	Difference
a-Si/µc-Si	29%	20%	9%
CIGS	25%	18%	7%
c-Si	21%	17%	4%
a-Si	23%	20%	3%
m-Si	21%	21%	0%
CdTe	23%	23%	0%

By default, PVsyst does not account for PID in its model. The user, however, can add this loss into the LID or Module Quality parameter of simulation. As shown in the previous section, m-Si modules were greatly affected by PID degradation in the # Capivari de Baixo-SC ES. This loss could be the reason why the measured losses are larger than the simulated losses for the # Itiquira-MT ES.

PVsyst also does not take into account spectral gains for thin-film CdTe modules in its model. As mentioned in the previous subsection, CdTe modules have a spectral advantage in climates such as Itiquira's, due to the fact that both the local spectral distribution of the irradiance and the spectral response of the PV technology are blue-shifted in relation to the standard ASTM G-173 spectrum. This spectral gain would mean lower simulated losses for this PV technology on both ESs.

Soiling losses were quantified through the measurement of I-V curves before and after cleaning the modules in the # Itiquira-MT ES. The experiment was carried out in September 2014, nine months after this system's commissioning. Figure 36 shows pictures of the CIGS, CdTe and m-Si PV systems before and after being manually cleaned. It can be observed that soiling seems to be significant and uniform for all three PV technologies. The results obtained are shown in Table 11. It can be observed that the measured soiling losses for a-Si and CdTe are much larger than the standard 3% soiling that PVsyst (and most of the PV project designers in Brazil and elsewhere) assume as the default value for soiling losses. These technologies are more affected by soiling because of their blue-shifted spectral response, and to the fact that soiling acts as a blue filter for incoming radiation. These larger soiling losses could explain the difference between measured and simulated losses for the thin-film a-Si PV technology.

Table 11 - Measured soiling losses at the # Itiquira-MT ES (17°S, 54°W).

PV Technology	Soiling Losses
a-Si	7.8%
CdTe	4.1%
CIGS	3.2%
a-Si/µc-Si	2.8%
c-Si	2.1%
m-Si	0.5%

Figure 36 - Images of the CIGS (a), CdTe (b) and m-Si (c) Itiquira MT ES PV systems before and after being manually cleaned (left- and right-hand side images, respectively). The soiling shown was accumulated between December 2013 and September 2014.

4.3. OVERIRRADIANCE IMPACTS ON PV SYSTEMS

4.3.1 Global Horizontal Irradiance - overirradiance events (GHI)

The highest overirradiance value measured in Brazil so far (GHI = 1845 W/m²) was recorded at the # Caucaia-CE SMS using a Delta SPN1 thermopile pyranometer. Figure 37 shows global horizontal irradiance (GHI), diffuse horizontal irradiance (DHI) and extraterrestrial global horizontal solar irradiance (ETH) during this overirradiance event.

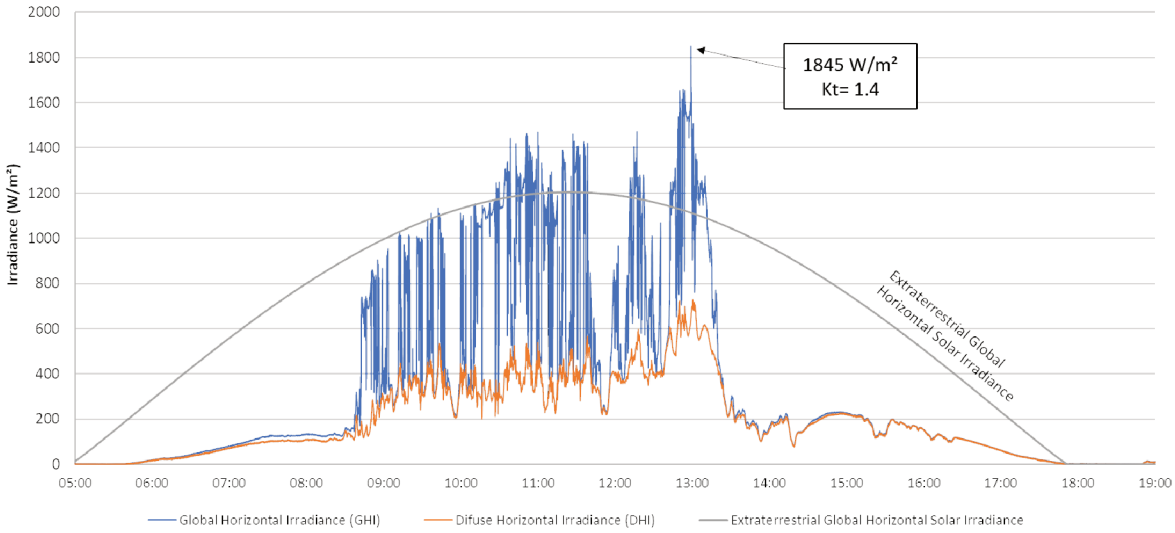

Figure 37 - Highest overirradiance event measured in Brazil so far (1845 W/m^2), using a Delta SPN1 thermopile pyranometer installed at the # Caucaia-CE SMS.

It is worth mentioning that the # Caucaia-CE SMS's altitude is only about 32 m above sea level, and there is no benefit from a reduced atmospheric absorption, as for example at the elevated test location (1829 m above sea level) used by Gueymard (2017) in the world-record 1891 W/m^2 overirradiance event reported for Colorado-USA.

Overirradiance events, as shown in Figure 37, are usually detected under broken cloud skies, when cloud enhancement effects lead to overirradiance values. During these overirradiance events, even DHI levels are extremely high as is also shown in Figure 37.

Figure 38 shows a picture from the sky recorded at the # Itiquira-MT SMS, during a typical situation of broken cloudy sky, with a visible cloud brightening due to cloud enhancement effects.

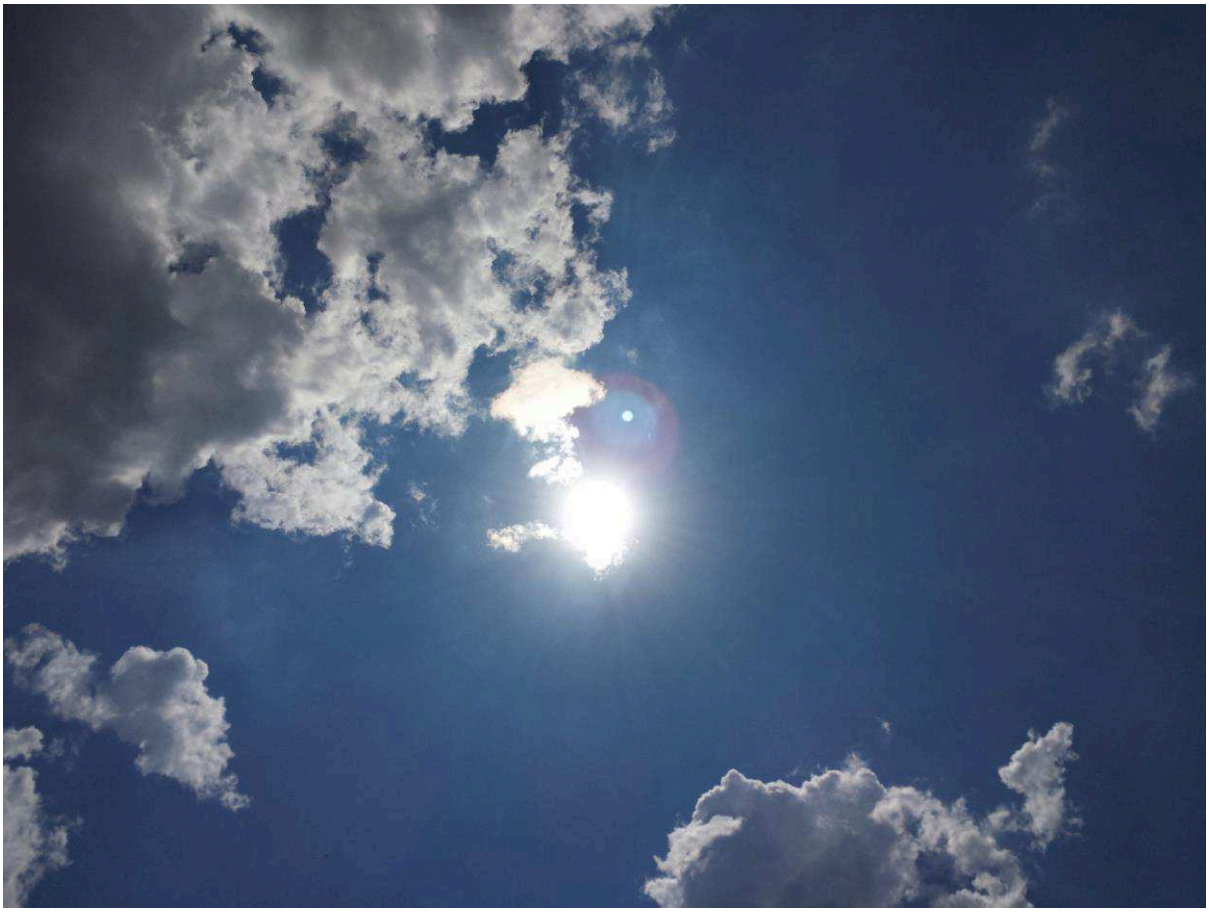

Figure 38 - Picture of a broken cloud sky with overirradiance event at the # Itiquira-MT SMS.

The record overirradiance events and the corresponding clearness index Kt, at each of the seven SMSs referred to in this thesis, are presented in Figure 39. The map shows, for all SMSs, the maximum overirradiance values measured by pyranometers (thermopile sensors), from different models and manufacturers, as detailed in Tables 5.

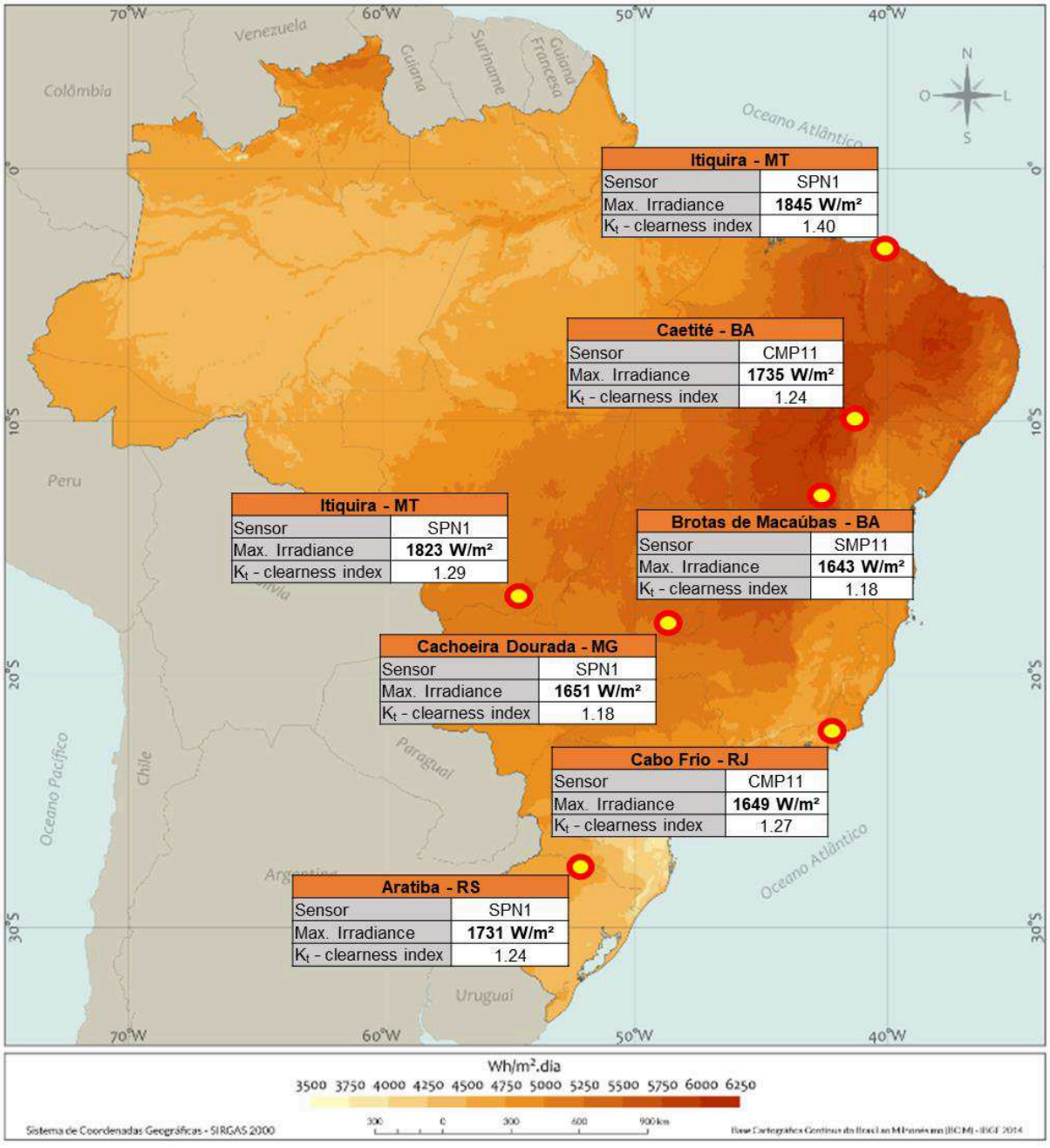

Figure 39 – Extreme overirradiance events recorded at each of the seven SMSs installed at different sites in Brazil, measured with pyranometers (thermopile sensors) from different models and manufacturers.

Since the three pyranometers, despite being all thermopile sensors, have different construction structures and different overall accuracy for individual readings (SPN1 ±8%, CMP11 ±2 and SMP11 ±2%), values recorded by each one, at the same site, could be different. An example of this situation is presented in Figure 40, for the highest global horizontal overirradiance (GHI) events, recorded at the # Brotas da Macaúbas-BA and # Itiquira-MT sites, with SPN1 and SMP11 pyranometers.

The highest difference between values measured with the different pyranometer models at the # Brotas de Macaúbas-BA site is 89 W/m^2 and at the # Itiquira-MT site is 105 W/m^2. These figures are consistent with pyranometers' accuracies at these high irradiance levels.

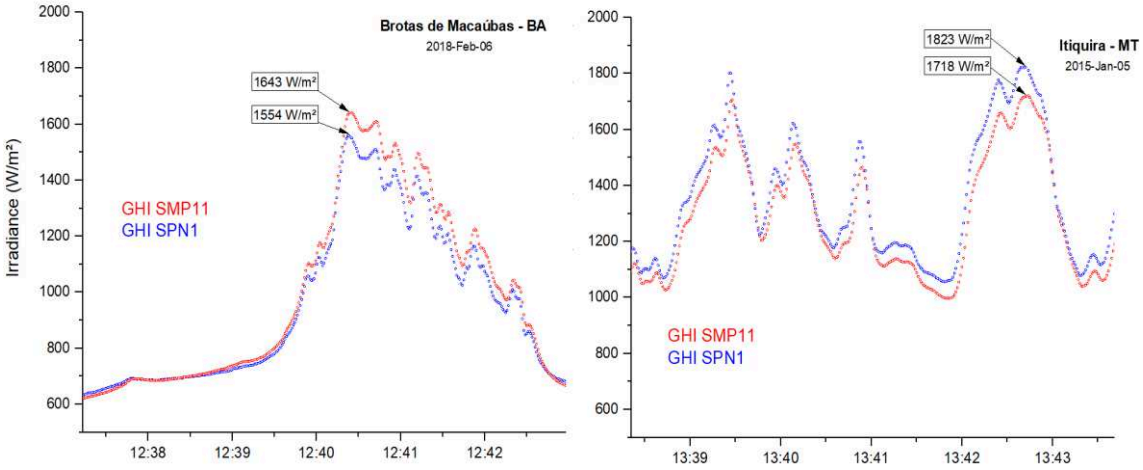

Figure 40 – Extreme global horizontal overirradiance (GHI) events, recorded at the # Brotas de Macaúbas-BA and # Itiquira-MT SMS, with SMP11 and SPN1 pyranometers (both are thermopile sensors).

Table 12 shows the maximum values of global horizontal irradiance (GHI) events recorded around the world. This table, adapted from Almeida *et al.* (2014) and Gueymard (2017a), is updated and includes location, elevation, clearness index (Kt), measurement time resolution, the instrument used in the measurement and instrument response time.

Table 12 - Maximum values of global horizontal overirradiance (GHI) events recorded around the world. Adapted from Almeida *et al.* (2014) and Gueymard (2017a) and updated, including location, elevation, clearness index (Kt), measurement time resolution, the instrument used in the measurement and instrument response time.

Pos.	Reference	Irradiance (W/m^2)	Location	Elevation (m)	K_T	Resolution (s)	Instrument	Response time (s)
1	Gueymard (2017)	1891	Colorado, USA	1829	1.62	1	LI-COR LI-200 (Photod.)	<<1
2	**This study (SMS #4)**	**1845**	**Caucaia, Brazil**	**32**	**1.40**	**1**	**SPN1**	**<0.2**
3	Emck and Richter (2008)	1832	Andes, Ecuador	3400	1.34	300	K&Z CM3	<18
4	**This study (SMS #3)**	**1823**	**Itiquira, Brazil**	**392**	**1.29**	**1**	**SPN1**	**<0.2**
5	**This study (SMS #5)**	**1735**	**Caetité, Brazil**	**1193**	**1.24**	**1**	**CMP11**	**<5**
6	**This study (SMS #1)**	**1731**	**Aratiba, Brazil**	**404**	**1.24**	**1**	**SPN1**	**<0.2**
7	**This study (SMS # 2)**	**1651**	**Cachoeira Dourada, Brazil**	**430**	**1.18**	**1**	**SPN1**	**<0.2**
8	**This study (SMS #6)**	**1649**	**Cabo Frio, Brazil**	**5**	**1.27**	**1**	**CMP11**	**<5**
9	Andrade and Tiba (2016)	1648	Maceió, Brazil	127	N/S	60	Eppley 8–48	<30
10	**This study (SMS #7)**	**1643**	**Brotas de Macaúbas, Brazil**	**1068**	**1.18**	**1**	**SMP11**	**<2**
11	Gueymard (2017)	1634	Colorado, USA	1829	1.37	60	LI-COR LI-200 (Photod.)	<<1
12	Emck and Richter (2008)	1630	Ecuador	1970	1.24	300	K&Z CM3	<18
13	Almeida et al. (2014)	1590	São Paulo, Brazil	760	1.14	1	MSX-10 (PV module)	<<1
14	Avila et al. (2019)	~1570	Bogotá, Colombia	2600	N/S	2	K&Z CM3	<18
15	Andrade and Tiba (2016)	1551	Água Branca, Brazil	593	N/S	60	Eppley 8–48	<30
16	Gueymard (2017)	1546	Colorado, USA	1829	1.30	60	K&Z CM22	<5
17	Tapakis and Charalambides (2014)	1533	Cyprus	360	1.19	5	EKO MS-802	<5
18	Ramgolam and Soyjaudah (2014)	1532	Mauritius	200	1.09	30	SolData 80SPC (cell)	<<1
19	Piacentini et al. (2003)	1528	Puna de Atacama, ARG	3900	1.13	5	Eppley PSP	<15
20	Weigl et al. (2012)	~1520	Oahu, Hawaii	<10	N/S	1	LI-COR LI-200 (Photod.)	<<1
21	Piacentini et al. (2011)	1477	Recife, Brazil	4	1.09	N/S	Eppley PSP	<15
22	Hansen et al. (2010)	~1450	New Mexico, USA	1657	N/S	60	K&Z CM2	<18
23	Pfister et al. (2003)	1450	New Zealand	370	N/S	60	K&Z CM11	<5
24	Gu et al. (2001)	~1400	Rondônia, Brazil	<400	N/S	60	Eppley PSP	<15
25	Inman et al. (2016)	1396	California, USA	N/S	1.10	30	Yankee MFR-7 (Photod.)	<<1
26	Inman et al. (2016)	1380	Hawaii, USA	N/S	1.04	30	Yankee MFR-7 (Photod.)	<<1
27	Walker (2001)	~1350	Australia	40	N/S	60	N/S (Photod.)	<<1
28	Luoma et al. (2012)	>1300	San Diego, USA	22	N/S	1	LI-COR LI-200 (Photod.)	<<1
29	Piedehierro et al. (2014)	1244	Granada, Spain	680	1.10	60	K&Z CM11	<5

4.3.2 Impacts on PV power performance

4.3.2.1 Fuse rating

Combiner boxes are used in both small and utility-scale PV projects in order to associate, add electrical protection, and monitor the strings of a PV system. To avoid ingress of animals, small insects, moisture and dust, usually combiner boxes have a high degree of environmental protection (high IP code rating, as defined by the IEC 60529 standard) which

unfortunately also causes a reduction in the internal ventilation and heat dissipation, leading to high operating temperatures of the components housed therein.

In utility-scale PV power plants the combiner boxes are typically fixed to PV modules mounting structures, or installed near those structures, quite often directly exposed to the sun, increasing, even more, the temperature of electrical components.

Fuses are used and installed in combiner boxes to protect PV module strings against reverse currents. PV module manufacturers' data sheets provide information on the "maximum series fuse rating" to be considered when sizing a PV array. Rating fuses above this maximum value could lead to risks in PV module safety and definitively void manufacturer's module warranty.

4.3.2.2 Fuse behavior with temperature

A fuse electrical current carrying capacity is typically rated at 20 ºC to 30 ºC, and with an increase in temperature, a "derating factor" must be applied. At 70 ºC the derating factor varies from ~0.73 to 0.80, depending on the fuse manufacturer (MERSEN, 2012; SIBA, 2012; ETI, 2013; SOCOMEC, 2014; BUSSMANN, 2017). At the seven PVES locations reported in this work, where the seven SMS are installed, and at most sites where PV plants in Brazil, now and in the future, will more and more operate, ambient temperatures and irradiance levels are high. Combiner boxes, where the above-mentioned fuses are installed, can reach temperatures higher than 70°C, as has been routinely measured throughout the current ESs (Rüther *et al.*, 2017).

Figure 41 shows a combiner box (containing a digital temperature meter), which had just been opened when the image was captured. The meter's thermocouple is inserted in the fuse holder. The digital meter's display presents two values: the instantaneous temperature of 66.3 ºC and the maximum temperature of 74.3 °C, both measured at the fuse holder.

Figure 41 - Operating temperature (66.3 ºC) and maximum temperature (74.3 ºC) measured in a fuse holder, inside a combiner box. The meter's thermocouple is inserted in the fuse holder.

Considering a condition as shown in Figure 41, a 15 A rated fuse, normally used with 60-cell crystalline-Si PV modules, in the worst case of temperature derating would behave as a

fuse with nominal capacity around 11 A. In the case of a typically higher voltage (and therefore lower current) thin-film module, the 2 A rated fuse recommended by the PV module manufacturer would behave like a 1.5 A fuse. This issue, associated with overirradiance events in the minute-range, can lead (and has led) to deleterious consequences to the operation and maintenance of PV power plants.

4.3.2.3 Blown fuses during overirradiance events

During overirradiance events, PV array DC output power might be higher than inverter nominal DC power ($P_{PV}>P_{INV}$), and the inverter will typically limit the output power to its nominal power. This control is performed by the inverter's MPPT algorithm, increasing the PV array operating voltage (V_{MPP}) towards open-circuit voltage (V_{OC}). This could lead to the conclusion that, in cases of long overirradiance events at warm sites, the inverter's MPPT will sweep towards V_{OC}, and all strings will operate at a higher voltage and lower current than in normal MPPT range operation.

However, in utility-scale PV power plants, with dozens of combiner boxes connected to a central inverter, it has already been noticed in field measurements (Nascimento *et al.*, 2018) what is suggested in literature: overirradiance events have only a small spatial footprint, because of their direct dependence on the sun-cloud edge-surface geometry (Gueymard, 2017a). This implies that during an overirradiance event, depending on cloud geometry, number of independent inverter MPPTs and ILR, some of the strings could be operating with currents proportional to the (over) irradiance levels, while the other strings could be under the cloud shadows, resulting in an inverter output power below inverter nominal power (Luoma *et al.*, 2012). In such scenario, the inverter will not limit the output power using the above-described MPPT control strategy, and, therefore, strings will operate with high currents, which associated with high fuse operating temperatures, might cause string fuses to blow. One of such situations was observed in a PV system located at the # Cabo Frio-RJ SMS. The system is composed of thin-film amorphous/microcrystalline silicon (a-Si/µc-Si) PV modules with strings having an operational current (I_{MPP}) of 1.17 A at STC. Each string has a 2 A series fuse, which is the maximum series fuse rating allowed by the PV module manufacturer in order not to void module warranty. The ratio of fuse-current by string operation-current at STC ($I_{maxFuse}/I_{MPP@STC}$) is 1.70. As previously presented, the derating factor for fuses at high operating temperatures will lead the 2 A rated fuses to behave as 1.5 A fuses. The ratio of this derated fuse current by string operation current at STC ($I_{maxfuse\_derated}/I_{MPP@STC}$) in this scenario will be 1.28.

Figure 42 shows the normalized current ($I_{MPP}/I_{MPP@STC}$) of two strings that have very similar behavior, following the simultaneous irradiance profile as expected. During an overirradiance event, at around 12:30, with values higher than 1500 W/m² lasting longer than five minutes, the fuse of string 2 has blown, with a normalized current value of 1.43.

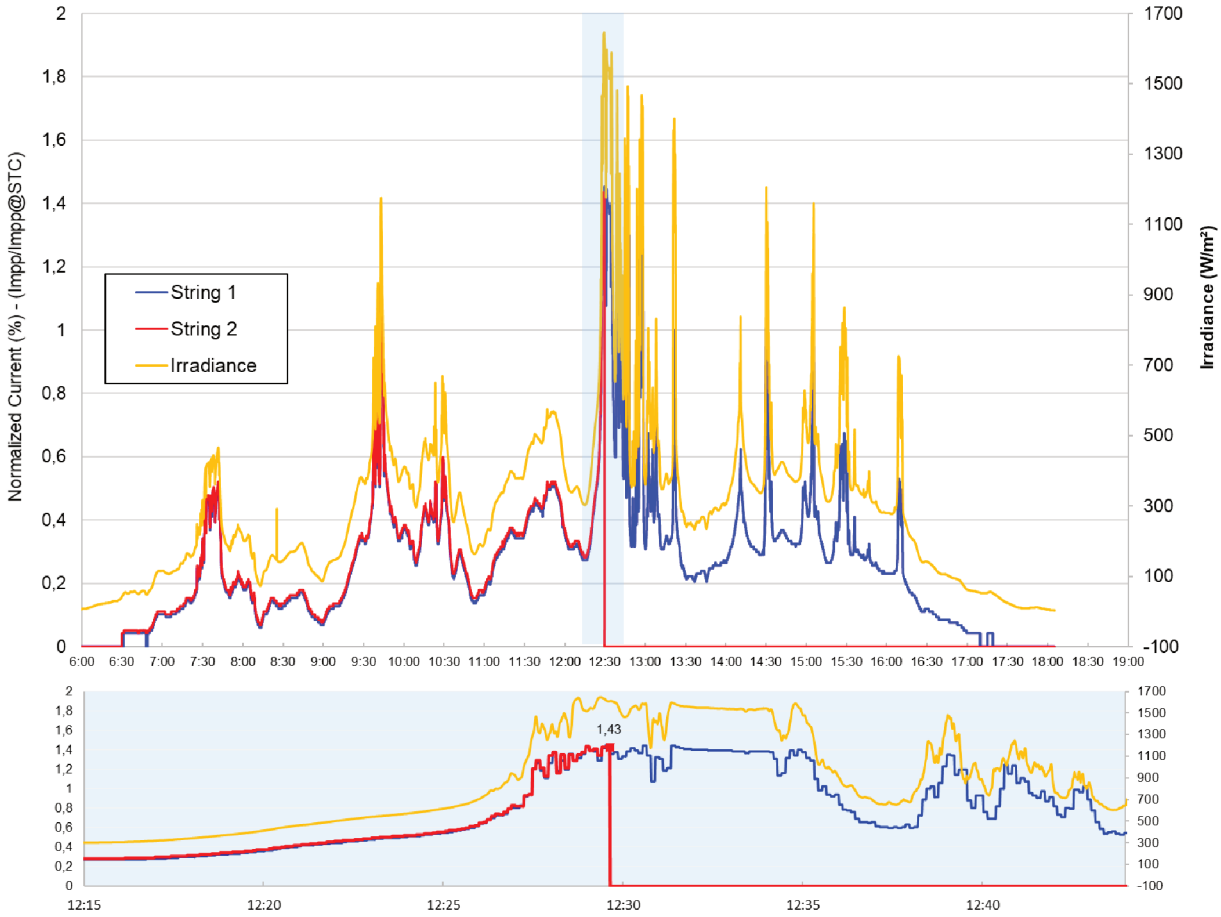

Figure 42 - Global tilted overirradiance event measured with a Kipp & Zonen CMP11 thermopile pyranometer at the # Cabo Frio-RJ SMS, around 12:30, with irradiances higher than 1500 W/m² and lasting longer than five minutes. The fuse of string 2 has blown with a normalized current value of 1.43.

Normally, due to fuse characteristics for PV applications (gPV fuse), even in situations as described above (PV operational current higher than derated fuse current), fuses are not expected to blow, since these events are transitory and not lasting long enough to trigger (fuse) the fuse. However, time spans in the minute-range will result in conditions that will lead to the blowing (fusing) of even slow-blow fuses, if they are sized as per the PV module manufacturer's specification.

This kind of event was noticed during the course of this thesis fieldwork in several other sites for different PV technologies (Braga *et al.*, 2018) and, based on these findings, it can be speculated that several such events will take place in many of the large-scale PV power plants being installed in Brazil. It is therefore recommended that PV module manufacturers reassess their maximum series fuse ratings in the light of this information, and utility-scale projects could size string boxes in a manner to keep fuses from reaching such high temperatures. Table 13 presents the number of high global tilted irradiance (GTI) events measured at the seven SMSs, with IMT reference cells, for time spans ranging from less than five seconds to more than five minutes. The number of events corresponds to measured irradiance values higher than G_0 (1367 W/m²). Average irradiance values were calculated using all instantaneous overirradiance values measured in the corresponding time span.

Table 13 - Number of high global tilted irradiance (GTI) events (irradiance higher than G_0, 1367 W/m²) measured at all seven SMS. Averaged irradiance is calculated using all instantaneous overirradiance values measured in the corresponding time span.

Time span		Aratiba-RS	Cachoeira Dourada-MG	Itiquira-MT	Caucaia-CE	Caetité - BA	Cabo Frio-RJ	Brotas de Macaúbas-BA
Shorter than 5s	Number of events	334	254	1242	351	2338	238	122
	Average irradiance (W/m²)	1392	1385	1388	1391	1408	1390	1347
Between 5s and 10s	Number of events	133	163	661	155	895	132	57
	Average irradiance (W/m²)	1414	1403	1408	1403	1434	1411	1380
Between 10s and 30s	Number of events	105	183	686	99	885	144	38
	Average irradiance (W/m²)	1423	1424	1423	1413	1443	1428	1370
Between 30s and 1min	Number of events	22	56	230	32	327	35	14
	Average irradiance (W/m²)	1436	1427	1436	1417	1447	1453	1408
Between 1min and 5min	Number of events	3	38	133	10	60	21	7
	Average irradiance (W/m²)	1408	1448	1436	1426	1441	1460	1390
Longer than 5min	Number of events	0	2	4	0	4	1	0
	Average irradiance (W/m²)	-	1456	1418	-	1417	1415	-

4.3.2.4 Inverter overload losses

When sizing a PV plant most PV software's use average hourly irradiance data for simulation, and this typical one-hour resolution often underestimates high irradiance levels (Ransome and Funtan, 2005). In practice underestimating high irradiance will directly affect systems with relatively high ILRs, since inverter saturation will be reached at a lower irradiance limit. In an evaluation taking into account site-dependent peculiarities of ambient temperature, inverter operating temperature and solar irradiance distribution characteristics, Burger and Rüther (2006) have shown that inverter sizing could lead to more than 10% differences in overloading when using hourly data compared to minute data for Southern Brazil. For San Diego, California, at a site with frequent overirradiance events, more than 18% difference in overloading for optimal inverter sizing was observed when using hourly data compared to one-sec data (Luoma *et al.*, 2012). Table 14 shows percentages of GTI annual solar energy (irradiation, H, kWh/m^2.year) measured at the # Itiquira-MT SMS, distributed by different ranges of irradiance (G) and averaged using different periods (one-second to one-hour). Irradiation data logged using one-second and ten-seconds averaging periods show, in both cases, that around 22% of the annual solar irradiation (kWh/m^2.year) occurred at irradiance levels at or above 1000 W/m², typically caused by overirradiance events.

When a one-hour averaging period is used the result is considerably different and shows that only around 10% (less than a half of previous value of 22%) of the annual solar irradiation occurs at the same irradiance range (≥ 1000 W/m²) considered for one-second and ten-seconds averaging periods.

Table 14 - Annual GTI solar energy distribution (in % of annual irradiation) measured at Itiquira-MT SMS, for different ranges of irradiance (G) and different averaging periods.

Averaging period	Irradiance ranges (W/m²)				
	G < 300	**300 ≤ G < 700**	**700 ≤ G < 1000**	**1000 ≤ G < 1200**	**G ≥ 1200**
1 second	11.1%	28.8%	37.9%	18.3%	3.8%
10 seconds	11.1%	28.9%	38.2%	18.2%	3.6%
1 minute	11.0%	29.2%	39.1%	18.0%	2.8%
10 minutes	10.5%	30.8%	43.1%	15.1%	0.6%
1 hour	9.7%	34.6%	45.3%	10.4%	0.0%

The results, shown in Table 14, demonstrate that the commonly used hourly averages induce an experimental artifact that hides important energy information, and is not representative of the actual solar energy distribution profile. These different results have a direct impact on inverter sizing and PV system performance.

ILRs for crystalline-Si PV systems varying from 100% to 140% are presented in Figure 43, using different data averaging periods (one-second to one-hour). The PV system is operating at the # Itiquira-MT site, with an average performance ratio (PR) of 75%.

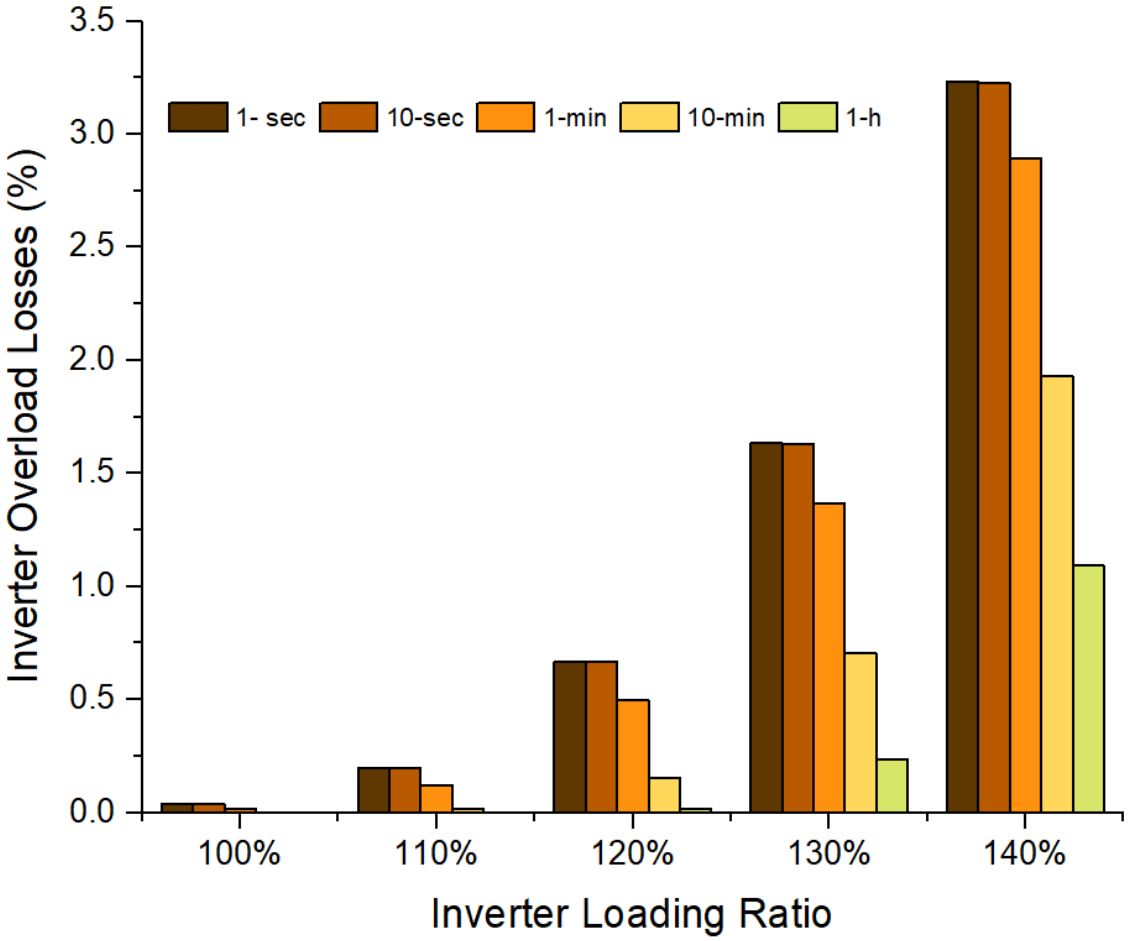

Figure 43 – Inverter overload losses for a crystalline-Si PV system at the # Itiquira-MT ES, with an average PR of 75%, and ILRs varying from 100% to 140% using different data averaging intervals.

It can be noted that for a 130% ILR, typical for recent Brazilian PV power plants, simulations using hourly data show inverter overload losses of 0.2%, while the estimation using one-second data reveals losses of 1.6%. Losses are even more pronounced for systems with higher ILR. These results also demonstrate that one-minute and one-second, or ten-second data averaging, are very similar to each other and do not justify the extra file sizes and computation times incurred by the instant one-second values as compared to the one-minute averages.

4.3.2.5 Irradiance variability and impacts on MPPT efficiency

The operation of PV systems under high irradiance variability has not drawn much attention given the limited availability of high time-resolution data, even though a PV system inverter should be able to quickly adapt MPPT input impedance to any weather conditions (Piotrowicz and Marańda, 2013). For measurements of inverter MPPT efficiency, the European standard EN 50530 – "Overall efficiency of grid-connected photovoltaic inverters"

(CENELEC, 2010), provides a procedure to measure both static and dynamic MPPT efficiency. In the case of dynamic MPPT efficiency, the goal is to assess how the inverter will behave in irradiance ramps sloping from 0.5 W/m²/s up to 100 W/m²/s. Figure 44 shows the frequency distribution of irradiance ramps, with 50 W/m²/s slope intervals, at the # Itiquira-MT SMS, where the highest number of solar overirradiance events has been recorded.

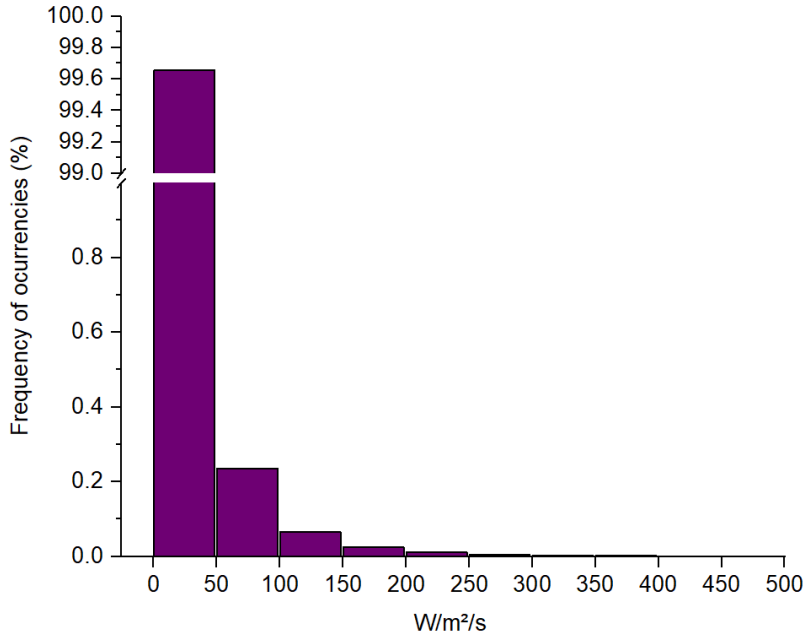

Figure 44 - Frequency distribution of irradiance ramps, for 50 W/m²/s slope intervals, at the # Itiquira-MT SMS.

The irradiance distribution in Figure 44 shows that more than 99.9% of irradiance ramps occur with slopes up to 100 W/m²/s revealing that, besides the high values of overirradiance events, the actual irradiance slope fits within the values specified by the above-mentioned inverter (MPPT) efficiency standard.

5 CONCLUSIONS

In this thesis, the performance assessment of six different PV technologies for utility-scale applications in eight warm and sunny sites in Brazil has been described and evaluated in a medium-term scientific experiment. The results presented in this thesis give a concise overview of the main aspects (overirradiance effects, fuse design/rating, PID, simulation uncertainties and soiling losses) that will have to be considered in more detail as utility-scale PV power plants start to emerge in large amounts in warm and sunny countries.

The results also present the performance assessment of the PV technologies installed at each of the eight ES. Thin-film PV technologies with a low-temperature coefficient of power presented superior output performance. Mono- and multi-crystalline silicon PV devices (p-type PV cells using Tedlar-type back sheets) revealed intense degradation in coastal areas with high temperature and high relative humidity, reaching power reductions up to 60% and 40% for individual modules, respectively. The results also show low measured peak power for a-Si/µc-Si modules that had been operating for two consecutive years, indicating a 7% reduction in nominal power, which could be associated with an initial degradation greater than expected. I-V curve measurements carried out on CIGS modules indicate an average power reduction of 6.2% relative to nameplate peak power for brand-new modules. Even though a small sample was analyzed, this could indicate a discrepancy between nameplate and actual power for these modules and manufacturer.

The comparison between measured and simulated losses showed differences of up to 11% for the # Itiquira-MT site and 9% for the # Aratiba-RS site, both for a-Si/µc-Si PV systems. No significant difference was observed between the simulated and measured performance of CdTe PV systems for both sites. Most of the differences between simulation and measured results are a consequence of PID effects, marked initial degradation, and soiling rates different from standard simulation values, and are not necessarily only due to simulation uncertainties.

Even though six different PV technologies were assessed, the results presented in this thesis are directly related to the specific manufacturers of the modules employed in the project, and not necessarily reflect the PV technologies' behavior as a whole.

The effects of solar overirradiance events, on top of being of scientific and technological interest, will have important impacts on the operational performance of utility-scale PV power plants. Seven of the ten highest overirradiance events taking place worldwide and recorded in the literature took place in Brazil and were measured in the R&D project that led to this thesis. These solar overirradiance events all occurred at sites where utility-scale PV power plants are being deployed in Brazil, and all these sites are located at relatively low altitudes where there

is no benefit from a reduced atmospheric absorption, making these observations even more remarkable. The highest overirradiance event recorded at the # Caucaia-CE SMS, at an altitude of about 32 m above sea level was 1845 W/m² (Kt = 1.40). The measured value is similar to those reported for Colorado-USA, where 1891 W/m² was recorded at 1829 m above sea level, and for Andes-Ecuador, where 1832 W/m² was measured at 3400 m above sea level, and where utility-scale PV power plants are not likely to be installed in the near future.

The impacts of these extreme solar overirradiance values on utility-scale PV power plants were also addressed. Results showed that when long overirradiance events, with a time span longer than five minutes, are associated with the very high fuse operating temperatures prevailing in the field, deleterious consequences can be observed. These impacts can include the blowing of even slow-blow fuses if they are sized as per the PV module manufacturer's specification. It is therefore recommended that PV module manufacturers reassess their maximum series fuse ratings in the light of this information, and utility-scale projects could size string boxes in a manner to keep fuses from reaching such high temperatures.

Under the conditions shown in this thesis, PV system design of utility-scale PV power plants needs to be carried out with care due to the large fraction of solar energy available at irradiance values above the standard 1000 W/m^2 STC irradiance, typically caused by overirradiance events and clear sky exceedances. For such cases, one-minute data averaging intervals have presented satisfactory results for PV modeling and sizing. High time-resolution measurements of solar irradiance in the field all over the globe might reveal solar overirradiance events like the ones presented in this thesis to be even more common than reported here. Especially at sites in which utility-scale PV power plants will be extensively deployed in the future, the issue raised in this thesis is not only of scientific and technological interest but of economic importance as well.

REFERENCES

60904-9, I. **Photovoltaic devices - Part 9: Solar simulator performance requirements**: International Electrotechnical Commission 2007.

60904-13, I. **Photovoltaic devices – Part 13: Electroluminescence of photovoltaic modules**: INTERNATIONAL ELECTROTECHNICAL COMMISSION 36 p. 2018.

ABNT. **NBR 10899:2006 - Energia Solar Fotovoltaica - Terminologia** 2006.

ALMEIDA, M. P.; ZILLES, R.; LORENZO, E. Extreme overirradiance events in São Paulo, Brazil. **Solar Energy,** v. 110, p. 168-173, 2014. ISSN 0038-092X. Disponível em: < http://www.sciencedirect.com/science/article/pii/S0038092X14004423 >.

ALVARES, C. A. S., JOSÉ LUIZ; SENTELHAS, PAULO CESAR; DE MORAES GONÇALVES, JOSÉ LEONARDO; SPAROVEK, GERD. Köppen's climate classification map for Brazil. **Meteorologische Zeitschrif,** v. 22, n. 6, p. 711-728, 2013.

AMILLO, A. M. G.; HULD, T.; VOURLIOTI, P.; MÜLLER, R.; NORTON, M. Application of Satellite-Based Spectrally-Resolved Solar Radiation Data to PV Performance Studies. **Energies,** v. 8, n. 5, 2015.

ANDRADE, R. C. D.; TIBA, C. Extreme global solar irradiance due to cloud enhancement in northeastern Brazil. **Renewable Energy,** v. 86, p. 1433-1441, 2016/02/01/ 2016. ISSN 0960-1481. Disponível em: < http://www.sciencedirect.com/science/article/pii/S0960148115302913 >.

ASHRAE. **Methods of Testing to Determine the Thermal Performance of Solar Collectors**. ASHRAE, 1978.

ASTM-G173.03. **Standard Tables for Reference Solar Spectral Irradiances: Direct Normal and Hemispherical on 37° Tilted Surface** 2012.

AVANCIS. **PowerMax® STRONG** 2011.

AVILA, A.; VIZCAYA, P. R.; DIEZ, R. Daily irradiance test signal for photovoltaic systems by selection from long-term data. **Renewable Energy,** v. 131, p. 755-762, 2019/02/01/ 2019. ISSN 0960-1481. Disponível em: < http://www.sciencedirect.com/science/article/pii/S0960148118308681 >.

BOLINGER, M.; WEAVER, S.; ZUBOY, J. Is $50/MWh solar for real? Falling project prices and rising capacity factors drive utility-scale PV toward economic competitiveness. **Progress in Photovoltaics: Research and Applications,** v. 23, n. 12, p. 1847-1856, 2015/12/01 2015. ISSN 1062-7995. Disponível em: < https://doi.org/10.1002/pip.2630 >.

BOSIO, A.; ROSA, G.; ROMEO, N. Past, present and future of the thin film CdTe/CdS solar cells. **Solar Energy**, 2018/01/31/ 2018. ISSN 0038-092X. Disponível em: < http://www.sciencedirect.com/science/article/pii/S0038092X18300306 >.

BRAGA, M.; CAMPOS, R. A.; NASCIMENTO, L. R. D.; SANTOS, E. M.; RÜTHER, R. **AVALIAÇÃO DE DESEMPENHO DE DIFERENTES TECNOLOGIAS FOTOVOLTAICAS EM IRECÊ, BA**. VII Congresso Brasileiro de Energia Solar. Gramado - SC: Anais do VII CBENS 2018.

BURGER, B.; RÜTHER, R. Inverter sizing of grid-connected photovoltaic systems in the light of local solar resource distribution characteristics and temperature. **Solar Energy,** v. 80, n. 1, p. 32-45, 2006. ISSN 0038-092X. Disponível em: < http://www.sciencedirect.com/science/article/pii/S0038092X05003099 >.

BUSSMANN. **Photovoltaic Fuses - Technical Data 10121**. Eaton's Bussmann Series 2017.

CARON, J. R.; LITTMANN, B. Direct Monitoring of Energy Lost Due to Soiling on First Solar Modules in California. **IEEE Journal of Photovoltaics,** v. 3, n. 1, p. 336-340, 2013. ISSN 2156-3381.

CENELEC. **EN 50530 - Overall efficiency of grid connected photovoltaic inverters**: European Committee for Electrotechnical Standardization**:** 38 p. 2010.

CHEN, S.; LI, P.; BRADY, D.; LEHMAN, B. The impact of irradiance time behaviors on inverter sizing and design. 2010 IEEE 12th Workshop on Control and Modeling for Power Electronics (COMPEL), 2010, 28-30 June 2010. p.1-5.

CLIFFORD W. HANSEN, J. S. S., AND ABRAHAM ELLIS **Statistical Criteria for Characterizing Irradiance Time Series** Sandia National Laboratories Albuquerque, New Mexico 2010

DESCHAMPS, E. M.; RÜTHER, R. Optimization of inverter loading ratio for grid connected photovoltaic systems. **Solar Energy,** v. 179, p. 106-118, 2019/02/01/ 2019. ISSN 0038-092X. Disponível em: < http://www.sciencedirect.com/science/article/pii/S0038092X1831226X >.

DIAS, J. B. **Instalação Fotovoltaica Conectada à Rede: Estudo Experimental para Otimização do Fator de Dimensionamento**. 2006. Tese de Doutorado PROMEC/UFRGS, Porto Alegre, Brasil.

DIERAUF, T.; GROWITZ, A.; KURTZ, S. R.; CRUZ, J. L. B.; RILEY, E.; HANSEN, C. **Weather-Corrected Performance Ratio**. National Renewable Energy Laboratory. 2013

DIRNBERGER, D.; BLACKBURN, G.; MÜLLER, B.; REISE, C. On the impact of solar spectral irradiance on the yield of different PV technologies. **Solar Energy Materials and Solar Cells,** v. 132, p. 431-442, 2015/01/01/ 2015. ISSN 0927-0248. Disponível em: < http://www.sciencedirect.com/science/article/pii/S0927024814005169 >.

DUCK, B. C.; FELL, C. J. Comparison of methods for estimating the impact of spectrum on PV output. Photovoltaic Specialist Conference (PVSC), 2015 IEEE 42nd, 2015, 14-19 June 2015. p.1-6.

DUFFIE, J. A.; BECKMAN, W. A. Solar Radiation. In: (Ed.). **Solar Engineering of Thermal Processes**: John Wiley & Sons, Inc., 2013. p.3-42. ISBN 9781118671603.

DUPONT. **DuPont Apollo A Series Thin Film Modules** 2011.

_____. **DuPont Apollo C Series Thin Film Modules** 2012.

DYNGE, A. S.-N. **Optical Modelling for Photovoltaic Panels**. 2013. (Master Thesis). University of Agder

EL CHAAR, L.; LAMONT, L. A.; EL ZEIN, N. Review of photovoltaic technologies. **Renewable and Sustainable Energy Reviews,** v. 15, n. 5, p. 2165-2175, 2011. ISSN 1364-0321. Disponível em: < http://www.sciencedirect.com/science/article/pii/S1364032111000050 >.

EMCK, P.; RICHTER, M. An Upper Threshold of Enhanced Global Shortwave Irradiance in the Troposphere Derived from Field Measurements in Tropical Mountains. **Journal of Applied Meteorology and Climatology,** v. 47, n. 11, p. 2828-2845, 2008/11/01 2008. ISSN 1558-8424. Disponível em: < https://doi.org/10.1175/2008JAMC1861.1 >.

ESTUPINAN, J. G.; RAMAN, S.; CRESCENTI, G. H.; STREICHER, J. J.; BARNARD, W. F. Effects of clouds and haze on UV-B radiation. **Journal of Geophysical Research,** v. 101, p. 16807-16816, 1996. ISSN ISSN 0148-0227
EISSN 2156-2202.

ETI. **Protection of Photovoltaic Systems (gPV - Fuse-links)**. Green Protect - DC 2013.

FELDMAN, D.; BARBOSE, G.; MARGOLIS, R.; BOLINGER, M.; CHUNG, D.; FU, R.; SEEL, J.; DAVIDSON, C.; WISER, R. **Photovoltaic System Pricing Trends - Historical, Recent, and Near-Term Projections**. 2015

FIRST-SOLAR. **FS SERIES 2 SOLAR MODULE** 2007.

FORNIÉS, E.; NARANJO, F.; MAZO, M.; RUIZ, F. The influence of mismatch of solar cells on relative power loss of photovoltaic modules. **Solar Energy,** v. 97, p. 39-47, 2013. ISSN 0038-092X. Disponível em: < http://www.sciencedirect.com/science/article/pii/S0038092X13003149 >.

FRAUNHOFER. **Photovoltaics Report** ISE, I. F. S. E. S.-. 2012.

_____. **Photovoltaics Report** ISE, I. F. S. E. S.-. 2018.

GALLAGHER, R. P.; LEE, T. K. Adverse effects of ultraviolet radiation: A brief review. **Progress in Biophysics and Molecular Biology,** v. 92, n. 1, p. 119-131, 2006/09/01/ 2006. ISSN 0079-6107. Disponível em: < http://www.sciencedirect.com/science/article/pii/S0079610706000137 >.

GOSTEIN, M.; CARON, J. R.; LITTMANN, B. Measuring soiling losses at utility-scale PV power plants. 2014 IEEE 40th Photovoltaic Specialist Conference (PVSC), 2014, 8-13 June 2014. p.0885-0890.

GOTTSCHALG, R.; BETTS, T. R.; INFIELD, D. G.; KEARNEY, M. J. The effect of spectral variations on the performance parameters of single and double junction amorphous silicon solar

cells. **Solar Energy Materials and Solar Cells,** v. 85, n. 3, p. 415-428, 2005. ISSN 0927-0248. Disponível em: < http://www.sciencedirect.com/science/article/B6V51-4CYGVX3-1/2/0e75959018d7adbc682896373732dbe1 >.

GREEN, M. A. Recent developments in photovoltaics. **Solar Energy,** v. 76, n. 1–3, p. 3-8, 2004. ISSN 0038-092X. Disponível em: < http://www.sciencedirect.com/science/article/pii/S0038092X03000653 >.

_____. Third Generation Photovoltaics: Assessment of progress over the last decade. Photovoltaic Specialists Conference (PVSC), 2009 34th IEEE, 2009, 7-12 June 2009. p.000146-000149.

GREEN, M. A. Commercial progress and challenges for photovoltaics. **Nature Energy,** v. 1, p. 15015, 2016. Disponível em: < https://doi.org/10.1038/nenergy.2015.15 >.

GU, L.; FUENTES, J. D.; GARSTANG, M.; SILVA, J. T. D.; HEITZ, R.; SIGLER, J.; SHUGART, H. H. Cloud modulation of surface solar irradiance at a pasture site in southern Brazil. **Agricultural and Forest Meteorology,** v. 106, n. 2, p. 117-129, 2001/01/27/ 2001. ISSN 0168-1923. Disponível em: < http://www.sciencedirect.com/science/article/pii/S0168192300002094 >.

GUEYMARD, C. A. Cloud and albedo enhancement impacts on solar irradiance using high-frequency measurements from thermopile and photodiode radiometers. Part 1: Impacts on global horizontal irradiance. **Solar Energy,** v. 153, p. 755-765, 2017/09/01/ 2017a. ISSN 0038-092X. Disponível em: < http://www.sciencedirect.com/science/article/pii/S0038092X1730381X >.

_____. Cloud and albedo enhancement impacts on solar irradiance using high-frequency measurements from thermopile and photodiode radiometers. Part 2: Performance of separation and transposition models for global tilted irradiance. **Solar Energy,** v. 153, p. 766-779, 2017/09/01/ 2017b. ISSN 0038-092X. Disponível em: < http://www.sciencedirect.com/science/article/pii/S0038092X17303730 >.

HAAG, R. **ESTIMATIVA DA DISTRIBUIÇÃO ESPECTRAL DA RADIAÇÃO SOLAR SOBRE O TERRITÓRIO BRASILEIRO ATRAVÉS DE ANÁLISE MULTIINSTRUMENTAL**. 2013. (Tese). Pós-Graduação em Engenharia Mecânica, Universidade Federal do Rio Grande do Sul, Porto Alegre - Brasil.

HAAG, R.; KRENZINGER, A. **Espectro Solar Caracteristica para a região do semiárido Brasileiro**. VI Congresso Brasileiro de Energia Solar. Belo Horizonte - MG 2016.

HANWHA. **Hanwha SolarOne Poly x-tra** 2011.

HEEGER, A. Printable Organic Solar Cells - Challenges and Opportunities in Technology Transfer from Lab to Market. Nature Photonics Technology Conference - Future Perspectives on Photovoltaics, 2010, Tóquio - Japão.

HICKEL, B.; DESCHAMPS, E. M.; NASCIMENTO, L.; RÜTHER, R.; SIMOES, G. ANÁLISE DA INFLUÊNCIA DO ACÚMULO DE SUJEIRA SOBRE DIFERENTES

TECNOLOGIAS DE MÓDULOS FV: REVISÃO E MEDIÇÕES DE CAMPO. VI Congresso Brasileiro de Energia Solar, 2016, Belo Horizonte - Brasil. 04 a 07 de abril de 2016.

HOFFMANN, S.; KOEHL, M. Effect of humidity and temperature on the potential-induced degradation. **Progress in Photovoltaics: Research and Applications,** v. 22, n. 2, p. 173-179, 2014. ISSN 1099-159X. Disponível em: < http://dx.doi.org/10.1002/pip.2238 >.

HUSSIN, M. Z.; OMAR, A. M.; ZAIN, Z. M.; SHAARI, S.; ZAINUDDIN, H. Design Impact of 6.08 kWp Grid-Connected Photovoltaic System at Malaysia Green Technology Corporation. **INTERNATIONAL JOURNAL OF ELECTRICAL AND ELECTRONIC SYSTEMS RESEARCH,** v. 5, 2012

IEA. **Review of Failures of Photovoltaic Modules**. 2014. (Report IEA-PVPS T13-01:2014)

IEC-60891. **Photovoltaic devices - Procedures for temperature and irradiance corrections to measured I-V characteristics**: International Electrotechnical Commission 2009.

IEC-62804.1. **IEC TS 62804-1:2015: Photovoltaic (PV) modules - Test methods for the detection of potential-induced degradation - Part 1: Crystalline silicon**. 2015

INMAN, R. H.; CHU, Y.; COIMBRA, C. F. M. Cloud enhancement of global horizontal irradiance in California and Hawaii. **Solar Energy,** v. 130, p. 128-138, 2016/06/01/ 2016. ISSN 0038-092X. Disponível em: < http://www.sciencedirect.com/science/article/pii/S0038092X16001079 >.

IQBAL, M. **An Introduction to Solar Radiation**. Toronto: Academic Press, 1983.

ISHII, T.; OTANI, K.; TAKASHIMA, T. Effects of solar spectrum and module temperature on outdoor performance of photovoltaic modules in round-robin measurements in Japan. **Progress in Photovoltaics: Research and Applications,** v. 19, n. 2, p. 141-148, 2011. ISSN 1099-159X. Disponível em: < http://dx.doi.org/10.1002/pip.995 >.

ISLAM, M. A.; HASANUZZAMAN, M.; RAHIM, N. A. A comparative investigation on in-situ and laboratory standard test of the potential induced degradation of crystalline silicon photovoltaic modules. **Renewable Energy,** v. 127, p. 102-113, 2018/11/01/ 2018. ISSN 0960-1481. Disponível em: < http://www.sciencedirect.com/science/article/pii/S0960148118304592 >.

J. ZHU, D. M.-C., T.R. BETTS, R. GOTTSCHALG. Correlation of Degree of EVA Crosslinking with Formation and Discharge of Acetic Acid in PV Modules. 33rd European Photovoltaic Solar Energy Conference and Exhibition, 2017, Amsterdam. p.
1795 - 1798.

JAZAYERI, M.; JAZAYERI, K.; UYSAL, S. Adaptive photovoltaic array reconfiguration based on real cloud patterns to mitigate effects of non-uniform spatial irradiance profiles. **Solar Energy,** v. 155, p. 506-516, 2017/10/01/ 2017. ISSN 0038-092X. Disponível em: < http://www.sciencedirect.com/science/article/pii/S0038092X17305558 >.

JIANG, Z.; BRUNDLINGER, R.; BETTS, T. R.; GOTTSCHALG, R. Effect of Module Degradation on Inverter Sizing. Photovoltaic Specialists Conference, 2008. PVSC '08. 33rd IEEE, 2008, 11-16 May 2008. p.1-6.

JORDAN, D. C.; KURTZ, S. R. Photovoltaic Degradation Rates—an Analytical Review. **Progress in Photovoltaics: Research and Applications,** v. 21, n. 1, p. 12-29, 2013. ISSN 1099-159X. Disponível em: < http://dx.doi.org/10.1002/pip.1182 >.

KAVLAK, G.; MCNERNEY, J.; TRANCIK, J. E. Evaluating the causes of cost reduction in photovoltaic modules. **Energy Policy,** v. 123, p. 700-710, 2018/12/01/ 2018. ISSN 0301-4215. Disponível em: < http://www.sciencedirect.com/science/article/pii/S0301421518305196 >.

KEMPE, M. D.; JORGENSEN, G. J.; TERWILLIGER, K. M.; MCMAHON, T. J.; KENNEDY, C. E.; BOREK, T. T. Ethylene-Vinyl Acetate Potential Problems for Photovoltaic Packaging. 2006 IEEE 4th World Conference on Photovoltaic Energy Conference, 2006, 7-12 May 2006. p.2160-2163.

KING, D. L.; KRATOCHVIL, J. A.; BOYSON, W. E. Stabilization and performance characteristics of commercial amorphous-silicon PV modules. Photovoltaic Specialists Conference, 2000. Conference Record of the Twenty-Eighth IEEE, 2000, 2000. p.1446-1449.

KRATZENBERG, M. G.; DESCHAMPS, E. M.; NASCIMENTO, L.; RÜTHER, R.; ZÜRN, H. H. Optimal Photovoltaic Inverter Sizing Considering Different Climate Conditions and Energy Prices. **Energy Procedia,** v. 57, p. 226-234, 2014/01/01/ 2014. ISSN 1876-6102. Disponível em: < http://www.sciencedirect.com/science/article/pii/S1876610214013940 >.

LIOU, K.-N. **An Introduction to Atmospheric Radiation**. 2nd Edition. London: Academic Press, 2002. ISBN 0074-6142. Disponível em: < https://www.sciencedirect.com/bookseries/international-geophysics/vol/26/suppl/C >.

LONG, C. N.; DUTTON, E. G. **BSRN Global Network recommended QC tests, V2.0** 2002

LONG, C. N.; SHI, Y. An Automated Quality Assessment and Control Algorithm for Surface Radiation Measurements. **The Open Atmospheric Science Journal** v. 2, p. 23-37, 10/4/2008 2008.

LORENZO, E.; MORETÓN, R.; LUQUE, I. Dust effects on PV array performance: in-field observations with non-uniform patterns. **Progress in Photovoltaics: Research and Applications**, p. n/a-n/a, 2013. ISSN 1099-159X. Disponível em: < http://dx.doi.org/10.1002/pip.2348 >.

LUOMA, J.; KLEISSL, J.; MURRAY, K. Optimal inverter sizing considering cloud enhancement. **Solar Energy,** v. 86, n. 1, p. 421-429, 2012/01/01/ 2012. ISSN 0038-092X. Disponível em: < http://www.sciencedirect.com/science/article/pii/S0038092X11003793 >.

MACÊDO, W. N.; ZILLES, R. Operational results of grid-connected photovoltaic system with different inverter's sizing factors (ISF). **Progress in Photovoltaics: Research and Applications,** v. 15, n. 4, p. 337-352, 2007. ISSN 1099-159X. Disponível em: < http://dx.doi.org/10.1002/pip.740 >.

MANI, M.; PILLAI, R. Impact of dust on solar photovoltaic (PV) performance: Research status, challenges and recommendations. **Renewable and Sustainable Energy Reviews,** v. 14, n. 9, p. 3124-3131, 2010. ISSN 1364-0321. Disponível em: < http://www.sciencedirect.com/science/article/pii/S1364032110002455 >.

MANSHANDEN, P.; BRONSVELD, P. C. P. Investigation of Hydrogenation in n-type Wafers with Ring- and Disc-shaped Defect Zones. **Energy Procedia,** v. 92, p. 857-866, 2016/08/01/ 2016. ISSN 1876-6102. Disponível em: < http://www.sciencedirect.com/science/article/pii/S1876610216305197 >.

MARTÍNEZ-MORENO, F.; PIGUEIRAS, E. L.; VILLAGRÁ, R. M.; NARVARTE, L. Bankable procedures for the Technical quality assurance of large Scale PV plants. 29th European Photovoltaic Solar Energy Conference (PVSEC), 2014, Amsterdam.

MATEO, C.; HERNÁNDEZ-FENOLLOSA, M. A.; MONTERO, Á.; SEGUÍ-CHILET, S. Analysis of initial stabilization of cell efficiency in amorphous silicon photovoltaic modules under real outdoor conditions. **Renewable Energy,** v. 120, p. 114-125, 2018/05/01/ 2018. ISSN 0960-1481. Disponível em: < http://www.sciencedirect.com/science/article/pii/S0960148117312582 >.

MCCORMICK, P. G.; SUEHRCKE, H. The effect of intermittent solar radiation on the performance of PV systems. **Solar Energy,** v. 171, p. 667-674, 2018/09/01/ 2018. ISSN 0038-092X. Disponível em: < http://www.sciencedirect.com/science/article/pii/S0038092X18305942 >.

MEKHILEF, S.; SAIDUR, R.; KAMALISARVESTANI, M. Effect of dust, humidity and air velocity on efficiency of photovoltaic cells. **Renewable and Sustainable Energy Reviews,** v. 16, n. 5, p. 2920-2925, 2012. ISSN 1364-0321. Disponível em: < http://www.sciencedirect.com/science/article/pii/S1364032112001050 >.

MERSEN. **Photovoltaic Fuse - Ampere Rating Vs. Ambient Temperature**. Newburyport, MA - USA 2012.

MIMS III, F. M.; FREDERICK, J. E. **Cumulus clouds and UV-B**. Nature: Nature Publishing Group. 371**:** 291 p. 1994.

MINNAERT, B.; VEELAERT, P. A Proposal for Typical Artificial Light Sources for the Characterization of Indoor Photovoltaic Applications. **Energies,** v. 7, n. 3, p. 1500, 2014. ISSN 1996-1073. Disponível em: < http://www.mdpi.com/1996-1073/7/3/1500 >.

MORA SEGADO, P.; CARRETERO, J.; SIDRACH-DE-CARDONA, M. Models to predict the operating temperature of different photovoltaic modules in outdoor conditions. **Progress in Photovoltaics: Research and Applications,** v. 23, n. 10, p. 1267-1282, 2015. ISSN 1099-159X. Disponível em: < http://dx.doi.org/10.1002/pip.2549 >.

MUÑOZ-GARCÍA, M. A.; MARIN, O.; ALONSO-GARCÍA, M. C.; CHENLO, F. Characterization of thin film PV modules under standard test conditions: Results of indoor and outdoor measurements and the effects of sunlight exposure. **Solar Energy,** v. 86, n. 10, p. 3049-3056, 2012/10/01/ 2012. ISSN 0038-092X. Disponível em: < http://www.sciencedirect.com/science/article/pii/S0038092X12002770 >.

MUNOZ, M. A.; CHENLO, F.; ALONSO-GARCÍA, M. C. Influence of initial power stabilization over crystalline-Si photovoltaic modules maximum power. **Progress in Photovoltaics: Research and Applications,** v. 19, n. 4, p. 417-422, 2011. ISSN 1099-159X. Disponível em: < http://dx.doi.org/10.1002/pip.1052 >.

MYERS, D. R.; GUEYMARD, C. A. **Description and Availability of the SMARTS Spectral Model for Photovoltaic Applications** International Symposium on Optical Science and Technology, SPIE's 49th Annual Meeting. Denver, Colorado 2004.

N. REICH; W. VAN SARK; E. ALSEMA; S. KAN, S. S.; DER, A. V.; HEIDE, R. L., AND R. SCHROPP. Weak light performance and spectral response of different solar cell types. 20th European Photovoltaic Solar Energy Conference, 2005, Spain.

NASCIMENTO, L. **A Avaliação de Longo Prazo de um Sistema Fotovoltaico Integrado à Edificação Urbana e Conectado à Rede Elétrica Pública**. 2013. 95 (Dissertação de Mestrado). Departamento de Engenharia Civil - UFSC, Universidade Federal de Santa Catarina, Florianópolis - SC.

NASCIMENTO, L.; CAMPOS, R.; RÜTHER, R.; SIMÕES, G. AVALIAÇÃO DE DESEMPENHO DE DIFERENTES TECNOLOGIAS FOTOVOLTAICAS NO NORDESTE BRASILEIRO. VI Congresso Brasileiro de Energia Solar 2016, Belo Horizonte - Brasil. 04 a 07 de abril de 2016.

NASCIMENTO, L.; RÜTHER, R. Fifteen years and counting: The reliable long-term performance of the first grid-connected, building-integrated, thin-film photovoltaic installation in Brazil. 2014 IEEE 40th Photovoltaic Specialist Conference (PVSC), 2014, 8-13 June 2014. p.3372-3377.

NASCIMENTO, L. R. D.; BRAGA, M.; DOLLA, R.; CAMPOS, R. A.; RÜTHER, R. PV Systems in Warm and Sunny Climates: Performance Assessment of Commercially Available Solar Photovoltaic Technologies under Different Climatic Conditions in the Brazilian Energy Mix. 2018 IEEE 7th World Conference on Photovoltaic Energy Conversion (WCPEC) (A Joint Conference of 45th IEEE PVSC, 28th PVSEC & 34th EU PVSEC), 2018, 10-15 June 2018. p.0103-0108.

NOBRE, A. **SHORT-TERM SOLAR IRRADIANCE FORECASTING AND PHOTOVOLTAIC SYSTEMS PERFORMANCE IN A TROPICAL CLIMATE IN SINGAPORE**. 2015. 252 (Tese de Doutorado). Programa de PósGraduação em Engenharia Civil, Universidade Federal de Santa Catarina - UFSC, Florianópolis - SC.

NOBRE, A.; MONTENEGRO, A.; ZHEN, Y.; REINDL, T.; RÜTHER, R. **ON PV MODULE TEMPERATURES IN TROPICAL REGIONS – A COMPARISON BETWEEN SYSTEM LOCATIONS IN SINGAPORE AND BRAZIL** IV Congresso Brasileiro de Energia Solar e V Conferência Latino-Americana da ISES – São Paulo, 18 a 21 de setembro de 2012 2012.

NOTTON, G.; LAZAROV, V.; STOYANOV, L. Optimal sizing of a grid-connected PV system for various PV module technologies and inclinations, inverter efficiency characteristics and

locations. **Renewable Energy,** v. 35, n. 2, p. 541-554, 2010. ISSN 0960-1481. Disponível em: < http://www.sciencedirect.com/science/article/pii/S0960148109003085 >.

NREL. **Best Research-Cell Efficiencies:** NREL's "Best Research-Cell Efficiencies" Chart p. 2018.

NÚÑEZ, R.; JIN, C.; VICTORIA, M.; DOMÍNGUEZ, C.; ASKINS, S.; HERRERO, R.; ANTÓN, I.; SALA, G. Spectral study and classification of worldwide locations considering several multijunction solar cell technologies. **Progress in Photovoltaics: Research and Applications**, p. n/a-n/a, 2016. ISSN 1099-159X. Disponível em: < http://dx.doi.org/10.1002/pip.2781 >.

PARIDA, B.; INIYAN, S.; GOIC, R. A review of solar photovoltaic technologies. **Renewable and Sustainable Energy Reviews,** v. 15, n. 3, p. 1625-1636, 2011. ISSN 1364-0321. Disponível em: < http://www.sciencedirect.com/science/article/pii/S1364032110004016 >.

PARISI, A.; DOWNS, N. Variation of the enhanced biologically damaging solar UV due to clouds. **Photochemical and Photobiological Sciences,** v. 3, n. 7, p. 643-7, 2004.

PARISI, A. V.; SABBURG, J.; KIMLIN, M. G.; DOWNS, N. Measured and modelled contributions to UV exposures by the albedo of surfaces in an urban environment. **Theoretical and Applied Climatology,** v. 76, n. 3, p. 181-188, 2003/12/01 2003. ISSN 1434-4483. Disponível em: < https://doi.org/10.1007/s00704-003-0012-9 >.

PECENAK, Z. K.; MEJIA, F. A.; KURTZ, B.; EVAN, A.; KLEISSL, J. Simulating irradiance enhancement dependence on cloud optical depth and solar zenith angle. **Solar Energy,** v. 136, p. 675-681, 2016/10/15/ 2016. ISSN 0038-092X. Disponível em: < http://www.sciencedirect.com/science/article/pii/S0038092X16303036 >.

PEEL, M. C.; FINLAYSON, B. L.; MCMAHON, T. A. Updated world map of the Köppen-Geiger climate classification. **Hydrol. Earth Syst. Sci.,** v. 11, n. 5, p. 1633-1644, 2007. ISSN 1607-7938. Disponível em: < https://www.hydrol-earth-syst-sci.net/11/1633/2007/ >.

PFISTER, G.; MCKENZIE, R. L.; LILEY, J. B.; THOMAS, A.; FORGAN, B. W.; LONG, C. N. Cloud Coverage Based on All-Sky Imaging and Its Impact on Surface Solar Irradiance. **Journal of Applied Meteorology,** v. 42, n. 10, p. 1421-1434, 2003/10/01 2003. ISSN 0894-8763. Disponível em: < https://doi.org/10.1175/1520-0450(2003)042<1421:CCBOAI>2.0.CO;2 >.

PIACENTINI, R. D.; CEDE, A.; BÁRCENA, H. Extreme solar total and UV irradiances due to cloud effect measured near the summer solstice at the high-altitude desertic plateau Puna of Atacama (Argentina). **Journal of Atmospheric and Solar-Terrestrial Physics,** v. 65, n. 6, p. 727-731, 2003/04/01/ 2003. ISSN 1364-6826. Disponível em: < http://www.sciencedirect.com/science/article/pii/S1364682603000841 >.

PIACENTINI, R. D.; SALUM, G. M.; FRAIDENRAICH, N.; TIBA, C. Extreme total solar irradiance due to cloud enhancement at sea level of the NE Atlantic coast of Brazil. **Renewable Energy,** v. 36, n. 1, p. 409-412, 2011/01/01/ 2011. ISSN 0960-1481. Disponível em: < http://www.sciencedirect.com/science/article/pii/S096014811000265X >.

PIEDEHIERRO, A. A.; ANTÓN, M.; CAZORLA, A.; ALADOS-ARBOLEDAS, L.; OLMO, F. J. Evaluation of enhancement events of total solar irradiance during cloudy conditions at Granada (Southeastern Spain). **Atmospheric Research,** v. 135-136, p. 1-7, 2014/01/01/ 2014. ISSN 0169-8095. Disponível em: < http://www.sciencedirect.com/science/article/pii/S0169809513002342 >.

PINGEL, S.; FRANK, O.; WINKLER, M.; DARYAN, S.; GEIPEL, T.; HOEHNE, H.; BERGHOLD, J. Potential Induced Degradation of solar cells and panels. Photovoltaic Specialists Conference (PVSC), 2010 35th IEEE, 2010, 20-25 June 2010. p.002817-002822.

PINTO FILHO, G. F. P. **Degradação induzida pelo potencial em módulos e instalações fotovoltaicas de c-Si**. 2017. (Thesis). Universidade de São Paulo

PIOTROWICZ, M.; MARAŃDA, W. Report on efficiency of field-installed PV-inverter with focus on radiation variability. Proceedings of the 20th International Conference Mixed Design of Integrated Circuits and Systems - MIXDES 2013, 2013, 20-22 June 2013. p.440-443.

PVSYST. **Software for the Study and Simulation of Photovoltaic Systems**. Geneva, Switzerland 2016.

QASEM, H.; BETTS, T. R.; MÜLLEJANS, H.; ALBUSAIRI, H.; GOTTSCHALG, R. Dust-induced shading on photovoltaic modules. **Progress in Photovoltaics: Research and Applications**, p. n/a-n/a, 2012. ISSN 1099-159X. Disponível em: < http://dx.doi.org/10.1002/pip.2230 >.

RANSOME, S. J.; FUNTAN, P. **Why Hourly Averaged Measurement Data Insufficient to Model PVSystem Performance Accurately**. 20th European PVSEC Papers. Barcelona 2005.

REICH, N. H.; MUELLER, B.; ARMBRUSTER, A.; VAN SARK, W. G. J. H. M.; KIEFER, K.; REISE, C. Performance ratio revisited: is PR > 90% realistic? **Progress in Photovoltaics: Research and Applications,** v. 20, n. 6, p. 717-726, 2012. ISSN 1099-159X. Disponível em: < http://dx.doi.org/10.1002/pip.1219 >.

REICH, N. H.; SARK, W. G. J. H. M. V.; ALSEMA, E. A.; KAN, S. Y.; SILVESTER, S.; HEIDE, A. S. H. V. D.; LOF, R. W.; SCHROPP, R. E. I. Weak light performance and spectral response of different solar cell types. 20th European Photovoltaic Solar Energy Conference, 2005, Barcelona.

RODRIGO, P.M., FERNÁNDEZ, E.F., ALMONACID, F.M., PÉREZ-HIGUERAS, P.J., 2017. Quantification of the spectral coupling of atmosphere and photovoltaic system performance: indexes, methods and impact on energy harvesting. Sol. Energy Mater. Sol. Cells 163, 73–90. https://doi.org/10.1016/j.solmat.2017.01.018.

RUSCHEL, C. S.; GASPARIN, F. P.; COSTA, E. R.; KRENZINGER, A. Assessment of PV modules shunt resistance dependence on solar irradiance. **Solar Energy,** v. 133, p. 35-43, 2016. ISSN 0038-092X. Disponível em: < http://www.sciencedirect.com/science/article/pii/S0038092X16002449 >.

RÜTHER, R. **Edifícios Solares Fotovoltaicos** Florianópolis - Brasil: LABSOLAR/UFSC, 2004. 114 ISBN 858758304-2,.

RÜTHER, R.; DEL CUETO, J.; TAMIZH-MANI, G.; MONTENEGRO, A. A.; RUMMEL, S.; ANDERBERG, A.; VON ROEDERN, B. Performance test of amorphous silicon modules in different climates - year four: Progress in understanding exposure history stabilization effects. Photovoltaic Specialists Conference, 2008. PVSC '08. 33rd IEEE, 2008, 11-16 May 2008. p.1-5.

RÜTHER, R.; KLEISS, G.; REICHE, K. Spectral effects on amorphous silicon solar module fill factors. **Solar Energy Materials and Solar Cells,** v. 71, n. 3, p. 375-385, 2002. ISSN 0927-0248. Disponível em: < http://www.sciencedirect.com/science/article/B6V51-44SJ4C3-8/2/4c46052c333cad5d11026e582bb8db40 >.

RÜTHER, R.; LIVINGSTONE, J. Seasonal variations in amorphous silicon solar module outputs and thin film characteristics. **Solar Energy Materials and Solar Cells,** v. 36, n. 1, p. 29-43, 1995. ISSN 0927-0248. Disponível em: < http://www.sciencedirect.com/science/article/pii/092702489400165O >.

RÜTHER, R.; NASCIMENTO, L.; JUNIOR, J. U.; PFITSCHER, P.; VIANA, T. Long-term performance of the first grid-connected, building-integrated, thin-film amorphous silicon PV installation in Brazil. 35th IEEE Photovoltaic Specialists Conference, 2010a, Honolulu -HI, EUA. p.4.

_____. Performance assessment of a microcrystalline Si PV installation in a warm climate. 35th IEEE Photovoltaic Specialists Conference, 2010b, Honolulu -HI, EUA. p.4.

RÜTHER, R.; NASCIMENTO, L. R. D.; CAMPOS, R. A. Performance assessment issues in utility-scale photovoltaics in warm and sunny climates. **Renew. Energy Environ. Sustain.,** v. 2, p. 35, 2017. Disponível em: < https://doi.org/10.1051/rees/2017035 >.

RÜTHER, R.; TAMIZH-MANI, G.; DEL CUETO, J.; ADELSTEIN, J.; MONTENEGRO, A. A.; VON ROEDERN, B. Performance test of amorphous silicon modules in different climates: higher minimum operating temperatures lead to higher performance levels. Photovoltaic Energy Conversion, 2003. Proceedings of 3rd World Conference on, 2003, 12-16 May 2003. p.2011-2014 Vol.2.

SAGA, T. Advances in crystalline silicon solar cell technology for industrial mass production. **NPG Asia Mater,** v. 2, p. 96-102, 2010. ISSN 1884-4049. Disponível em: < http://dx.doi.org/10.1038/asiamat.2010.82 >.

SCHMIDT, H. B., B.; KIEFER, K. **Wechselwirkungen zwischen Solarmodulen und Wechselrichtern**. Freiburg/Brsg. 2007

SEFID, S. S. S. G.; MIRBAGHERI, S. M.; MOUSAVI, S. M. H.; SEFID, S. E. S. G. Investigation of solar cells lifetime in Iran. Power Electronics, Drives and Energy Systems (PEDES), 2012 IEEE International Conference on, 2012, 16-19 Dec. 2012. p.1-5.

SIBA. **Fuse.On**. SIBA technical background information:Know-how on electrical fuses. Lünen - Germany 2012.

SINHA, P.; HAYES, W.; LITTMANN, B.; NGAN, L.; ZNAIDI, R. Environmental variables affecting solar photovoltaic energy generation in Morocco. 2014 International Renewable and Sustainable Energy Conference (IRSEC), 2014, 17-19 Oct. 2014. p.230-234.

SKOPLAKI, E.; PALYVOS, J. A. On the temperature dependence of photovoltaic module electrical performance: A review of efficiency/power correlations. **Solar Energy,** v. 83, n. 5, p. 614-624, 2009. ISSN 0038-092X. Disponível em: < http://www.sciencedirect.com/science/article/pii/S0038092X08002788 >.

SOCOMEC. **Photovoltaic fuses - gPV curve**. Catalogue 2014 2014.

SOPORI, B.; BASNYAT, P.; DEVAYAJANAM, S.; SHET, S.; MEHTA, V.; BINNS, J.; APPEL, J. Understanding light-induced degradation of c-Si solar cells. Photovoltaic Specialists Conference (PVSC), 2012 38th IEEE, 2012, 3-8 June 2012. p.001115-001120.

STREVEL, N.; TRIPPEL, L.; KOTARBA, C.; KHAN, I. **Improvements in CdTe module reliability and long-term degradation through advances in construction and device innovation** Photovoltaics International. 22**:** 66-74 p. 2014.

SUEHRCKE, H.; MCCORMICK, P. G. The frequency distribution of instantaneous insolation values. **Solar Energy,** v. 40, n. 5, p. 413-422, 1988/01/01/ 1988. ISSN 0038-092X. Disponível em: < http://www.sciencedirect.com/science/article/pii/0038092X88900965 >.

TAPAKIS, R.; CHARALAMBIDES, A. G. Enhanced values of global irradiance due to the presence of clouds in Eastern Mediterranean. **Renewable Energy,** v. 62, p. 459-467, 2014/02/01/ 2014. ISSN 0960-1481. Disponível em: < http://www.sciencedirect.com/science/article/pii/S0960148113004023 >.

THUILLIER, G.; PERRIN, J.-M.; KECKHUT, P. L.; HUPPERT, F. Local enhanced solar irradiance on the ground generated by cirrus: measurements and interpretation. **Journal of Applied Remote Sensing** v. 7, n. 1, p. 18, 2013. Disponível em: < https://doi.org/10.1117/1.JRS.7.073543 >.

TOMSON, T.; TAMM, G. Short-term variability of solar radiation. **Solar Energy,** v. 80, n. 5, p. 600-606, 2006/05/01/ 2006. ISSN 0038-092X. Disponível em: < http://www.sciencedirect.com/science/article/pii/S0038092X05001398 >.

TRÄGER, F., Ed. **Radiation and Optics in the Atmosphere**. Handbook of Lasers and Optics: Springer-Verlag Berlin Heidelberg, Handbook of Lasers and Opticsed. 2012.

TSUJI, M.; RAHMAN, M. M.; HISHIKAWA, Y.; NISHIOKA, K.; MINEMOTO, T. Uniqueness verification of solar spectrum obtained from three sites in Japan based on similar index of average photon energy. **Solar Energy,** v. 173, p. 89-96, 2018/10/01/ 2018. ISSN 0038-092X. Disponível em: < http://www.sciencedirect.com/science/article/pii/S0038092X18307035 >.

VIRTUANI, A.; PAVANELLO, D.; FRIESEN, G. Overview of Temperature Coefficients of Different Thin Film Photovoltaic Technologies. 25th European Photovoltaic Solar Energy Conference and Exhibition / 5th World Conference on Photovoltaic Energy Conversion, 2010, Valencia - Spain.

WALKER, G. R. Evaluating MPPT converter topologies using a Matlab PV model. **Australian Journal of Electrical & Electronics Engineering, ,** v. 21, n. 1, p. pp. 49-55., 2001.

WEIZER, V. G.; BRANDHORST, H. W.; BRODER, J. D.; HART, R. E.; LAMNECK, J. H. Photon-degradation effects in terrestrial silicon solar cells. **Journal of Applied Physics,** v. 50, n. 6, p. 4443-4449, 1979. Disponível em: < http://scitation.aip.org/content/aip/journal/jap/50/6/10.1063/1.326437 >.

YINGLI. **Yingli Solar Panda** 2012.

YORDANOV, G. H. A study of extreme overirradiance events for solar energy applications using NASA's I3RC Monte Carlo radiative transfer model. **Solar Energy,** v. 122, p. 954-965, 2015/12/01/ 2015. ISSN 0038-092X. Disponível em: < http://www.sciencedirect.com/science/article/pii/S0038092X15005617 >.

YORDANOV, G. H.; MIDTGÅRD, O.; SAETRE, T. O.; NIELSEN, H. K.; NORUM, L. E. Overirradiance (Cloud Enhancement) Events at High Latitudes. **IEEE Journal of Photovoltaics,** v. 3, n. 1, p. 271-277, 2013. ISSN 2156-3381.

YORDANOV, G. H.; SAETRE, T. O.; MIDTGÅRD, O.-M. Extreme overirradiance events in Norway: 1.6 suns measured close to 60°N. **Solar Energy,** v. 115, p. 68-73, 2015/05/01/ 2015. ISSN 0038-092X. Disponível em: < http://www.sciencedirect.com/science/article/pii/S0038092X15000900 >.

YORDANOV, G. H.; SAETRE, T. O.; MIDTGÅRD, O. 1.6 suns at 58°20′N - the solar resource in Southern Norway. 2014 IEEE 40th Photovoltaic Specialist Conference (PVSC), 2014, 8-13 June 2014. p.0815-0820.

ZORRILLA-CASANOVA, J.; PILIOUGINE, M.; CARRETERO, J.; BERNAOLA-GALVÁN, P.; CARPENA, P.; MORA-LÓPEZ, L.; SIDRACH-DE-CARDONA, M. Losses produced by soiling in the incoming radiation to photovoltaic modules. **Progress in Photovoltaics: Research and Applications,** v. 21, n. 4, p. 790-796, 2013. ISSN 1099-159X. Disponível em: < http://dx.doi.org/10.1002/pip.1258 >.